ELECTRIC POWER
RESEARCH INSTITUTE

Divider Plate Cracking in Steam Generators

Results of Phase 1: Analysis of Primary Water Stress Corrosion Cracking and Mechanical Fatigue in the Alloy 600 Stub Runner to Divider Plate Weld Material

Divider Plate Cracking in Steam Generators

Results of Phase 1: Analysis of Primary Water Stress Corrosion Cracking and Mechanical Fatigue in the Alloy 600 Stub Runner to Divider Plate Weld Material

1014982

Final Report, June 2007

EPRI Project Manager
H. Cothron

ELECTRIC POWER RESEARCH INSTITUTE
3420 Hillview Avenue, Palo Alto, California 94304-1338 • PO Box 10412, Palo Alto, California 94303-0813 • USA
800.313.3774 • 650.855.2121 • askepri@epri.com • www.epri.com

DISCLAIMER OF WARRANTIES AND LIMITATION OF LIABILITIES

ORGANIZATION(S) THAT PREPARED THIS DOCUMENT

Westinghouse Electric Company

NOTE

For further information about EPRI, call the EPRI Customer Assistance Center at 800.313.3774 or e-mail askepri@epri.com.

CITATIONS

This report was prepared by

Westinghouse Electric Company
P.O. Box 158
Madison, PA 15663-0158

Principal Investigator
C.D. Cassino

This report describes research sponsored by the Electric Power Research Institute (EPRI).

This report is a corporate document that should be cited in the literature in the following manner:

Divider Plate Cracking in Steam Generators: Results of Phase 1: Analysis of Primary Water Stress Corrosion Cracking and Mechanical Fatigue in the Alloy 600 Stub Runner to Divider Plate Weld Material. EPRI, Palo Alto, CA: 2007. 1014982.

PRODUCT DESCRIPTION

Cracking in steam generator divider plate to stub runner welds has been reported by Electricité de France (EdF) plants. This report describes a conservative detailed analysis of a crack in the divider plate to stub runner weld of a domestic Westinghouse-designed steam generator. The crack growth analysis considers the effects of both mechanical fatigue and primary water stress corrosion cracking (PWSCC). There are no reports of divider plate cracking in the domestic market. The goal of this report is to determine if divider plate cracking is a concern for domestic nuclear power plants with Westinghouse steam generators.

Results & Findings

This report provides a conservative crack and fatigue life estimate analysis. Results show that currently observed cracks in the foreign steam generators are not capable of causing the divider plate to fail in the worst-case domestic steam generator during accident or normal operating conditions. However, it is possible for cracks in the divider plate to increase in both length and depth once they have initiated in the divider plate to stub runner weld. Vertical tubesheet displacement will increase by more than 2% for a crack greater than 64% into the depth of the divider plate for all operational conditions.

Challenges & Objective(s)

This report is intended for steam generator analysts and engineers in nuclear power. This report is mainly applicable to nuclear power plants that have Westinghouse-designed steam generators, without center stays or floating divider plates. The purpose of this report is to establish if divider plate cracking indications reported in foreign steam generators are a concern for the domestic steam generator fleet. Specifically, the purpose of the analysis is to determine

- the limiting case model of steam generators with respect to divider plate cracking,
- if a crack in the divider plate can increase vertical tubesheet displacements by more than 2%, and
- if a crack in the divider plate can propagate 100% through the weld material.

Applications, Values & Use

The results in this report will form the basis for future analyses that will mitigate or eliminate the need for divider plate inspections. The details listed herein also will be useful for steam generator engineers to use in writing degradation assessments for future steam generator outage work.

EPRI Perspective

This report is first of a kind. To date there is no other available analysis on the effect of divider plate cracking in Westinghouse steam generators.

Approach

The project team used finite element methods and a first principles engineering mechanics evaluation to determine the effect of a divider plate on the steam generator.

Keywords

Divider plate
Tubesheet displacement
Mechanical fatigue
PWSCC

ABSTRACT

Experience with foreign steam generators suggests that there is a possibility cracks may develop in the divider plate of non-center stayed steam generators due to the presence of Alloy 600 in the stub runner weld material and divider plate.

Current operating experience suggests that the cracks are due to material defects, weld defects, damage due to loose parts in the channel head and Primary Water Stress Corrosion Cracking (PWSCC). The cracks tend to occur in the heat affected zone of the stub runner to divider plate weld and have been observed to run nearly the length of the divider plate (~ 6 feet). As the cracks approach the triple point of the tubesheet-channel head (TS-CH) complex (the junction between the channel head, divider plate and tubesheet) the cracks begin to curve upwards. Current operating experience and non-destructive evaluation of steam generators that have developed these cracks indicates that the cracks remain shallow, in many cases less than 0.10 inch depth, and do not grow deeply into the divider plate.

However, the concern remains as to what effect a crack in the divider plate will have on the structural integrity of the lower steam generator complex. It is also important to develop a basis for understanding any crack propagation mechanism to predict the possibility of a crack running through the thickness of the divider plate if cracks do develop.

CONTENTS

LIST OF FIGURES

LIST OF TABLES

1 INTRODUCTION

There have been several documented cases of cracks and crack indications in the stub runner to divider plate weld in steam generators in operation outside of the United States [1, 2, 3, 4, 5].

The function of the divider plate in most Westinghouse steam generators is to provide a separation between the cold and hot legs of the channelhead as the primary water enters the steam generator. The divider plate is not considered a primary pressure boundary [6] in the context of this analysis. In most Model F, Model D and Model 51 steam generators the divider plate is also not considered a structural component of the lower steam generator complex.

In most Model F, Model D and Model 51 Westinghouse pressurized water reactor (PWR) steam generators the divider plate is initially welded to the channelhead and then attached to the tubesheet via a weld to a strip of metal on the primary side of the tubesheet called the stub runner. The weld between the stub runner and the divider plate is subject to bending and tension during regular operation of the steam generator. The tension on the divider plate occurs as the tubesheet bows from the difference between the primary and secondary operating pressures. The bending on the divider plate occurs because there is typically a temperature and a pressure difference between the hot leg and cold leg side of the tubesheet and divider plate [7]. The weld that connects the stub runner and the divider plate in some steam generators consists of Alloy 600 material. This metal is susceptible to primary water stress corrosion cracking (PWSCC).

The purpose of this report is to determine:

- The limiting case model of steam generator with respect to divider plate cracking.
- If a crack in the divider plate can increase vertical tubesheet displacements by more than 2%.
- If a crack in the divider plate can propagate 100% through the weld material.

Cracking in the divider plate is a concern because it affects tubesheet displacements. Tubesheet displacements may directly affect multiple regions in the SG that include such areas as:

- Stresses in the tubesheet-channelhead complex and connections
- Tube stress
- Plug retention/acceptability issues.

The results of the analysis do not specifically include details of divider plate cracking in designs without a stub runner. Cracking in the divider plate to channelhead weld connection is not examined. The effect that any stress increase in the lower steam generator complex due to divider plate degradation may cause is not examined.

2
SUMMARY OF RESULTS AND CONCLUSIONS

The most limiting steam generator model is the Westinghouse Model 51 steam generator. The Model 51 is the limiting case because it has the thinnest as-designed divider plate section under minimum material conditions and the greatest vertical displacements of the tubesheet under normal, accident and faulted conditions. The predicted mode of failure is a combination of PWSCC and mechanical fatigue of the stub runner to divider plate weld leading to a ductile failure of the material in the heat affected zone.

The region where the divider plate weld cracks have been detected is shown in Figure 2-1 and Figure 2-2. The assumed crack geometry is shown in Figure 2-3[1]. The results of the conservative crack and fatigue life estimate analysis, using the geometry from the most limiting steam generator model with a nominal divider plate thickness of 2.00 inches, show that the currently observed cracks in the foreign steam generators are not capable of causing the divider plate to fail in the worst case domestic steam generator during accident or normal operating conditions.

However, it is possible for cracks in the divider plate to increase in both length and depth once they have initiated in the divider plate to stub runner weld. The conservative crack geometry (i.e., an edge crack that runs the length of the divider plate) and assumptions used in the current FEA and crack growth analysis can be used to bound the scope of the problem in steam generators with typical divider plate geometries and PWSCC susceptible divider plate to stub runner welds.

Table 2-1 summarizes the number of calendar years required to grow a crack through the thickness of the divider plate to stub runner weld (100% through wall) so that the divider plate is unable to restrict the vertical displacement of the tubesheet.[2] The results in the table are discussed in Section 4.5 in more detail.

The significant conclusions from this analysis are:

1. Both the 2D and 3D crack models predict that a crack in the divider plate can exceed the threshold for propagation at relatively shallow depths (e.g. approximately 3% of the divider plate thickness) for all operational conditions.

1: The assumed crack geometry is based on the combination of worst case results from current foreign field inspections. To date, there is no evidence that such a crack geometry exists in a domestic steam generator.

2: In the event of a failed divider plate to stub runner weld it is still possible for the divider plate to maintain a pressure differential between the hot and cold legs of the steam generator.

2. The vertical tubesheet displacement will increase by more than 2% for a crack greater than 64% into the depth of the divider plate for all operational conditions.
3. The 3D results indicate that a crack with the assumed geometry can grow in the thickness direction of the divider plate for both normal and accident conditions.
4. 96% (1.92 inches) of the divider plate thickness must be cracked in order for the weld to plastically fail under NOP. 93% (1.85 inches) must be cracked in order for the weld to plastically fail during an SLB.
5. A divider plate with a crack that runs the entire length of the plate and 0.16 inch deep, twice the threshold for detection, has a safety margin of 750 with respect to the number of loading cycles at NOP service conditions.
6. The crack growth rate analysis shows that it will take 5.11 years for the weld to fail if PWSCC accelerates crack growth in a divider plate with a crack that runs the entire length of the plate and is initially 0.16 inch deep under NOP service conditions.
7. The current field data suggests that it may require more than two times the PWSCC analysis limit (i.e., more than 11 years) to grow the crack entirely through the weld.

The analysis results are sufficient to show that the currently observed shallow crack depths (up to a maximum of 0.28 inch) are not a structural concern for normal operation or during SLB accident conditions in the most limiting steam generator model that is susceptible to PWSCC and fatigue in the divider plate to stub runner weld.

The increasing displacements and stresses that can occur as the divider plate to stub runner weld degrades may affect other structures and aspects of steam generator operation. Some of the related structures and analyses that could be affected by a cracked divider plate include:

- Stresses in the TS-CH complex to lower shell connections
- Faulted transient (e.g. SLB, FLB) analysis inputs and effects
- LOCA inputs and effects
- Inspection limits defined by alternate repair criteria for the tube portion within the tubesheet
- Stresses in the lower portion of the tubes above the TS but below the first support plate (assuming locked collars in the tube support plates)

It is possible that other structures would be affected by a degraded or failed divider plate to stub runner connection. Additional work must be performed to verify that a failed divider plate weld is not a concern to other components in the steam generator during operations.

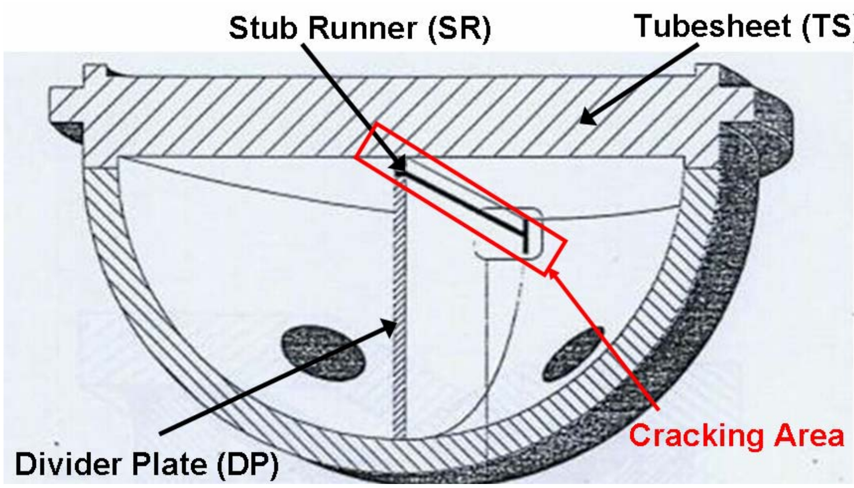

Figure 2-1
Sketch of the Tubesheet and Channelhead Complex Highlighting the Stub Runner the Region of Observed Cracking

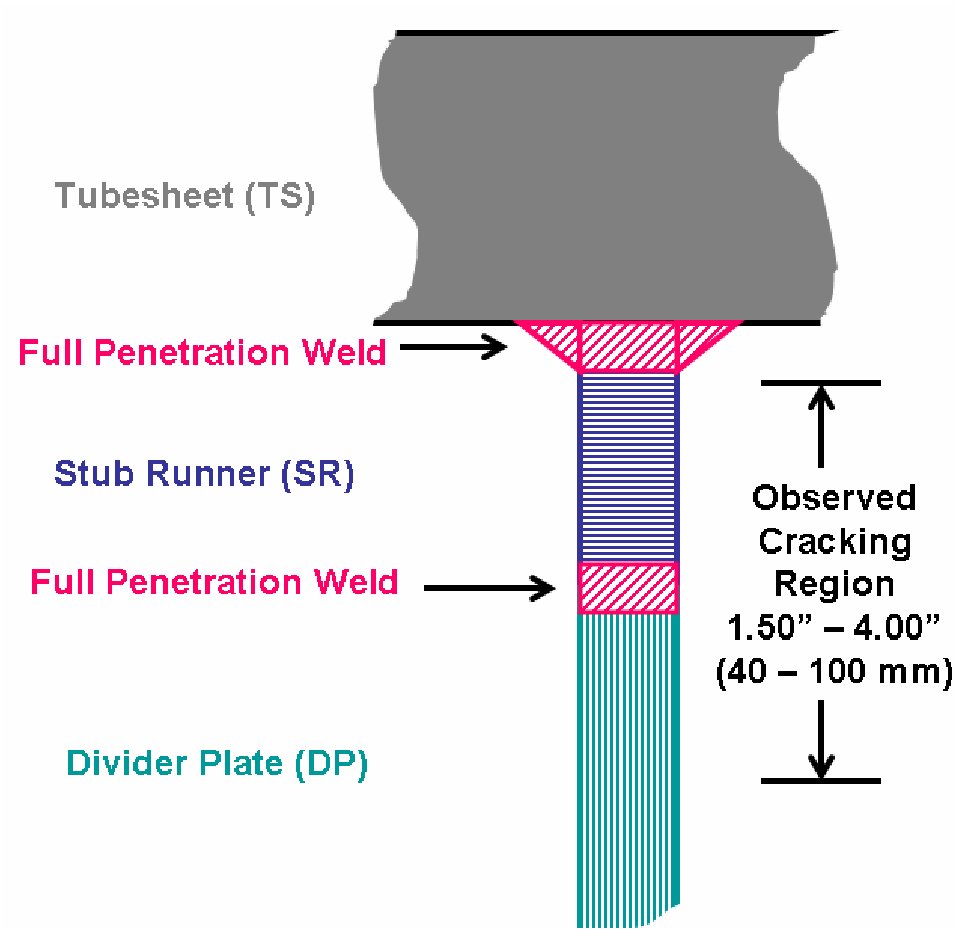

Figure 2-2
Sketch of the Affected Cross-section in the Divider Plate and Stub Runner

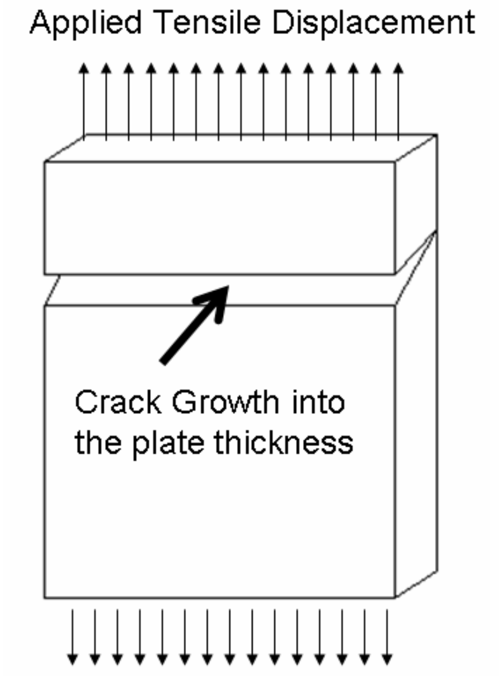

Figure 2-3
Assumed Crack Geometry in Fracture Analysis

Table 2-1
Summary of Estimated Fatigue Life of a Cracked Divider Plate during NOP Assuming an Initial 0.16 inch Crack Depth

Source	Years
FEA w/Ringhals Data	805.1
FEA w/Plastic Failure Limit	751.8
N_f - N_{CHEM}	698.6
Finite Element CGR Estimate	5.1

3
ANALYSIS OF THE LIMITING STEAM GENERATOR

3.1 Introduction

The most limiting model of steam generator in the domestic fleet is determined by examining the geometry, structural properties and thermal conditions of the tubesheet-channelhead (TS-CH) complex. Combustion Engineering (CE) steam generators are not considered in the following analysis. This is because steam generators with a central stay, and/or a floating divider plate, do not have a stub runner to divider plate weld and do not take credit for any structural connection between the divider plate and the tubesheet. The OEM Stress Report analyses of the divider plates in Westinghouse Model 51, Model F and Model D steam generators used a series of three dimensional finite element models to qualify the divider plate. The current analysis method uses two dimensional finite element studies to determine which steam generator model is most susceptible to cracking in the divider plate to stub runner weld and three dimensional finite element models in order to be able to compare the limiting model results to the original stress report results. The effect of a crack in a divider plate is explored using the two dimensional finite element methods. The purpose for the two different types of finite element model approaches is:

- To use a two dimensional finite element study to ascertain the decrease in divider plate stiffness due to a crack in the load path between the divider plate, stub runner and tubesheet.
- To use a three dimensional finite element study that takes the results of the two dimensional study to ascertain the magnitude of the stresses and displacements in the TS-CH steam generator complex with a degraded divider plate.

In each finite element study the crack is assumed to be only in the weld between the stub runner and the divider plate. The crack is also assumed to run the full length of the tubesheet and propagate into the depth of the divider plate. See Figure 2-1 and Figure 2-2 for sketches of the TS-CH steam generator complex and the region of observed cracking. See Figure 2-3 for a sketch of the assumed crack geometry.

The effect of residual stresses in the weld is not examined using this approach. It is possible to approximate the effects of residual stresses in the heat affected zone using other techniques. However, the assumption of the crack propagating through the thickness of the divider plate along the entire length of the divider plate simplifies the analysis because the onset of cracking has been assumed a priori. If it were necessary to determine the onset of cracking the residual stress in the welds would need to be included in the model.

The tubesheet is a complex structure. It is a thick perforated plate with several regions of solid material. The weld attachments between the tubesheet and the divider plate are also complex in geometry. See Figure 3-1 for a typical sketch of a recent finite element model of the lower steam generator region. See Figure 3-2 for a typical sketch of an older finite element model of the lower steam generator region. The tubesheet has been represented using one of several different methods in past finite element studies:

- An Axisymmetric Solid with Anisotropic Material Properties [6]
- A 3D Anisotropic Shell with Scaled Nominal Material Properties [7]
- A 3D Isotropic Solid with Scaled Nominal Material Properties [8]
- A 2D Isotropic Solid with Scaled Nominal Material Properties [9]
- A Three Dimensional Solid with Anisotropic Material Properties [10]

The previous analysis methods were used because of limits in computer power and software that made more detailed finite element techniques uneconomical or in some cases unfeasible. The previous studies also relied upon test data from a scaled steam generator model [6]. If drawings, specific dimensions, or manufacturing details could not be found in the archive appropriate values were taken from Reference 11. The previous analysis approaches developed different conservative estimates of the stresses and deformations in the TS-CH steam generator complex. Current advances in computing power and finite element analysis software make it possible to approach the problem more realistically and with a higher level of detail.

The presence of the perforations in the structure act to make the tubesheet behave differently from a solid homogeneous and isotropic material. It is important to note that in any of the methods above, the strict nominal properties of the tubesheet (without scaling or considered as anisotropic effects) are not used in the finite element model. Neglecting the change in radial and bending stiffness in the tubesheet due to the perforations may generate non-conservative results in any 3D structural analysis. See Appendix A for more details on the approximate material modeling approach.

The 2D dimensional finite element studies rely on a small section of the tubesheet, called the tubelane, which can be treated as a linear elastic homogenous isotropic solid because it is not perforated. However, this choice of material model for the two dimensional finite element study means that the stress results cannot be compared to the 3D dimensional studies. Only the vertical displacement results from the 2D finite element studies are used as input to the 3D finite element studies.

The tubesheet was modeled as a 3D solid with anisotropic material properties for this analysis using the method described by Slot [12]. See Appendix A for a description of how to calculate the appropriate anisotropic constants for the material model. The tubelane and annular material were modeled as solid, non-perforated, isotropic materials. See Table 3-1 for a list of the materials and material models used in the creation of the finite element model. The materials and material properties were taken from Reference 9. The values of the material properties for each material are listed in Table 3-2.

Two different values of tubesheet stiffness are used in the analysis. The first value for the vertical (E_{yy}) stiffness is derived from the nominal properties using the method described in Slot [12]. The second value is an increased stiffness to reflect the effect of the tube material within the tubesheet that can act to resist bending using a method described by Terakawa [13].

Assuming that the tubes have been sufficiently expanded into the tubesheet, and that the tube end weld is intact, the tubes can act to provide resistance to in-plane bending of the tubesheet due to a pressure drop from the primary to secondary side. This extra stiffness is conservatively derived by taking 50% of the tube wall thickness and linearly combining it with the stiffness of the nominal tubesheet material [13].

The equation for calculating the additional stiffness contribution due to the tube material within the tubesheet is:

$$E' = E_{Tube} n \frac{A_t}{A_c}$$

Where E_{Tube} is the elastic modulus of the tube material, n is the number of tubes within the tubesheet, A_t is half of the cross sectional area of a tube and A_c is the cross sectional area of a hypothetical solid cylinder which has an outer diameter equal to the outer limit circle.

It is important to note that this additional stiffness only applies to loading in the vertical direction and has no effect on displacements or stresses in the radial direction of the tubesheet. The modified tubesheet stiffness is then used to calculate the effective anisotropic constant for the E_{yy} value in the material model. All of the analysis results presented in this study include a comparison of the nominal and tube stiffness modified data.

Table 3-1
Table of Materials and Material Models in 2D and 3D FEM

Component	Material	Material Model
Channelhead	SA-216 WCC	Linear Elastic
Tubesheet (Solid)	SA-508 Class 2	Linear Elastic
Tubesheet (Perforated)	SA-508 Class 2	Linear Anisotropic Elastic
Stub Barrel	SA-533 Gr. A Class 1	Linear Elastic
Divider Plate	Alloy 600 TT	Linear Elastic
Stub Runner	Alloy 600 TT	Linear Elastic
Stub Runner/Divider Plate Weld	Alloy 600	Linear Elastic

Table 3-2
Table of Unmodified Model 44F and 51 Material Properties at 600 ºF

Tubesheet	SA-508 Class 2	
Young's Modulus	26.4 10^6	psi
Poisson's Ratio	0.3	
Stub Barrel	SA-533 Grade A Class 1	
Young's Modulus	26.4 10^6	psi
Poisson's Ratio	0.3	
Channel Head	SA-216 WCC	
Young's Modulus	26.7 10^6	psi
Poisson's Ratio	0.3	
Alloy 600 Data		
Young's Modulus	28.7 10^6	psi
Poisson's Ratio	0.3	

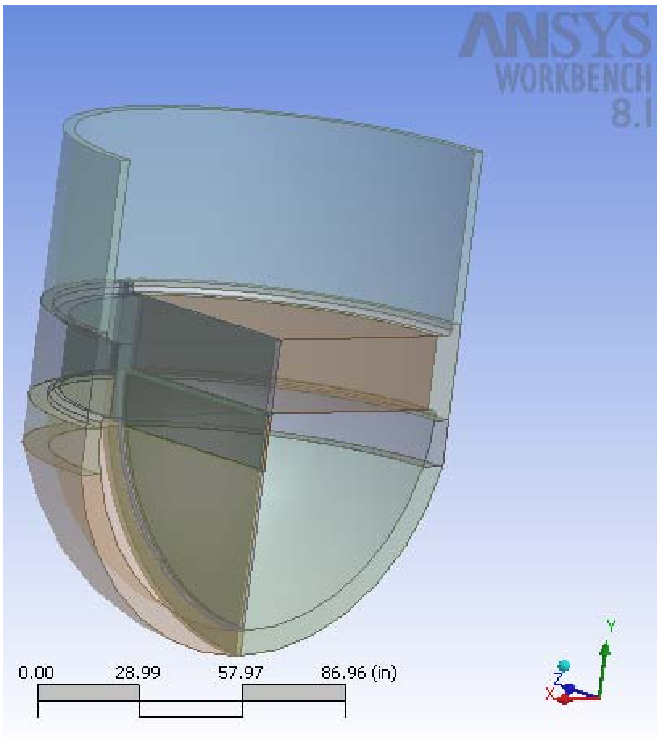

Figure 3-1
Typical Sketch of a Recent 3D Solid Model of the TS-CH Steam Generator Complex (Channelhead, Divider Plate, Tubesheet and Stub Barrel)

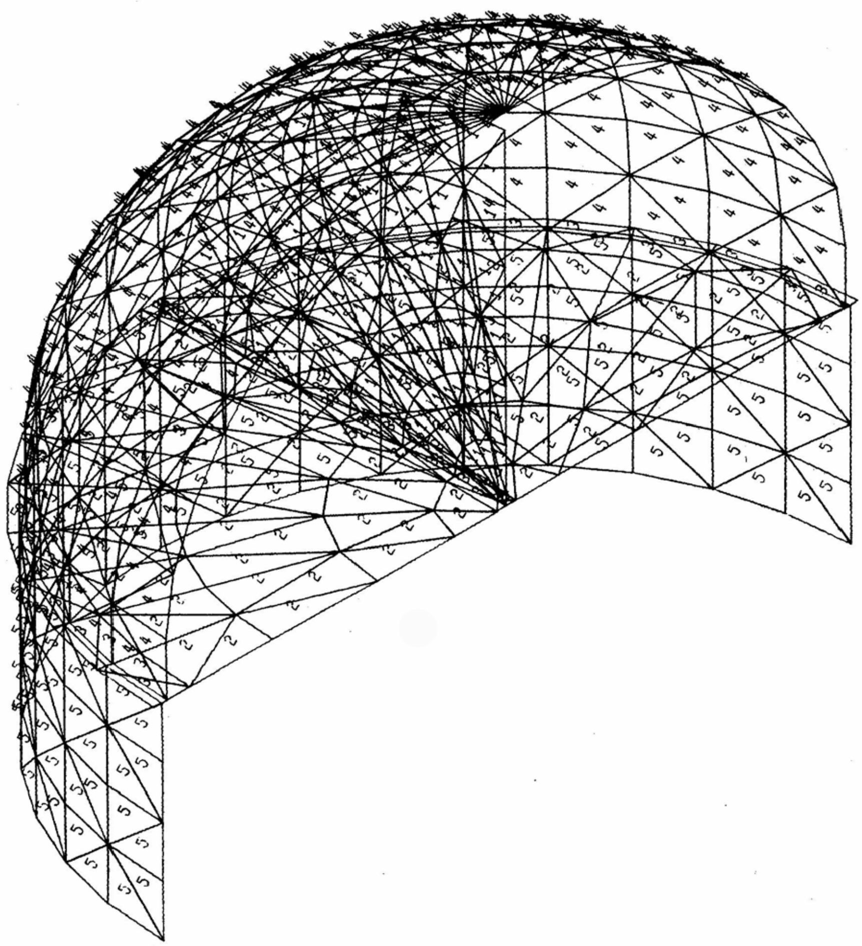

Figure 3-2
Typical Sketch of Previous Finite Element Solid Model of the TS-CH Steam Generator Complex (Channelhead, Divider Plate, Tubesheet and Stub Barrel) [7]

3.2 Preliminary Assessment of Limiting Steam Generator Model

There are 34 steam generator units in the Westinghouse fleet that may be susceptible to PWSCC in the stub runner to divider plate weld, however, several of the steam generators will be replaced in the near term. Table 3-3 lists the steam generator models and locations that are not expected to be replaced in the near term and are potentially susceptible to cracking in the stub runner to divider plate weld.

The limiting case steam generator will be the model SG that has a tubesheet with the largest potential vertical and radial displacements due to operating conditions. The maximum radial displacements are estimated from previous alternate repair criteria analysis [14]. The maximum vertical displacements are estimated via a simple circular plate deflection analysis considering the tubesheet as a solid plate [15]. The bending constant, *D*, must be modified to account for the perforated nature of the tubesheet. The equation for the modified bending constant is:

$$D_{Eff} = \frac{t^3}{12 \big/ 1 - \nu_{TS}} \left[E_{TS} \frac{A_{TS}}{A_{TOT}} + E_T \frac{A_T}{A_{TOT}} \right]$$

Where:

t = Tubesheet thickness = 21.03 in

ν_{TS} = Tubesheet Poisson's Ratio = 0.3

E_{TS} = Tubesheet Young's modulus, psi

E_T = Tube Young's modulus, psi

A_{TS} = Area of the solid portion of the tubesheet, in^2

A_T = Area of ½ of the tube material within the tubesheet

A_{TOT} = Total area of the tubesheet

The values of ν_{TS}, E_{TS}, E_T, A_{TS}, A_T and A_{TOT} will change depending on which model of steam generator is being considered. Note that A_T is equal to one-half of the annular area of the tube material within the tubesheet. Reducing the effective area of the tubes within the tubesheet is a conservative measure outlined in Reference 13. A_{TS} is equal to the solid portion of the tubesheet, excluding the area of the perforations, and A_{TOT} is the total area of the tubesheet calculated as if the entire tubesheet were a solid cylinder. The equations for the deflection of a pressure loaded plate are given in Reference 15 as cases 10a and 10b (maximum deflection of a simply supported a circular plate and a circular plate with fixed edges) for an applied pressure load of 1000 psi.

The dimensions, materials and specifications for the components in the finite element models were taken from the drawings below. In the event that the relevant dimensions were not found on the master drawings, assembly drawings, or as-built drawings, the general assembly and arrangement drawings referred to in the master drawing for the steam generator model was used to find the relevant drawing. In the event that the specific dimension or detail could not be found in the drawing archive, the data was taken from Reference 11. The actual material properties for the component material were taken from the ASME Code [16] once the appropriate material specification for a component was identified.

Table 3-4 lists the drawings that were used to find general dimensions and other drawings for details on the specific steam generator models. Table 3-5 lists the tube material classifications. Table 3-6 lists the drawings that were specifically used as references for the Model 51 steam generator. Table 3-7 lists the drawings that were specifically used as references for the Model 44F and F steam generators. Table 3-8 lists the drawings that were specifically used as references for the Model 51F and 54F steam generators.

Figure 3-3 and Figure 3-4 show the radial displacements of the tubesheet and channelhead near the centerline of the tubesheet. The data for Figure 3-3 and Figure 3-4 were taken from analyses in support Reference 17 for the Model F data, Reference 18 for the Model D5 and D3 data, Reference 14 for the Model 51 data and Reference 19 for the Model 44F data.

If the channelhead and tubesheet are more flexible (i.e. similar to a pinned connection) less of the radial deformation will then be forced into the potentially cracked divider plate and stub runner connection. The radial displacements of the channelhead and tubesheet shown in Figure 3-3 and Figure 3-4 indicate that the stiffest tubesheet and channelhead connections at the centerline of the tubesheet are present in the Model 51 and Model 44F steam generator models.

The presence of a crack will have a greater effect in a thinner divider plate cross section. Table 3-9 lists the minimum material conditions for the divider plates in each of the steam generator models. The Model 51 has the smallest divider plate cross section using minimum material conditions. The Model 44F has the second smallest divider plate cross section using minimum material conditions.

Table 3-10 summarizes the estimated maximum vertical displacements of the steam generator models. The vertical displacements were estimated using the data in Table 3-11 and the equations in Reference 15 (Page 488, Equations 10a and 10b, with $r_0 = 0$) with a modified bending constant as described in this section. The Model 51 has the largest predicted vertical TS displacements.

The vertical and radial TS displacements calculated from the list of steam generator models show that the Model 44F and Model 51 steam generators are likely candidates for the limiting case. The Model 51 and Model 44F steam generators are also the steam generators with the thinnest divider plates as specified in the original design specifications and drawings. Therefore, the Model 44F and Model 51 steam generators required further analysis using finite element techniques to determine which model was the limiting case. The unmodified material properties and values used in the 2D and 3D finite element studies are listed in Table 3-2 and Appendix A. In summary, the Model 44F and Model 51 are considered the potential structurally limiting cases because:

- The Model 51 has the thinnest as-designed divider plate cross-section using minimum material conditions. The Model 44F has the second thinnest cross-section.
- The Model 51 has the largest predicted vertical displacements at the centerline of the tubesheet.
- The Model 44F has the stiffest connection between the tubesheet and divider plate, which is likely to transmit large stresses and displacements to a cracked section.

Table 3-3
List of Potentially Limiting Steam Generators and Models with Stub Runner to Divider Plate Welds and Alloy 600/182 Weld Material[3]

Plant Name	Model	Alpha
Watts Bar Unit 1	D3	WAT
Byron Unit 2	D5	CBE
Braidwood Unit 2	D5	CDE
Catawba Unit 2	D5	DDP
Commanche Peak Unit 2	D5	TCX
Salem Unit 1	F	PSE
Kori 2	F	KPR
Kori 3	F	KGA
Kori 4	F	KHB
Maanshan 1	F	TWP
Maanshan 2	F	TXP
Millstone 3	F	NEU
Napot Point 1	F	PLA
Seabrook 1	F	FLA
Seabrook 2	F	NCH
Sizewell B	F	SWB
Vandellos Unit 2	F	EAS
Vogtle Unit 1	F	GAE
Vogtle Unit 2	F	GBE
Wolf Creek Unit 2	F	SAP
Yeonggwang Unit 1	F	KSR
Yeonggwang Unit 2	F	KTR
Point Beach Unit 1	44F	WEP
H.B. Robinson Unit 2	44F	CPL
Turkey Point Unit 3	44F	FPL
Turkey Point Unit 4	44F	FLA
Indian Point Unit 2	44F	IPP
Salem Unit 2	51	PNJ
Sequoyah Unit 2	51	TEN
Beaver Valley Unit 2	51M	DMW
Surry Unit 1	51F	VPA
Surry Unit 2	51F	VIR
D.C. Cook Unit 2	54F	AMP

[3] : Table 3.1-1 is not intended to be a complete listing of all plants that may be susceptible to the divider plate cracking phenomena. It is merely intended to list the potential steam generator models and operating conditions that were considered in this report.

Table 3-4
List of Drawings used to Find General Dimensions for FE Models

Plant Name	Model	Alpha	Master Drawing	As-Built Drawing
Salem Unit 2	51	PNJ	1097J56	6521D25
Beaver Valley Unit 2	51M	DMW	1104J89	1101J46
Salem Unit 1	F	PSE	717J361	1098J17
Seabrook 1	F	NAH	1513E33	1512E31
Turkey Point Unit 4	44F	FLA	675J676	4432D73
Surry Unit 1	51F	VPA	718J537	4484D53
Watts Bar Unit 1	D3	WAT	1101J22	1102J54
Byron Unit 2	D5	CBE	1103J99	1512E57
Braidwood Unit 2	D5	CDE	1101J40	1183J90

Table 3-5
Summary of Tube Materials in SG Models

SG Model	Tube Material	TS Material
D3	I600	A-508 Class 2
D5	I600TT	A-508 Class 2a
F	I600TT	A-508 Class 2a
51F	I600TT	A-508 Class 2a
54F	I600TT	SA-508 Class 3
44F	I600TT	A-508 Class 2a
51	I600	A-508 Class 2
51M	I600	A-508 Class 2

Table 3-6
Model 51 Drawing Data

Outline Drawing	717J360 Rev. 18
Lower Shell	4432D78
Assembly Tube Plate	1098J29A01
Channel Head	717J362A02
Tube Support Plate	717J368A01/2

Table 3-7
Model 44F and F Drawing Data

Outline Drawing	613E19 Rev. 2
Lower Shell Assembly	6135E84G01, Rev. 4
Tube Plate	6137E65 6137E78
Channel Head	6135E81G01, Rev. 4

Table 3-8
Model 51F and 54F Drawing Data

Outline Drawing	1105J19
Tube Plate	Reference 11
Channelhead	1104J78A01
Tube Support Plate	1104J76

Table 3-9
List of Minimum Material Divider Plate Thickness

SG Model (#)	DP Thickness (in)
51	1.19
44F	1.26
51F	1.90
51M	1.90
54F	1.90
D3	1.90
D5	1.90
F	1.90

Table 3-10
Summary of Calculated Vertical Displacements

	Deff	Yc	
Model SG	lb-in	Simple, in	Fixed, in
51	12503677837	0.106	0.026
44F	13947197604	0.051	0.012
51F	12503677837	0.067	0.016
D3	12503677837	0.070	0.017
D5	12503677837	0.070	0.017
F	12503677837	0.067	0.016

Table 3-11
List of Tube and Tubesheet Properties

		D5	D3	44F	F	51F	51	51M	54F
Tubesheet Thickness	in	21.03	21.03	21.81	21.03	21.03	21.03	21.03	21.03
Tubesheet Diameter	in	121.57	121.57	115.56	120.50	120.45	135.00	135.88	135.94
Number of Tubes	#	4674	4674	3214	5626	3342	3388	3376	3592
Tube Wall Thickness	in	0.043	0.043	0.050	0.041	0.050	0.050	0.050	0.050
E_{TS}	psi	26700000	26700000	26700000	26700000	26700000	26700000	26700000	26700000
E_T	psi	28500000	28500000	28500000	28500000	28500000	28500000	28500000	28500000
Tube Diameter	in	0.75	0.75	0.875	0.6875	0.875	0.875	0.875	0.875
A_{TS}	in^2	11607.91	11607.91	10487.43	11403.23	11395.09	57255.53	58004.4	58055.64
A_T	in^2	446.40	446.40	416.50	469.03	433.09	439.05	437.50	465.49
Tube Area Ratio	in^2/in^2	0.038	0.038	0.040	0.041	0.038	0.008	0.008	0.008
TS Area Ratio	in^2/in^2	0.822	0.822	0.816	0.817	0.824	0.964	0.965	0.963
Effective Bending Constant	lb-in	1.25E+10	1.25E+10	1.39E+10	1.25E+10	1.25E+10	1.41E+10	1.41E+10	1.41E+10

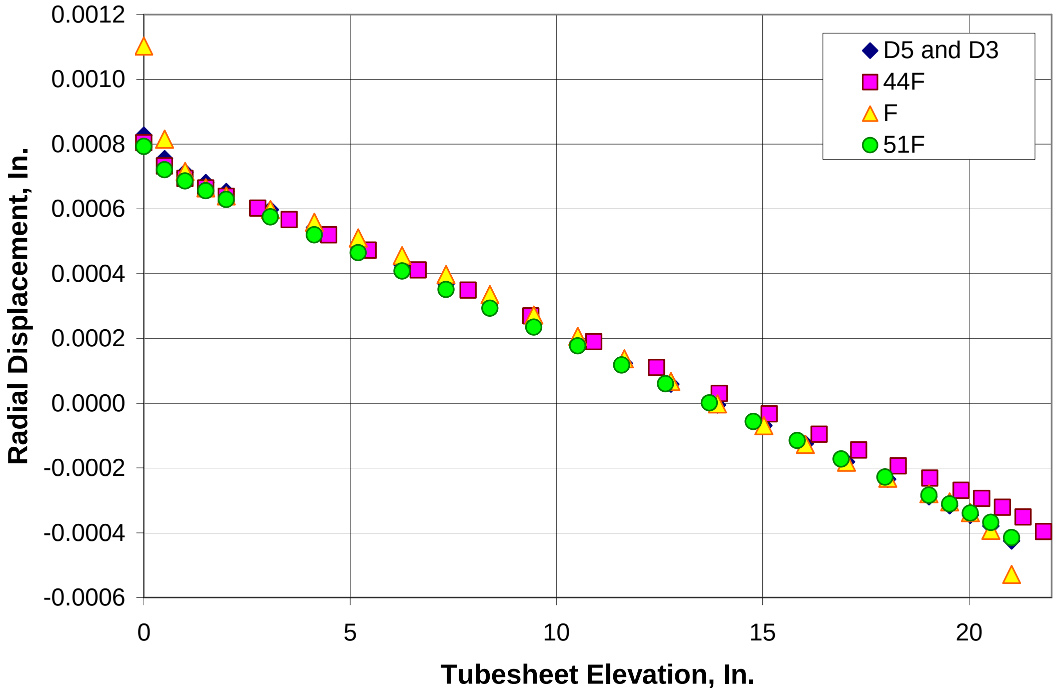

Figure 3-3
Radial Channelhead Displacement near the Tubesheet Centerline

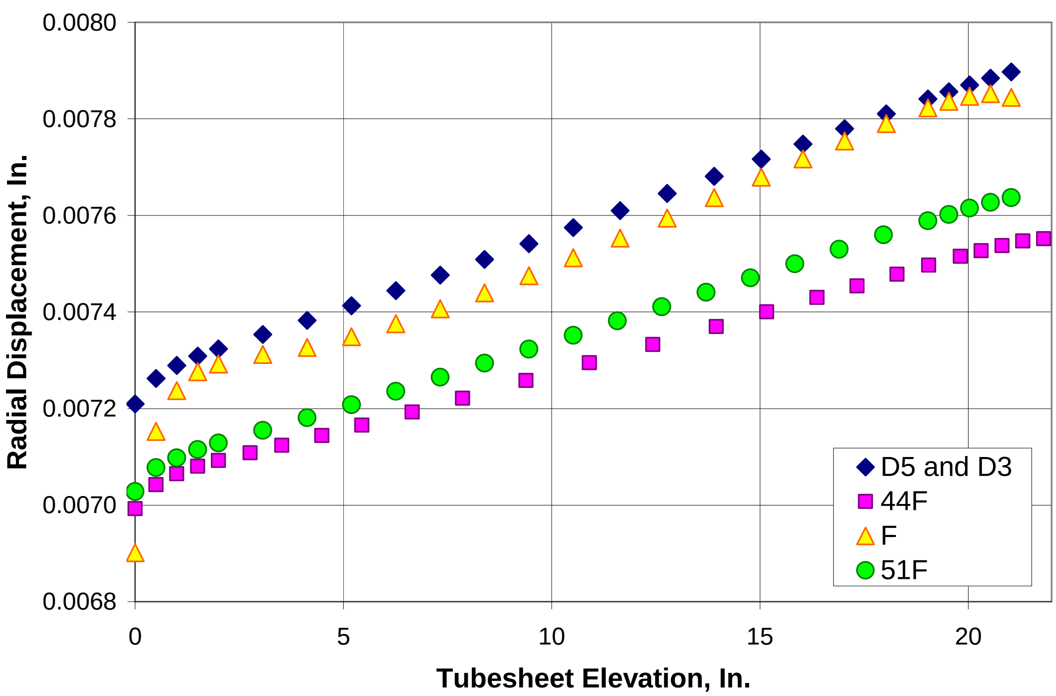

Figure 3-4
Radial Tubesheet Displacement near the Centerline of the Tubesheet

3.3 2D Finite Element Model Studies

The purpose of the 2D model studies is to:

1. Determine whether the Model 44F or Model 51 Steam Generator is the limiting case for a crack in the load path of the divider plate, divider plate to stub runner weld, stub runner and tubesheet.
2. Ascertain the effect that a propagating edge crack in the load path of the divider plate/stub runner/tubesheet connection will have on the vertical displacements of the tubesheet.

The results from the 2D finite element studies will be applied to a 3D finite element study of the TS-CH steam generator complex. An important result from the 3D finite element study will be a new limiting value for the divider plate factor to be used in future analyses. Historically, the divider plate factor was defined as the ratio of the maximum vertical displacements of the tubesheet centerline with the divider plate present to the maximum vertical tubesheet displacements without the divider plate providing any support.

A divider plate factor of 0.76 has typically been used in past analyses of steam generators when the deflection of the tubesheet was considered an important input parameter [9]. The DP of 0.76 has been used in the analysis of Model D, Model F, Model 51, Model 54F, Model 51F and Model 44F steam generators [17]. The DP factor was applied such that

$$DP = \frac{u_{\text{present}}}{u_{\text{weak plate}}} = \frac{u_{\text{uncracked}}}{u_{\text{cracked}}}$$

This gives a value of 1.00 in the case where the divider plate is assumed to not be present, or otherwise not capable of restricting the vertical deflection of the tubesheet.

The same relationship can be applied in the case of a crack propagating through the divider plate thickness, although for small cracks (a<0.50 in), the ratio will yield a value of nearly 1.00, because the difference in stiffness between the cracked and uncracked conditions will be small.

Note that in cases where the geometry or materials of the tubesheet, channel head or divider plate were significantly different from a similar analysis, the results were scaled to approximate the relevant situation. This is the case for most of the older analyses [6]. For instance, a detailed study of the divider plate and tubesheet displacements was performed for the Model D steam generator, which resulted in the DP factor of 0.76. These results were then applied in various forms to similar analyses of the F, Model 44F and Model 51 steam generators.

The divider plate factor must take into account 3D effects on stress and displacement of the tubesheet and divider plate. The result of the 2D finite element studies will be a vertical displacement ratio that will scale the stiffness of the stub runner material in the finite element model. It is time consuming to model a small crack in a large 3D structure such as the divider plate. This situation is ideal for a global/local model approach, in which a small scale and refined model is used to provide input to a global or large scale model that has a coarser mesh that accommodates the larger domain.

The 2D studies were performed using a section of the divider plate, stub runner, weld material and tubelane with a unit negative pressure load applied to the top face of the tubelane. All of the 2D finite element models applied static loads and conditions at an assumed worst case steady state temperature. See Figure 3-5 and Figure 3-6 for a sketch of the 2D finite element model and the applied boundary conditions.

The results of these studies were then applied to a half symmetry model of the TS-CH steam generator complex (channel head, divider plate, tubesheet and stub barrel). The ratio of the vertical displacement of the centerline of the tubesheet in the 2D unit load studies with an undamaged divider plate to a case with a crack in the divider plate load path will define a vertical displacement ratio (VDR). The VDR is calculated using the equation:

$$VDR = \frac{U_{uncracked}}{U_{\%cracked}}$$

Where $U_{uncracked}$ refers to the vertical displacement of the centerline of the tubesheet tubelane in the 2D studies under a unit pressure drop across the tubesheet and $U_{\%cracked}$ refers to the vertical displacement of the centerline of the tubesheet tubelane in the 2D studies for a specific crack depth. The VDR is used to scale the stiffness of the divider plate/stub runner/tubesheet connection for use in the 3D models. For example, if the 2D divider plate with a crack that penetrates 15% through the thickness is 26% less stiff than the uncracked divider plate the resulting 3D model for a divider plate with a 15% deep crack will reduce the stiffness of the stub runner region of the divider plate by 26%. The VDR is not the same as the DP factor, which is defined using 3D finite element results.

The two dimensional models used in the VDR study are based on minimum material conditions at the highest nominal operating temperature the TS-CH complex of the steam generator will see during design, upset or faulted conditions (600 ºF). There are no applied thermal boundary conditions in the finite element models. See Table 3-6 and Table 3-7 for a list of the drawings used to create the 2D finite element representations of the Model 51 and Model 44F steam generators. See Table 3-2 for a list of the unmodified material properties used in the analysis. See Appendix A for a discussion on the modified material properties.

A 1000 psi pressure load was used in the 2D modeling studies.[4] The pressure load was applied on the top surface of the models as shown in Figure 3-6.Two different kinds of steam generators were analyzed using the 2D models: a Model 51 and a Model 44F. Both models were chosen because of the high ligament efficiency of the tubesheet, thin divider plate cross sections and the potential for large vertical tubesheet displacements if the divider plate became unable to restrict the motion of the tubesheet.

[4] : A mesh convergence study using the maximum axial (σ_{yy}) far field stress was performed on both the 2D and 3D model meshes.

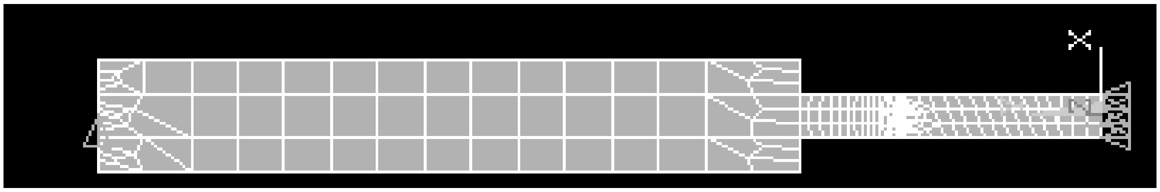

Figure 3-5
Plot of 2D Boundary Conditions. Showing a pinned central node at top edge (UX=0) and pinned nodes at the lower edge (UY=0).

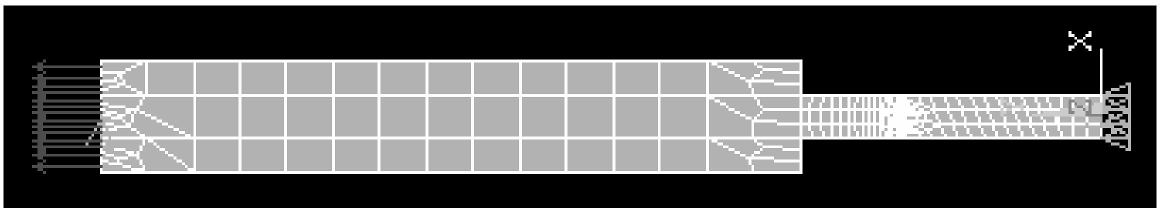

Figure 3-6
Plot of Applied Pressure Load (shown as arrows) on typical 2D Mesh.

3.4 3D Finite Element Model Studies

A parametric three dimensional half symmetry model of the Model 51 TS-CH steam generator complex was constructed using ANSYS Workbench [21] based on the results of the 2D finite element studies. The results of the 2D finite element studies, discussed in section 3.2, showed that for the minimum material conditions the Model 51 steam generator is the limiting case steam generator with respect to cracking in the divider plate. The minimum material conditions included loss of material on the secondary side due to corrosion and maximum machining tolerances.

The exception to the minimum material conditions was the tubesheet, in which case material was removed from the secondary side to represent corrosion loss but not due to machining tolerances. There are two reasons for not reducing the thickness of the tubesheet below nominal dimensions:

1. The tubesheet is an important primary structural element in the problem so variations in its thickness will have significant effects on other structures.
2. Decreasing the thickness of the tubesheet will increase the magnitude of the calculated displacements in the divider plate above an appropriately conservative level.

The dimensions of the 3D model representation of the Model 51 steam generator were taken from the drawings listed in Table 3-6. However, there are two differences between the details in the drawings of the Model 51 and the 3D finite element representation.

- The finite element model does not have a support ring.
- The divider plate in the finite element model is 2.00 inches thick.

The details listed above were used in the limiting geometry model because the goal of the 3D finite element analysis was to provide results for a generally applicable study. While the results of the preliminary analysis and the 2D finite element studies indicated that the Model 51 steam generator was the limiting steam generator, the Model 51 steam generator does not share dimensional and operational similarities with many other steam generator models. Therefore, the 3D finite element model was created to represent a more generically applicable case that was based on the physical parameters of the Model 51 steam generator. The modified stiffness values of the stub runner from the 2D Model 51 studies are still used in the 3D analysis with the thicker divider plate because the VDR ratio represents a percent decrease in stiffness which is valid regardless of the divider plate thickness.

The analysis described in this report is different from the prior divider plate and TS-CH steam generator complex analysis models. The specific differences between the current approach and the previous approaches are:

1. 3D solid elements are used instead of shell or axisymmetric elements. Specifically type 186 (20 node structural bricks) and type 187 (10 node structural tetrahedral) elements.
2. The tubelane is included and modeled as a solid, isotropic structure.
3. The channelhead to divider plate weld is included.
4. The divider plate connection to the stub runner and tubesheet is included.

The level of modeling detail was increased in the current analysis in order to quantify the effects of the assumed conservatisms in previous analyses. See Figure 3-7, Figure 3-8 and Figure 3-9 for pictures of the 3D finite element mesh. Figure 3-10 shows the stub runner region of the steam generator model. The stub runner region identified in the finite element model is larger than the stub runner region identified in the Model 51 drawings in order to represent the region noted as having cracks in the field examinations [22, 23]. The elements in the stub runner region were suppressed in the case of a fully cracked divider plate. Suppressing the stub runner elements made the analysis more efficient by not creating a potentially non-linear contact problem. See Figure 3-11 for an example of the solid model with the stub runner elements removed.

The drawings and material properties for the Model 51 steam generator are shown in Sections 3.1 and 3.2. Figure 3-12 and Figure 3-13 show that there are several boundary conditions applied to the 3D finite element model. There is a symmetry condition on the cut-face for the half-symmetry plane of the model. There is an applied end cap pressure load on the top surface of the stub barrel. There is a fully fixed support in the rear that represents the bearing pad of the lower steam generator support. There are also applied primary pressures on the cold and hot leg compartments of the channelhead and a secondary side pressure applied to the secondary surface of the tubesheet and stub barrel.

The stresses and displacements in the finite element model were evaluated for three different operating conditions: normal operation (NOP), the worst case upset condition and the worst case accident condition. The data for the applied Model 51 transient conditions is taken from References 6, 7 and 9. The worst case upset condition for the Model 51 steam generator is the loss of load (LOL) condition because of the maximum applied secondary and primary pressures combined with the pressure drop across the divider plate. The worst case accident condition is the main feedline break (FLB) condition because of the maximum pressure drop across the tubesheet. Table 3-12 lists the magnitude of the applied pressures for each analysis condition. A 10% plugging level was assumed in calculating the pressure loads. During a transient condition, such as SLB or LOL, the time point with the highest pressures, or the worst pressure drop across the divider plate and tubesheet, was assumed to be the steady state condition.

The 3D finite element model was meshed using higher order bonded surface contact elements to allow region and part based meshing features (ANSYS element types 170 and 174). The ANSYS Workbench Design Modeler database file and the batch run input files for the 3D finite element analysis are attached to this report in EDMS.

Table 3-12
List of Applied Pressures for the Model 51 Steam Generator Model

Category	Condition	Div. Plate ΔP (psi)	Pri. Press. (psi)	Sec. Press. (psi)	End Cap Press. (psi)
Design	Normal Operating	50	2250	735	8473
Upset	Loss of Load	45	2531	695	8012
Faulted	Feed Line Break	0	2650	0	0

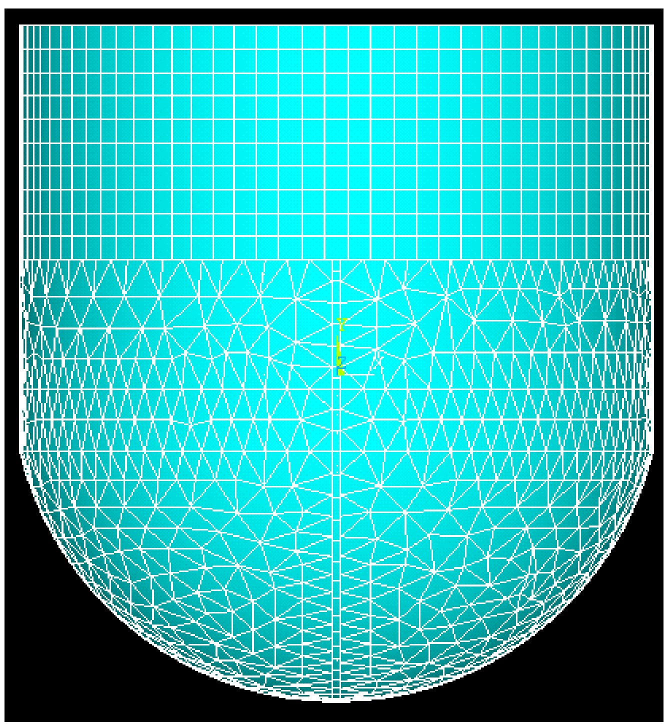

Figure 3-7
Screen Capture of 3D Finite Element Mesh, Rear View

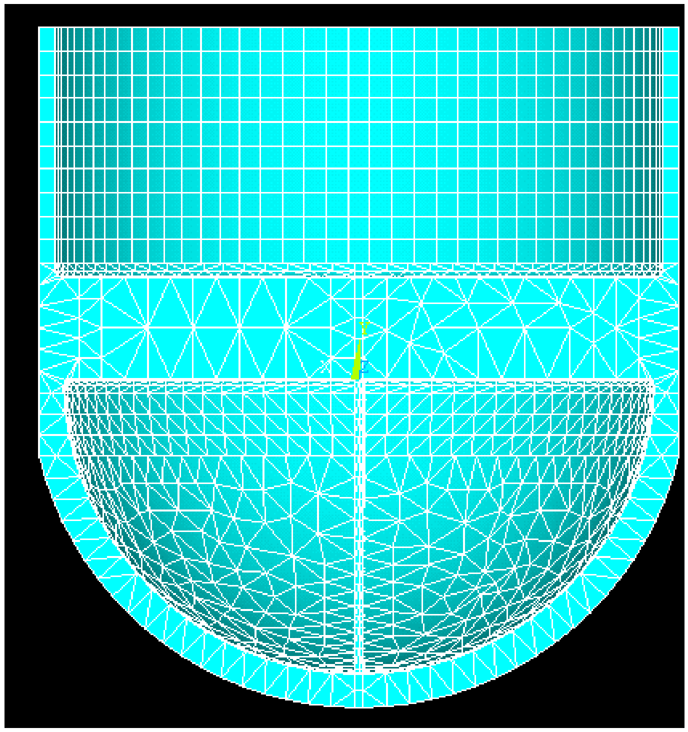

Figure 3-8
Screen Capture of 3D Finite Element Mesh, Front View

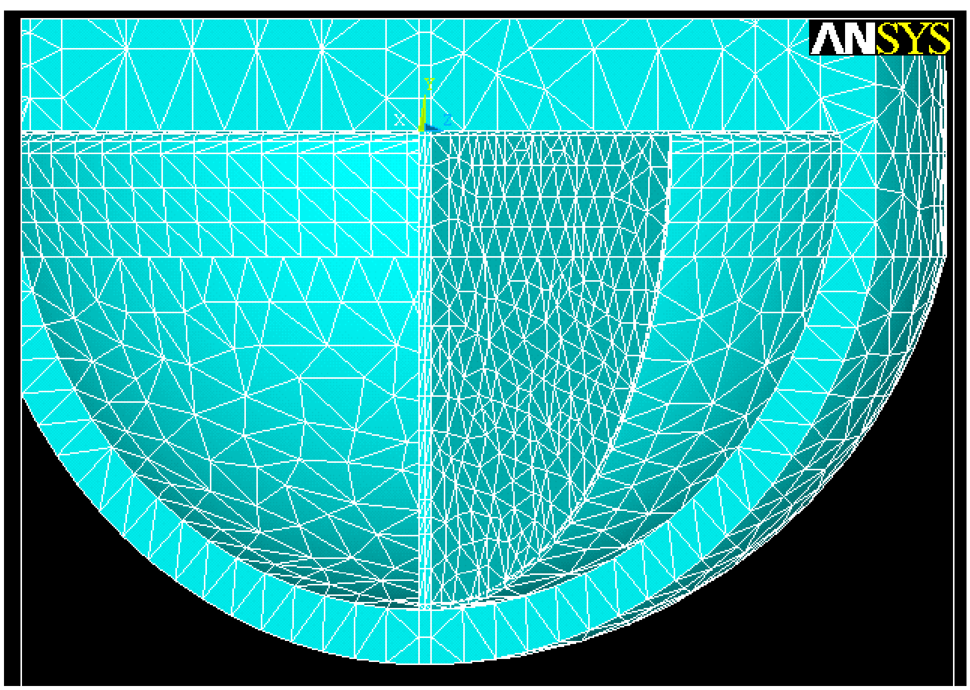

Figure 3-9
Screen Capture of 3D Finite Element Mesh; Close Up of Divider Plate Region (note that there are four elements through the thickness of the divider plate)

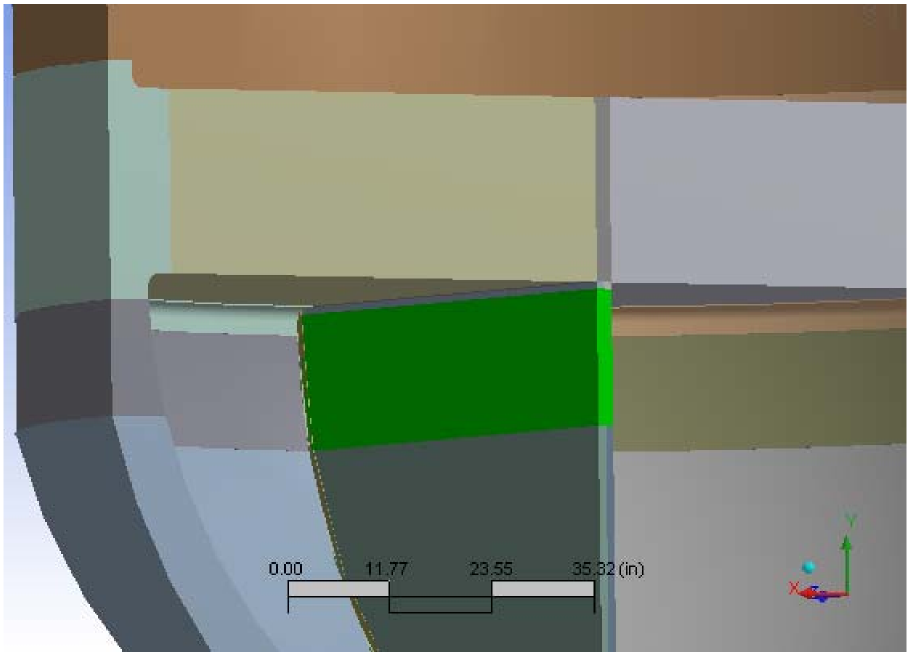

Figure 3-10
Plot of Model 51 Finite Element Solid Model Representation with Stub Runner Region Highlighted

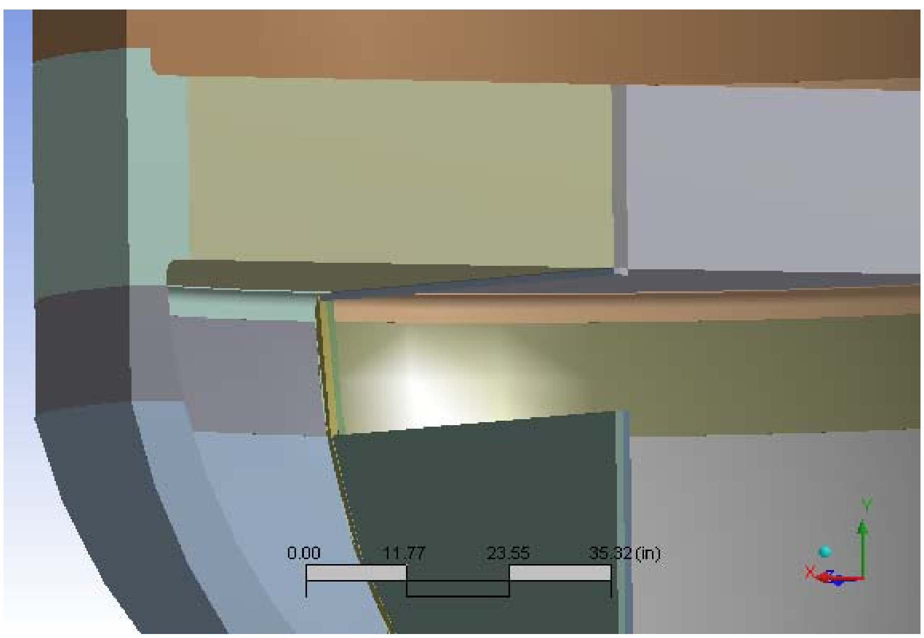

Figure 3-11
Plot of Model 51 Finite Element Solid Model Representation with Stub Runner Region Suppressed

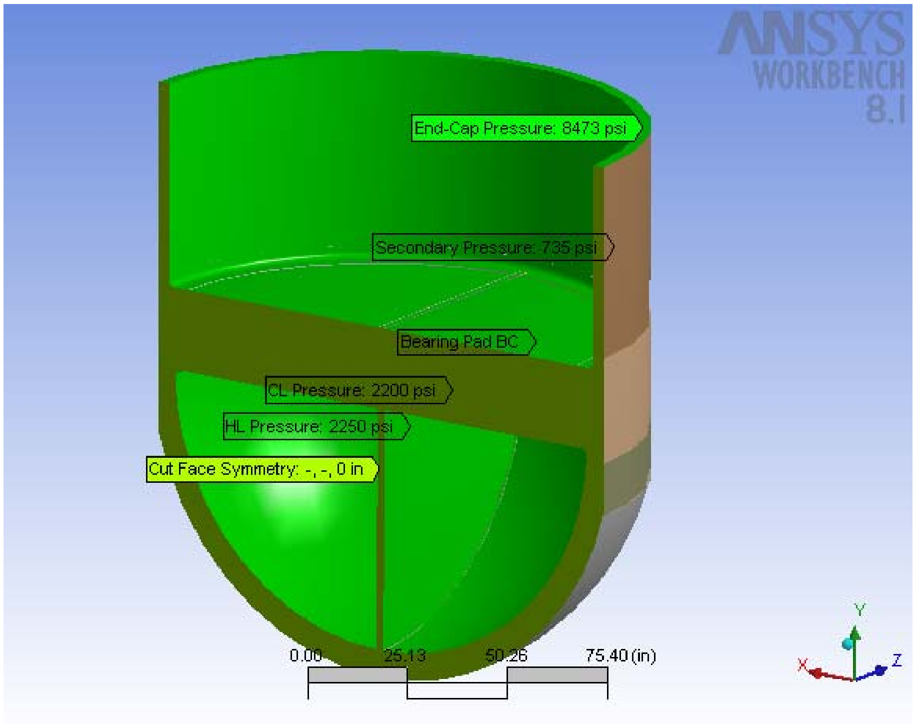

Figure 3-12
3D Finite Element Model NOP Boundary Conditions, Front View

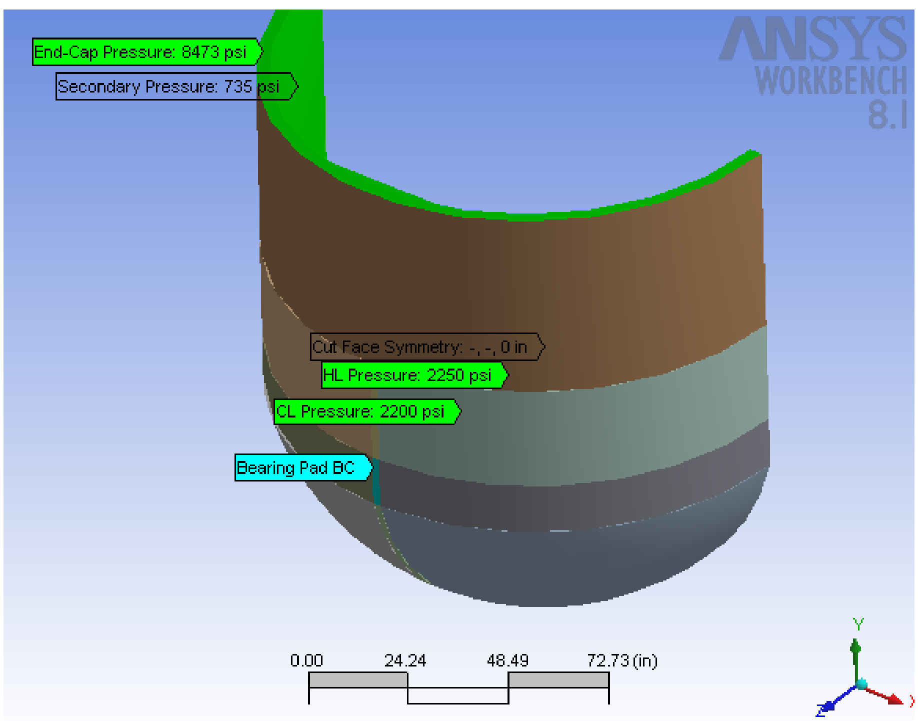

Figure 3-13
3D Finite Element NOP Boundary Conditions, Rear View

3.5 2D Finite Element Results

The converged vertical displacements of the finite element models at the top surface of the tubelane were used to calculate the VDR for the Model 44F and Model 51 steam generators. See Figure 3-14 through Figure 3-23 for plots of the deformed and undeformed model meshes at various crack lengths. See Figure 3-24 for a plot of the VDR as a function of the crack size in the divider plate. The displacement results shown in the figures are focused on the cracked region and have been magnified 100 times.

The results in Figure 3-24 show that for a crack of the same length, in two different models with identical meshes, the Model 51 structure has larger vertical displacements than the Model 44F for every value of a except at a =1.14 in. However, it is likely that a crack would be detected before it could propagate through 90% or more of the divider plate thickness. Therefore, the Model 51 steam generators are the worst case for a divider plate crack because the Model 51 finite element results predict a larger vertical displacement for the constant applied load due to a crack growing in the load path at cracks smaller than 90% of divider plate. This is a reasonable result considering that some of the foreign nuclear plants experiencing this kind of degradation also have Model 51 steam generators. Table 3-13 below summarizes the VDR results for the Model 44F and Model 51 steam generators. The values for the Model 51 steam generator will be used to scale the Young's Modulus of the stub runner in the 3D finite element study to represent the effect that increasing crack size has on stiffness. See section 3.2 for discussion of how the VDR is used to scale the stiffness of the 3D finite element model.

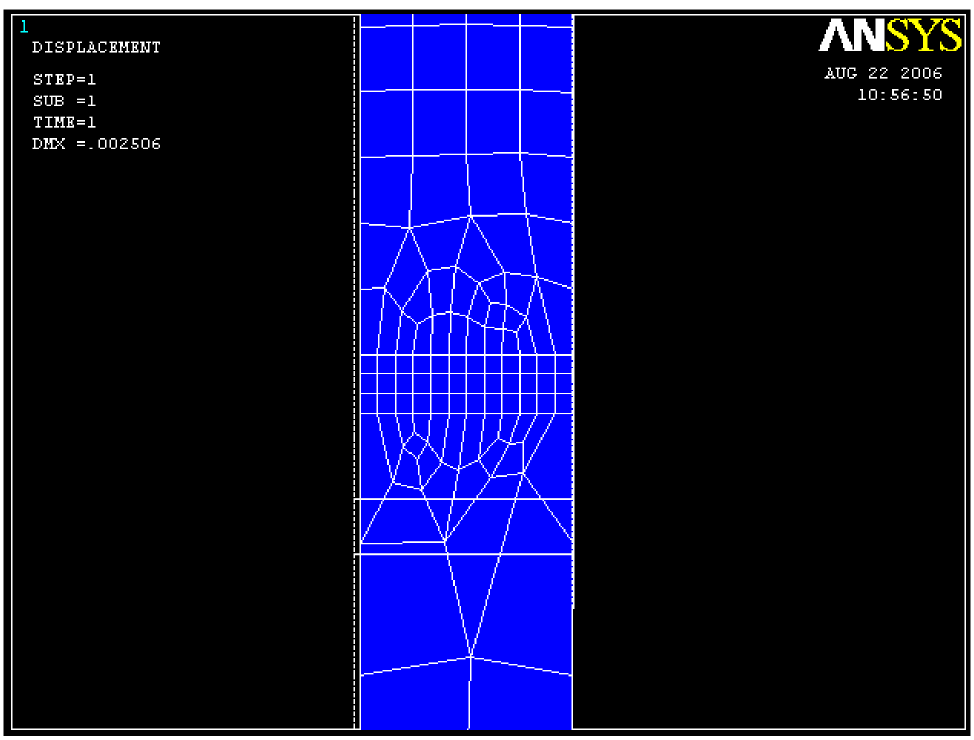

Figure 3-14
Uncracked Model 44F Displacement

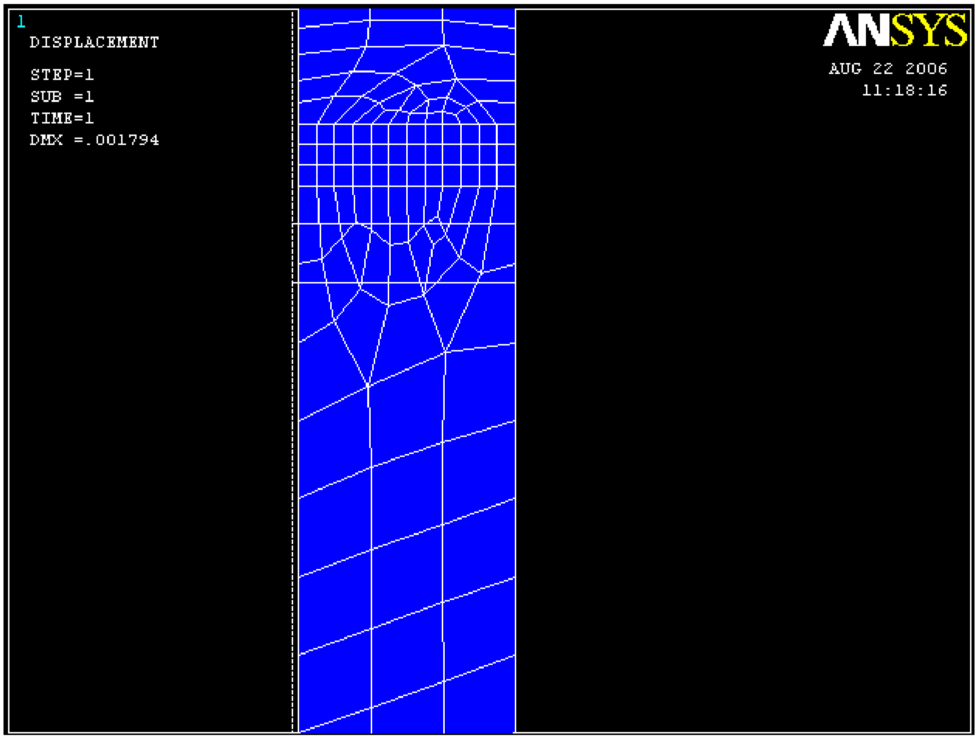

Figure 3-15
Uncracked Model 51 Displacement

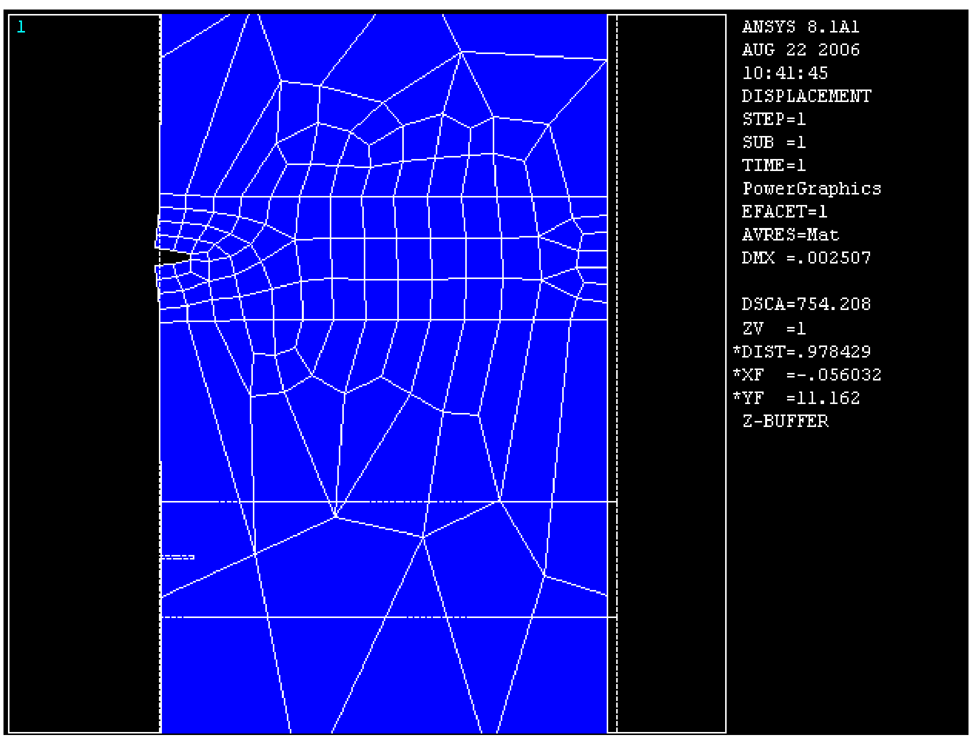

Figure 3-16
8% Cracked Model 44F Displacement.

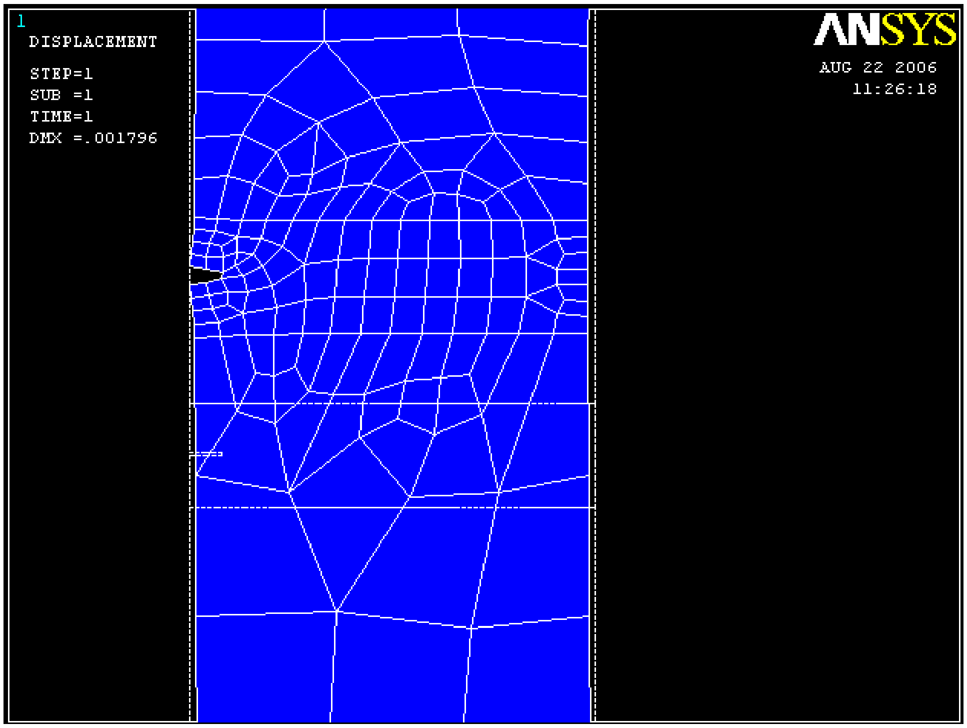

Figure 3-17
8% Cracked Model 51 Displacement

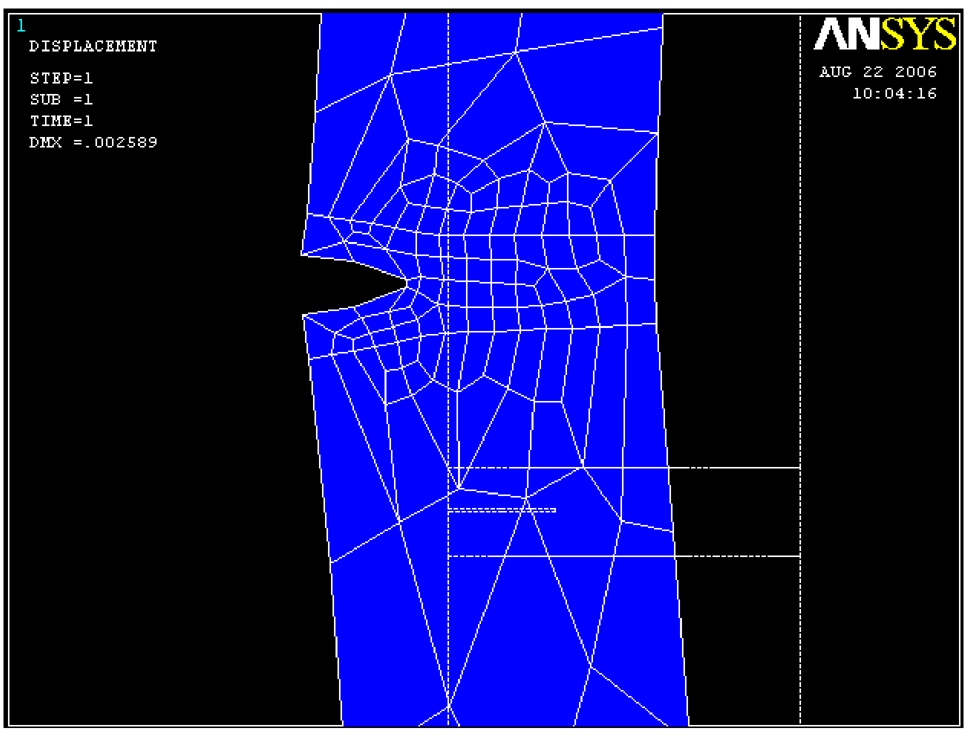

Figure 3-18
32% Cracked Model 44F Displacement.

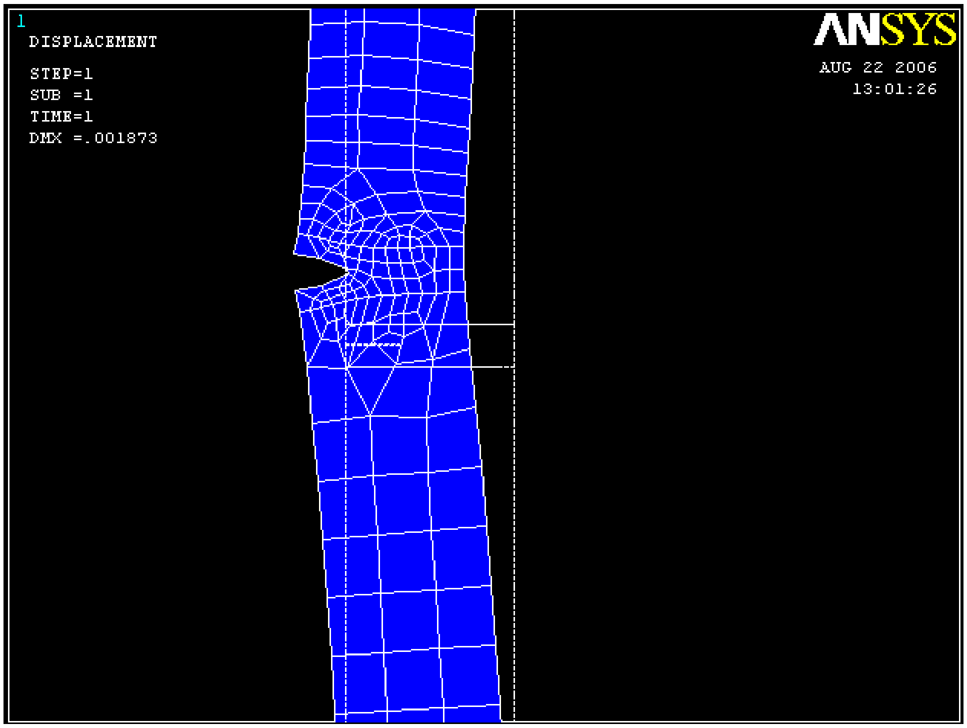

Figure 3-19
32% Cracked Model 51 Displacement.

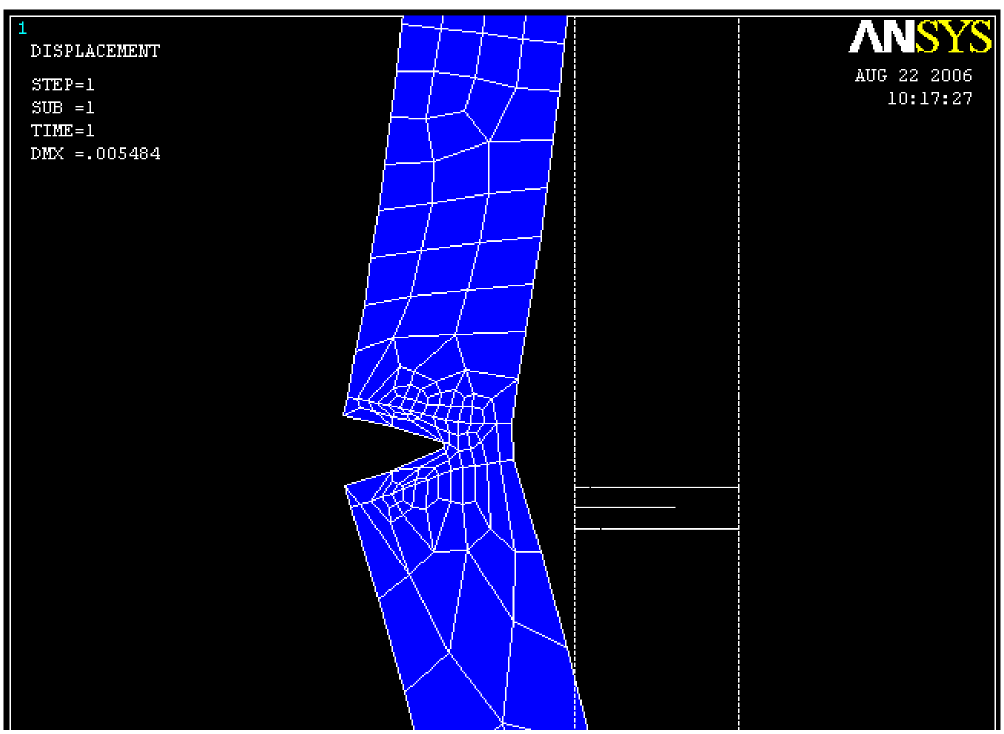

Figure 3-20
64% Cracked Model 44F Displacement.

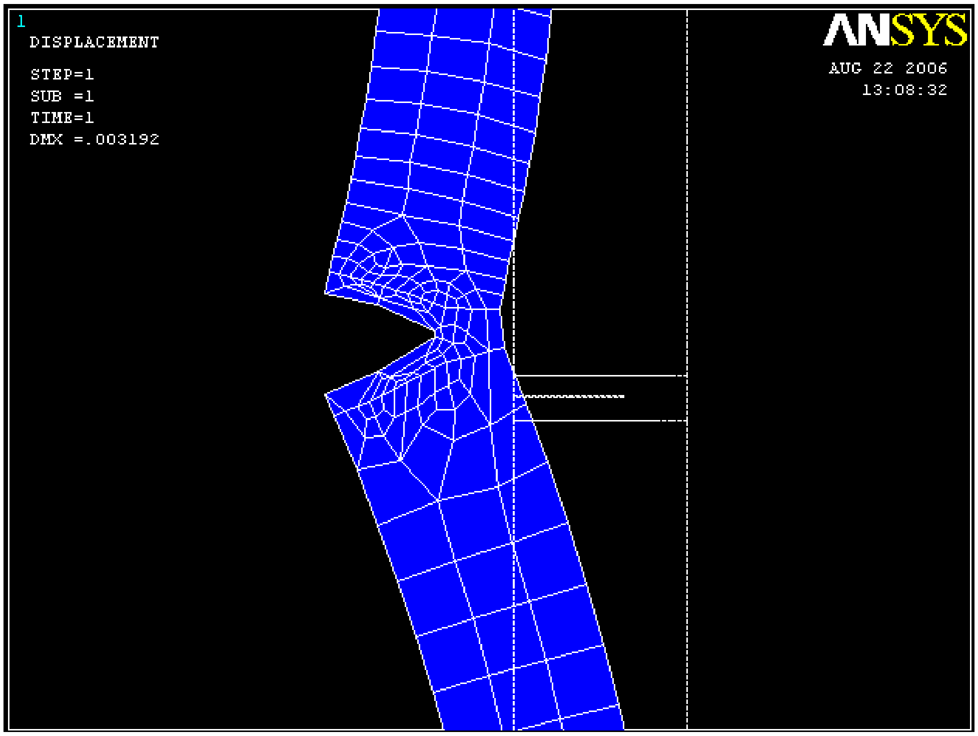

Figure 3-21
64% Cracked Model 51 Displacement.

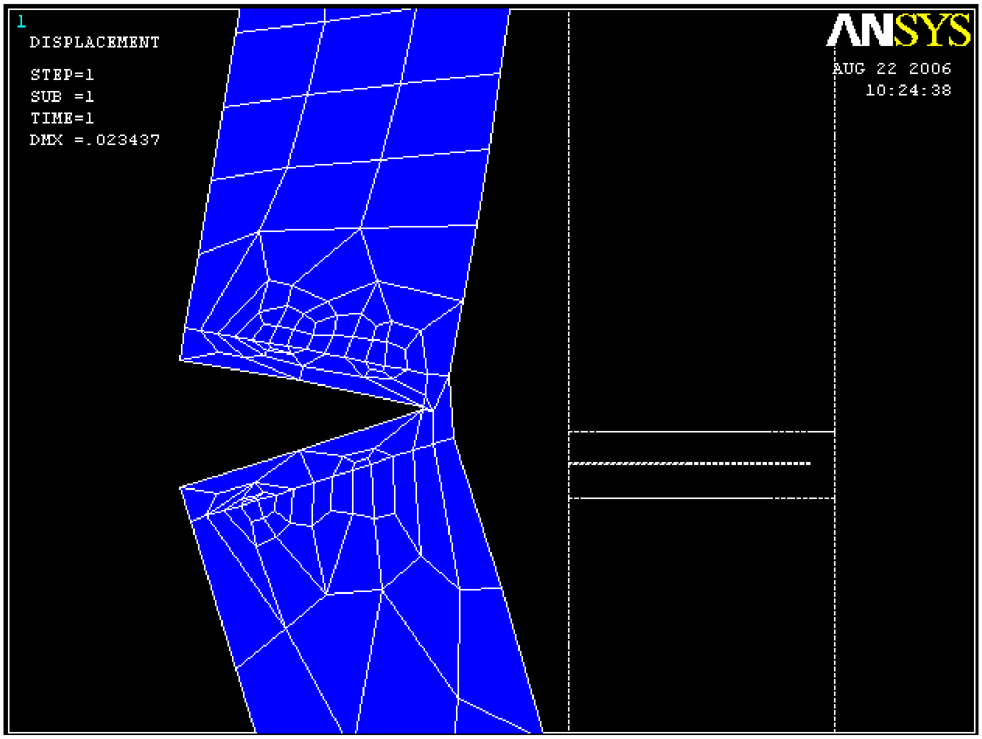

Figure 3-22
96% Cracked Model 44F Displacement.

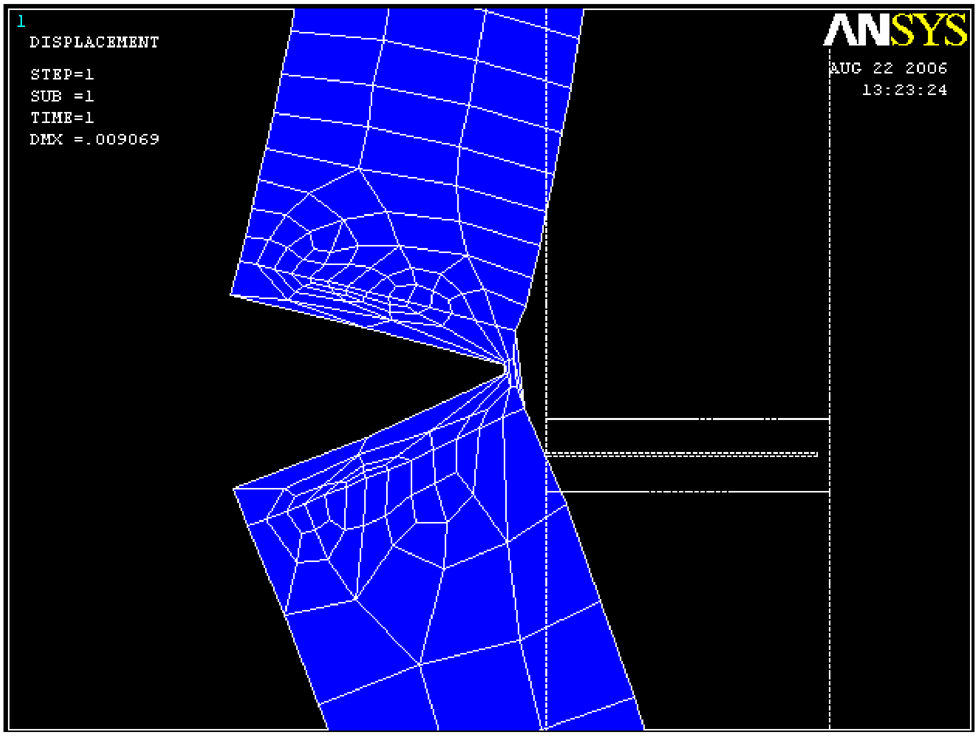

Figure 3-23
96% Cracked Model 51 Displacement.

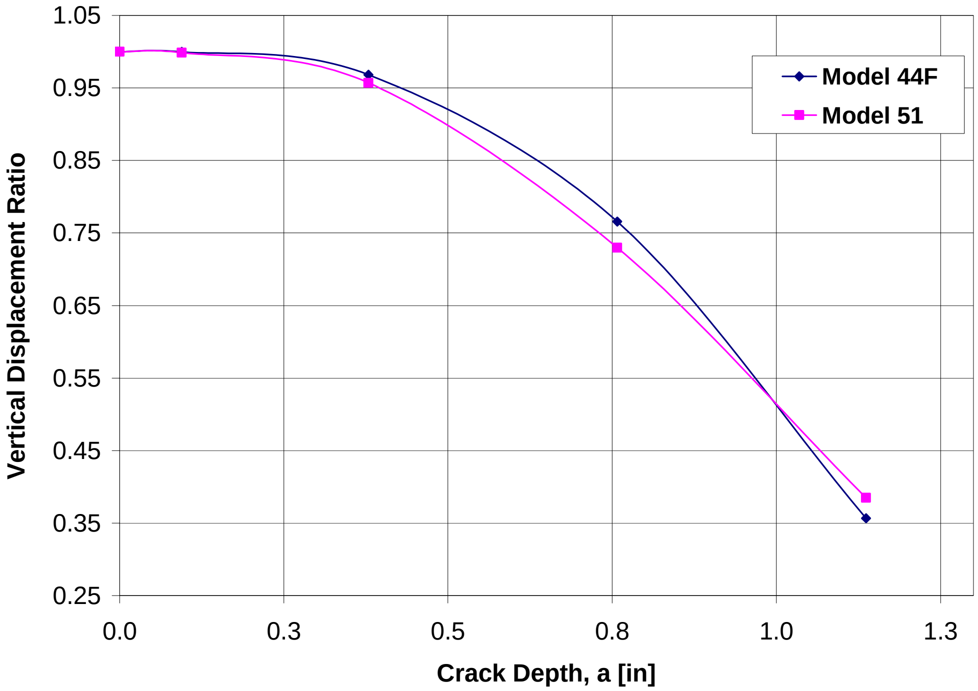

Figure 3-24
Plot of VDR for Model 44F and Model 51 as a Function of Crack Depth.

Table 3-13
Summary of Model 44F and Model 51 VDR Results

A (in)	VDR	
	Model 51	Model 44F
0.000	1.0000	1.0000
0.095	0.9985	0.9997
0.379	0.9571	0.9681
0.758	0.7297	0.7658
1.136	0.3849	0.3565

3.6 3D Finite Element Results

The Model 51 steam generator, as originally designed, was determined to be the limiting case for all of the steam generators susceptible to PWSCC due to the thin cross section of the divider plate and stub runner and the large displacements that the tubesheet experiences under operating, accident and faulted conditions. A detailed finite element analysis of the effect that a crack in the region of the stub runner to divider plate weld has on the tubesheet-channelhead (TS-CH) complex of a Westinghouse Model 51 steam generator was performed. The data from the 3D analysis of the Model 51 steam generator is intended to be used as the basis for the detailed fracture mechanics assessment on the affects of a crack propagating into the depth of the divider plate at the elevation of stub runner to divider plate weld.

The analysis of the Model 51 steam generator was compared to the results from a simple boundary value analysis listed in Reference 15. Case 30 on page 497 and Case 9 on page 510 were used as rough estimates of the expected stress magnitudes that the finite element results should approach. See Figure 3-25 and Figure 3-26 for sketches of the problem geometries in Case 30 and Case 9. See Figure 3-27 for a sketch of the global coordinate system in the 3D FEA with respect to the divider plate. The values from the simple boundary value analysis predicted that for a one half circular plate with fixed edges and a sliding support at the center of the plate the axial stresses near the elevation of the stub runner weld should be on the order of 25 ksi to 51 ksi. In the finite element model the largest axial component stresses at the elevation of the stub runner to divider plate weld ranged from 27 ksi to 44 ksi. The axial stress component is the stress that acts parallel to the global Y-axis shown in Figure 3-27 and Figure 3-29 for a plot of the linear average axial stresses for each operating condition in an uncracked divider plate.

The finite element analysis of the TS-CH steam generator complex included modeling the tubesheet as a solid structure with anisotropic perforated plate properties and cases where the stub runner elements were completely removed to simulate a 100% cracked divider plate cross section. The presence of the tubes within the tubesheet did affect the distribution of the stresses in the divider plate at the elevation of the stub runner. See Figure 3-28 for a plot of the axial stress components on the HL surface of the divider plate at the elevation of the stub runner during NOP for the uncracked condition.

The tubesheet displacements for the cracked and uncracked conditions were used to calculate a divider plate factor for each of the operating conditions. There is an additional stiffness provided by the tubes within the tubesheet in a steam generator with a damaged divider plate that becomes noticeable during upset and accident events [13]. The additional stiffness provided by the tubes in the tubesheet is capable of reducing the maximum tubesheet displacements by much less than 1%. See Figure 3-30 and Figure 3-31 for the plots of the divider plate factor for a Model 51 steam generator with and without the additional stiffness of the tubes within the tubesheet. The new limiting divider plate factor is the ratio of the maximum vertical displacements for the uncracked condition to the case with the stub runner removed in the worst case accident condition (FLB). However, removing the elements that represent the stub runner changes the stiffness of the divider plate to tubesheet connection. There is roughly a 5% difference between the stiffness of the tubesheet-channelhead-divider plate connection with the stub runner elements removed and the stiffness of the tubesheet-channelhead-divider connection with the stub runner elements present. The divider plate factor should take the stiffness difference into account. Therefore, the divider plate factor is calculated as

$$DP = \frac{1}{1.05}\frac{0.08225}{0.1962} = \frac{0.4191}{1.05} = 0.399 \approx 0.40$$

The previous value for the divider plate factor [8] was 0.76. The current analysis shows that there is substantially more resistance to tubesheet displacement in the lower steam generator region with an intact divider plate than was originally assumed.

The maximum vertical nodal displacements of the primary face of the tubesheet centerline were recorded for the three different operating conditions and the five different crack depths. The nodal axial stress components on the cold and hot leg faces of the divider plate at the elevation of the stub runner weld were also recorded for each case. The magnitude of the maximum and minimum stresses in the TS-CH complex, and the divider plate, were also compared to the results from the boundary value analysis from Reference [15].

Figure 3-32 through Figure 3-34 show the vertical displacement component contours plotted on the deformed configurations of the tubesheet and divider plate for each operating condition with a 64% cracked divider plate. As shown in Figures 3.30 and Figure 3-38, the stiffness of the connection between the divider plate and the tubesheet is drastically reduced once the crack progresses deeper into the weld than 64% of the divider plate thickness. The figures showing the displacement contours with a 64% deep crack in the divider plate to stub runner weld are useful to see what changes in the results at the transition between a stiff connection and a weak connection. Similarly, Figure 3-35 through Figure 3-37 show the axial nodal stress intensity contours for each operating condition with a 64% cracked divider plate. In both the sets of figures the deformed configuration results have been magnified by a factor of 2.00.

The results of the analysis indicate that a degraded divider plate does have an effect on the structural integrity of the TS-CH complex. In a Model 51 steam generator (SG), the divider plate is not considered a pressure boundary component and is not required to be present for the tubesheet or the channel head to meet ASME Code allowable stress limits or fatigue limits [8]. However, it is mentioned in several related documents [14] that the divider plate is considered an important structure with respect to limiting the vertical displacements of the tubesheet.

The maximum vertical displacement of the tubesheet under normal operating conditions for a case where the stub runner is completely cracked through the thickness of the divider plate is 0.120 inch. The maximum vertical displacement of the tubesheet under normal operating conditions with an intact divider plate is 0.052 inch. See Table 3-14 for a summary of the maximum vertical displacements of the centerline of the tubesheet from the 3D finite element analysis. Figure 3-38 shows the percent increase in maximum vertical tubesheet displacement as a function of increasing crack depth.

The stresses in the TS-CH complex and at the boundaries of the divider plate do not significantly change in the event of a crack in the divider plate. The maximum stress intensity in the TS-CH complex for the uncracked normal operating condition is 60.1 ksi. Note that in the context of this report, the term stress intensity refers to the maximum value of the difference between the principal stresses and not the calculated energy at the stress intensity at the crack tip. The maximum stress intensity in the TS-CH complex for a stub runner with a crack 96% through the thickness of the divider plate under normal operating conditions is 77.5 ksi. The maximum stress intensity in the TS-CH complex for the uncracked feed line break condition is 70.9 ksi. The maximum stress intensity in the TS-CH complex for a stub runner with a crack 96% through the thickness of the divider plate under feed line break conditions is 109.1 ksi.

The difference between the normal and feed line break principal stress intensity for the uncracked case is approximately 15.3%, or 10.8 ksi. The difference between the normal and feed line break stress intensities is approximately 29%, or 31.6 ksi, for the 96% cracked case. Therefore, the net effect to the stress state for a crack propagating nearly through the divider plate on the TS-CH complex is a change in the stress intensity of 20.8 ksi.

The results of the current analysis indicate that cracks less than 8% into the depth of the divider plate do not present a cause for concern. This is because a crack that is less than 30% of the divider plate thickness will not significantly change the stiffness of the tubesheet-channelhead-divider plate connection. Similarly, cracks that are less than 8% into the depth of the divider plate are not predicted to significantly increase the stress in the surrounding structures or the displacements of the tubesheet. As the crack depth progresses into the divider plate, assuming the crack that runs the entire length of the divider plate, the ability of the divider plate to restrain the tubesheet displacements will decrease. Similarly, an increase in the crack depth in the divider plate will cause an increase in stresses in the surrounding structural components. In the event of a crack present in the region of the stub runner to divider plate weld, the current analysis results show that the crack would need to be at least 64% through the thickness of the divider plate before the displacements would increase more than 5% relative to the undamaged condition of the divider plate.

It is important to realize that the increase in stress intensity in the TS-CH complex due to the presence of cracks in the stub runner weld region may exceed the ASME Code allowable stresses or fatigue limits in other components (e.g. channelhead, tubesheet, tubes). However, the effects of such an increase in stress intensity on other components in the lower steam generator region are outside of the scope of the current analysis.

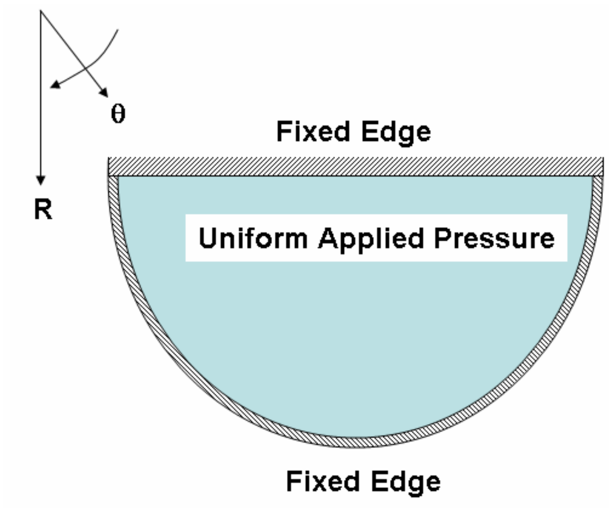

Figure 3-25
Sketch of Coordinate System and Problem Geometry for Case 30, page 497 of Ref. 15

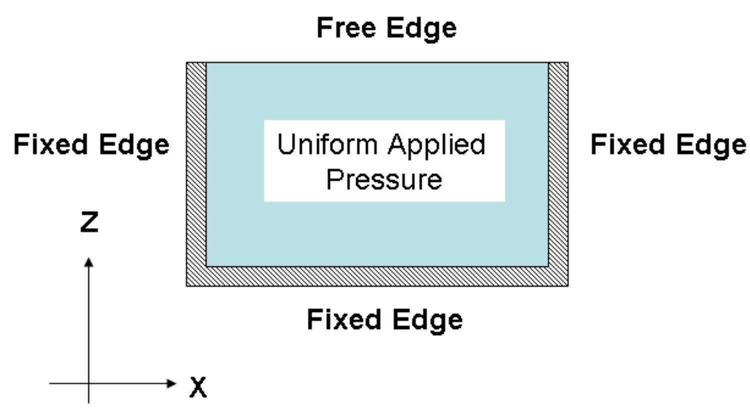

Figure 3-26
Sketch of Coordinate System and Problem Geometry for Case 10, Page 513 of Ref. 15

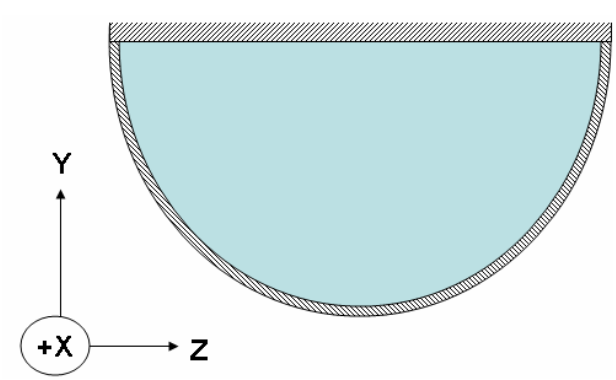

Figure 3-27
Global Coordinate System with Respect to the Divider Plate in 3D FE Model

Table 3-14
Summary of Maximum Vertical Tubesheet Displacements comparing a 100% Through Wall Crack to the Uncracked Condition

Maximum Vertical TS Displacement		NOP (in)	LOL (in)	FLB (in)
No Tube Stiffness	Uncracked	0.05152	0.06127	0.08225
w/Tube Stiffness	Uncracked	0.05153	0.06129	0.08232
No Tube Stiffness	100% Cracked	0.12022	0.14364	0.19624
w/Tube Stiffness	100% Cracked	0.12018	0.14359	0.19621

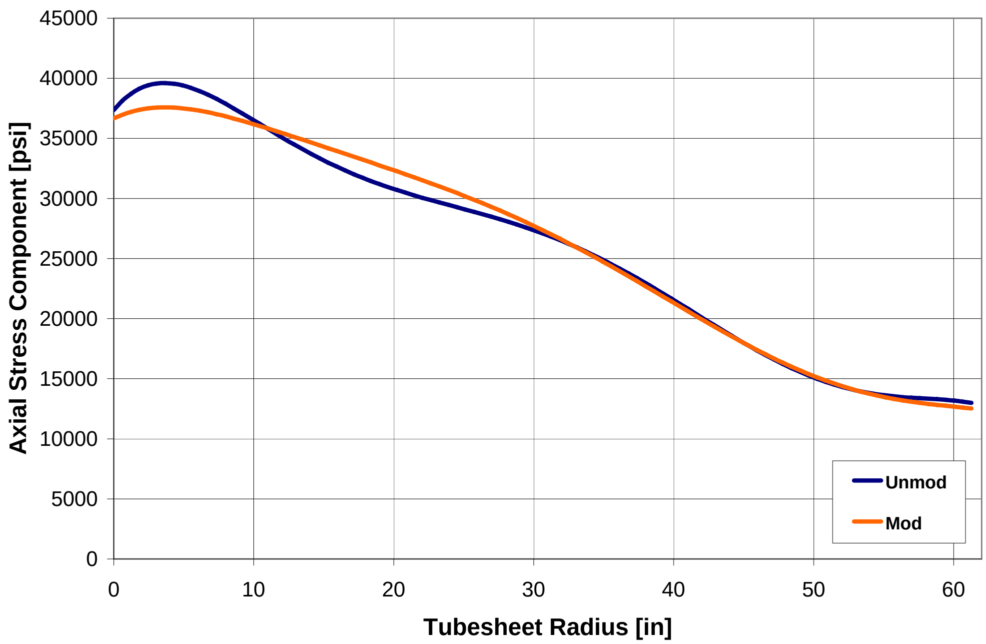

Figure 3-28
Plot of the Smooth Fit of the Tubesheet Stiffness Modified and Unmodified Values for the HL Surface Axial Stress Component at the Elevation of the Stub Runner to Divider Plate Weld for the Uncracked NOP Condition.

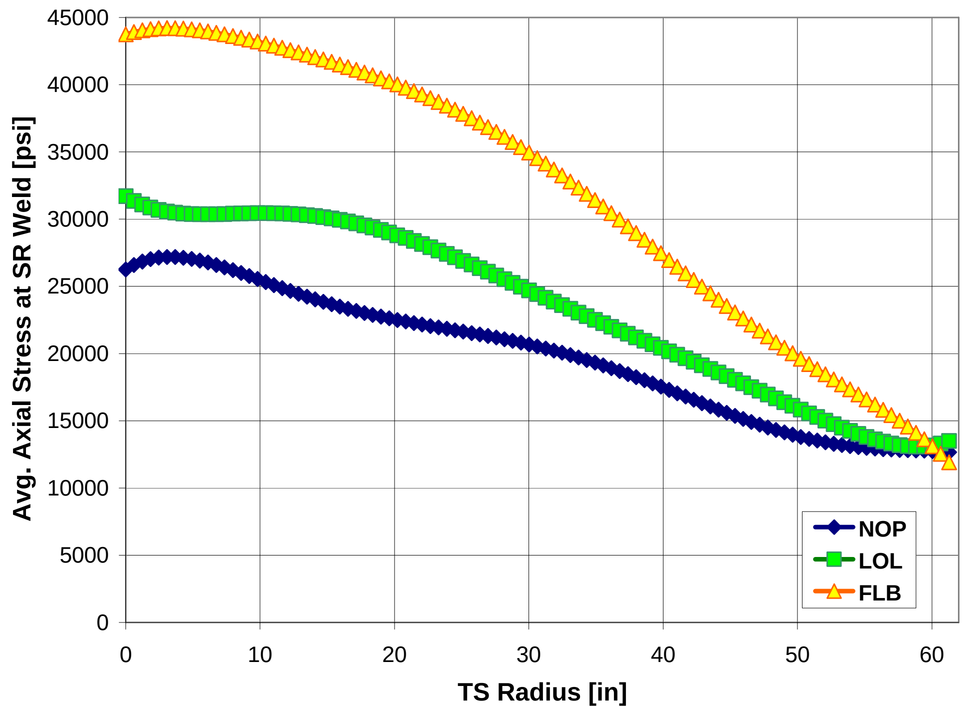

Figure 3-29
Plot of Linear Average Axial Stress Components for the Uncracked Condition at the Elevation of the Stub Runner to Divider Plate Weld in a Model 51 Steam Generator.

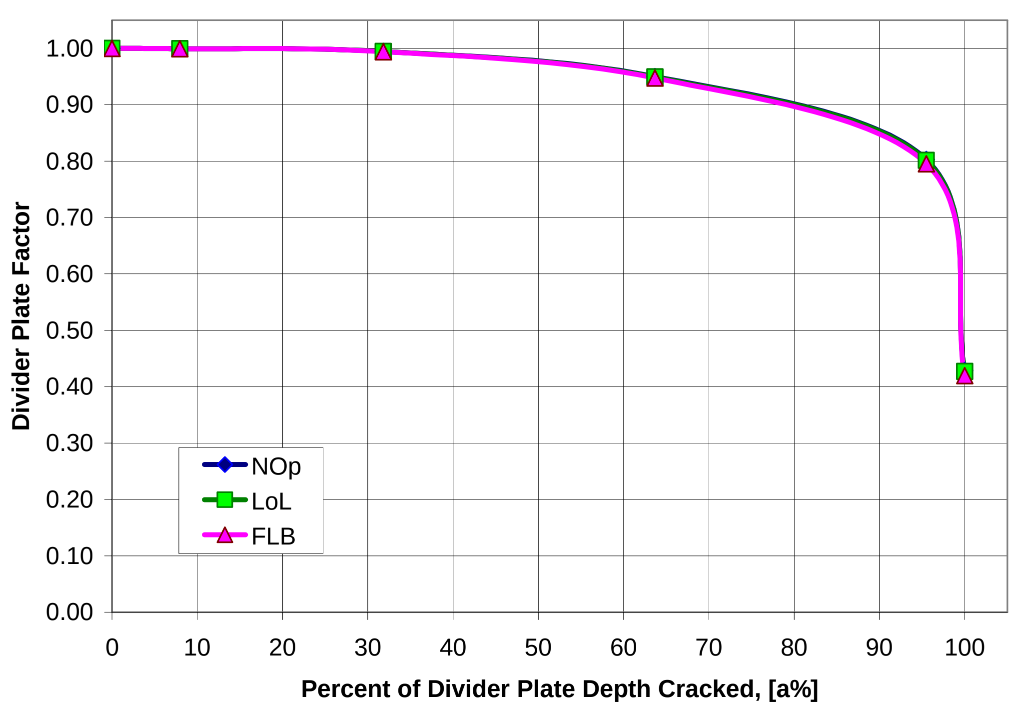

Figure 3-30
Plot of Divider Plate Factor for a Model 51 SG with Unmodified Tubesheet Stiffness

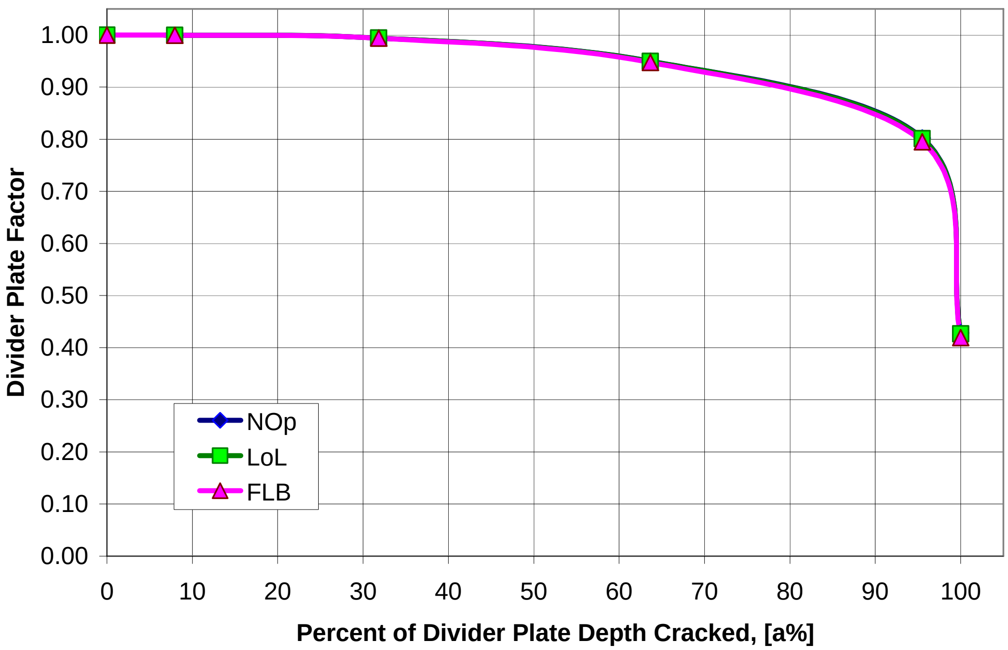

Figure 3-31
Plot Divider Plate Factor for a Model 51 SG with Additional Stiffness from the Tubes within the Tubesheet

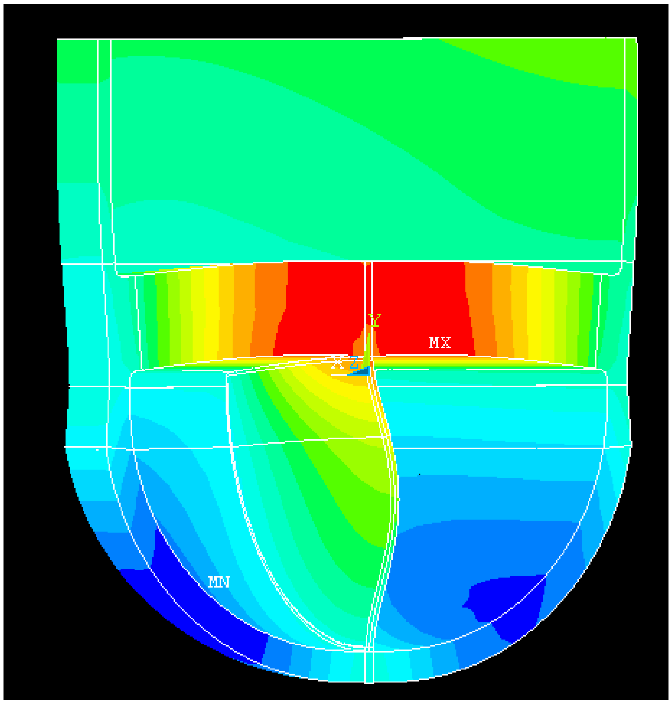

Figure 3-32
64% Cracked NOP Vertical Displacement Contours Plotted on the Deformed Model Configuration with Maximum and Minimum Location Identified.

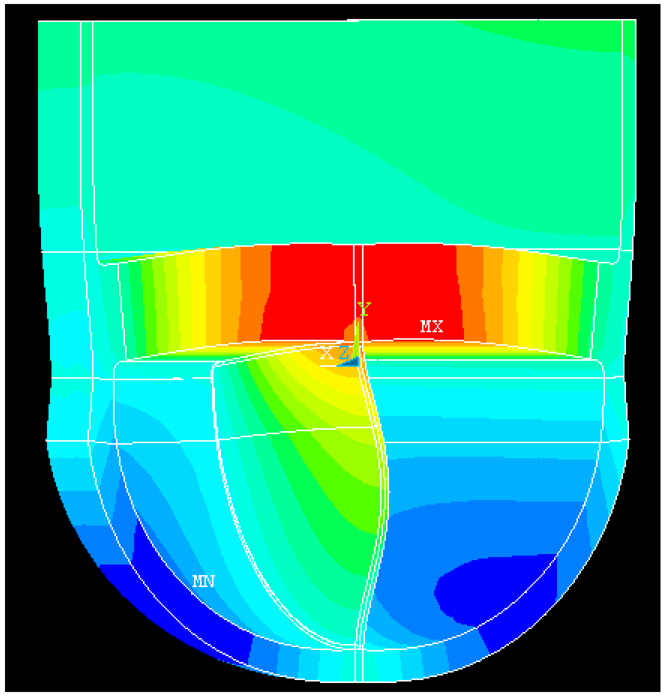

Figure 3-33
64% Cracked LOL Vertical Displacement Contours Plotted on the Deformed Model Configuration with Maximum and Minimum Location Identified.

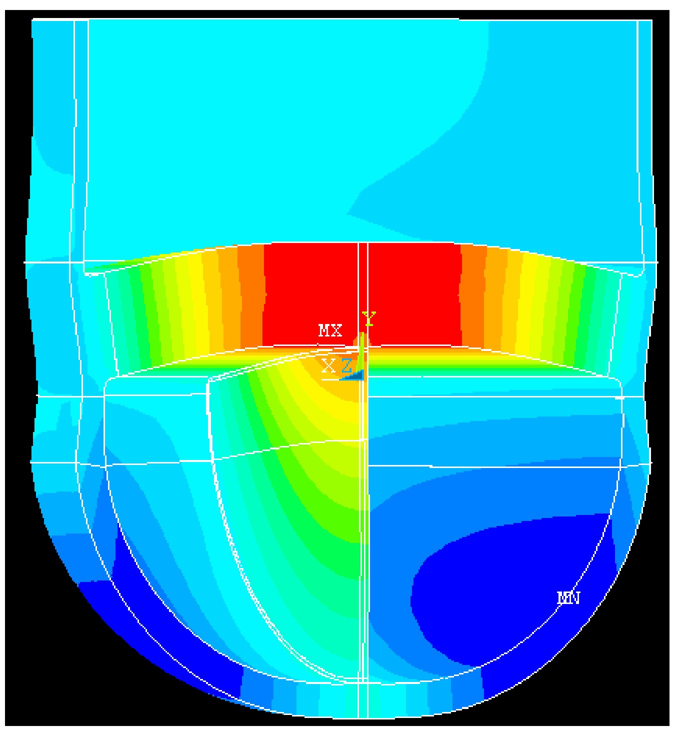

Figure 3-34
64% Cracked FLB Vertical Displacement Contours Plotted on the Deformed Model Configuration with Maximum and Minimum Location Identified.

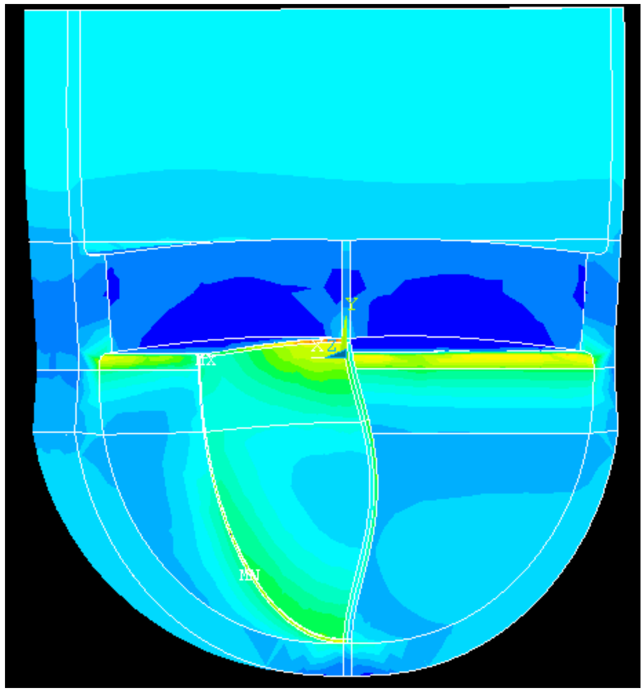

Figure 3-35
64% cracked NOP stress intensity contours plotted on the deformed model configuration with maximum and minimum location identified.

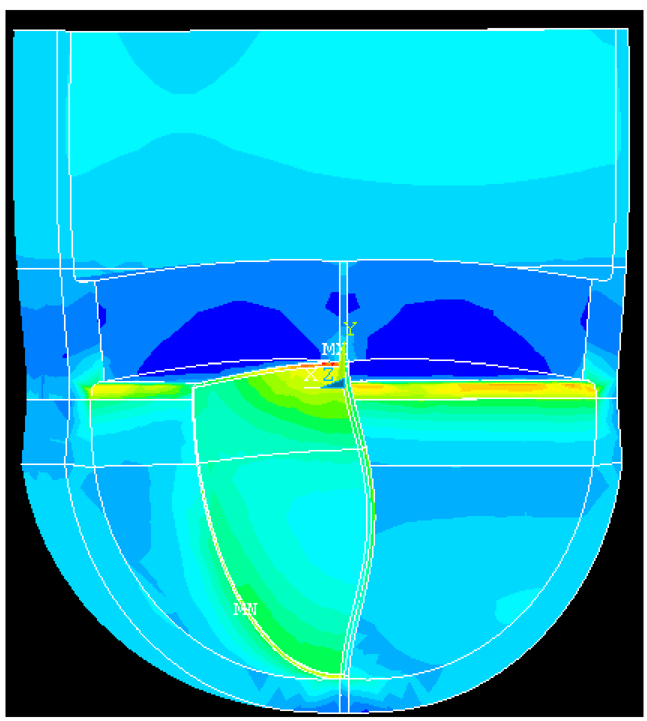

Figure 3-36
64% Cracked LOL Stress Intensity Contours Plotted on the Deformed Model Configuration with Maximum and Minimum Location Identified

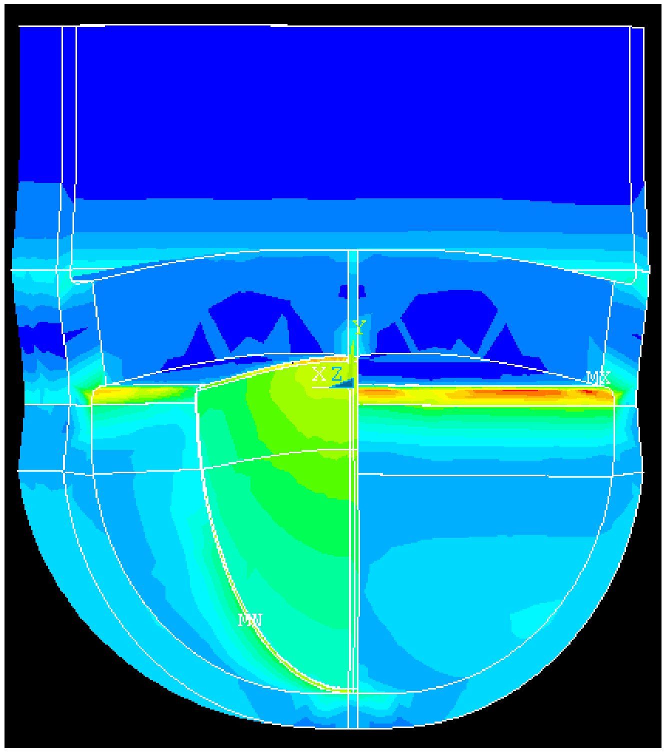

Figure 3-37
64% Cracked FLB Stress Intensity Contours Plotted on the Deformed Model Configuration with Maximum and Minimum Location Identified

3.7 Summary of Limiting Steam Generator Finite Element Analysis

The results of the analysis show that a degraded divider plate does have an effect on the stresses and displacements of the TS-CH complex. The Model 51 steam generator is the limiting SG case for a cracked divider plate.

The current analysis results show that a crack in the divider plate to stub runner weld would need to be at least 64% through the thickness of the divider plate before the displacements would increase more than 2% relative to the undamaged condition of the divider plate during normal operation. The maximum vertical displacement of the tubesheet under normal operating conditions for a case where the stub runner is completely cracked through the thickness of the divider plate is 0.120 inch. The maximum vertical displacement of the tubesheet under normal operating conditions with an intact divider plate is approximately 0.052 inch. See Table 3-14 for a summary of the maximum vertical displacements of the centerline of the tubesheet from the 3D finite element analysis. See Figure 3-38 for a plot of the percent increase in tubesheet displacements as a function of percent of the divider plate depth cracked.

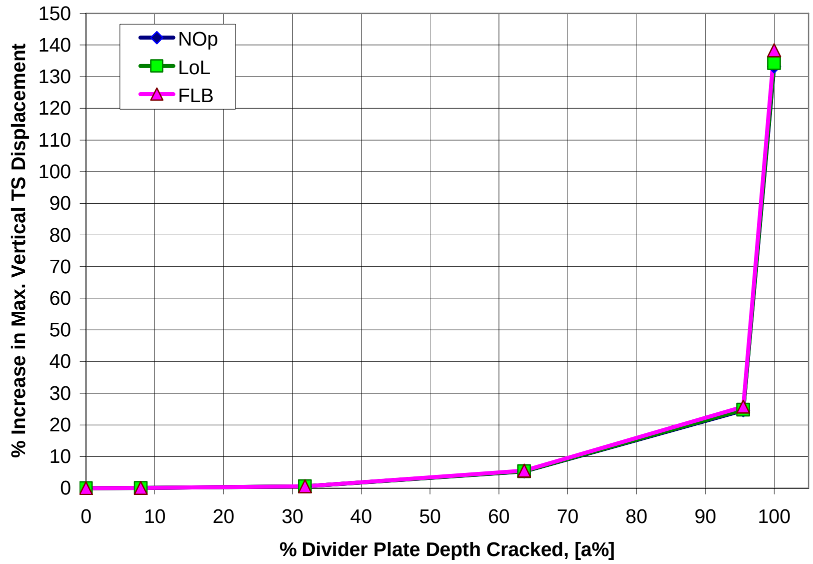

Figure 3-38
Plot of the Percent Increase in Maximum Vertical Tubesheet Displacements as a Function of the Percent Increase in Crack Depth in the Divider Plate

There is an additional stiffness provided by the tubes within the tubesheet in a steam generator with a damaged divider plate that becomes noticeable during upset and accident events [13]. The additional stiffness provided by the tubes in the tubesheet is capable of reducing the maximum tubesheet displacements by a small amount, much less than 1% of the total deflection.

Previous analysis determined the DP to be 0.76 [8]. The current analysis proves that there is substantially more resistance to tubesheet displacement in the lower steam generator region than that was originally assumed. Comparing the results of the 2D and 3D finite element studies indicates that the average divider plate ratio for a steam generator with an uncracked divider plate is about 0.40.

The current limit on the detection of cracks in the divider plate using NDE techniques is 2 mm (0.078 in) which is equal to roughly 4% of the thickness of a 2.00 inch thick divider plate. The results indicate that cracks less than 8% into the depth of the divider plate, or twice the minimum depth threshold for detection, do not present a cause for concern. Furthermore, cracks less than 8% into the depth of the divider plate should not cause a significant increase in stress or displacement in the TS-CH complex. The maximum vertical tubesheet displacements are not predicted to increase more than 2% relative to the non-degraded normal operating condition until the crack has progressed more than 64% into the depth of the divider plate.

4
FRACTURE CALCULATIONS AND METHODS

4.1 Method Discussion

Cracks have been observed in the Alloy 600 weld between the stub runner and the divider plate in foreign steam generators. The divider plate, stub runner and weld material in this analysis are assumed to be homogenous materials. This is an important assumption to clarify because regions of cold working, such as those created by loose parts impingement, in the Alloy 600 material have potential to significantly affect crack growth. The presence of cracks and other damage in a material typically create regions of inhomogeniety within a structure.

See Figure 2-1 and Figure 2-2 for a sketch of the stub runner and divider plate in the tubesheet-channelhead (TS-CH) complex. See Figure 2-3 for a sketch of the assumed model crack geometry.

The assumed crack geometry results in a plane strain edge crack that can be analyzed using either two dimensional or three dimensional methods. The edge crack is a well known model and has been extensively studied in the literature [24]. For any given two dimensional crack the stress intensity can be calculated using the equation

$$K = FS_g\sqrt{\pi a} \qquad (1)$$

Where F is the geometry factor for the applied loading and the specimen response, S_g is the gross section stress applied in the far field with respect to the crack in the specimen and a is the crack depth. See Figure 4-1 for a sketch of the typical edge crack specimen geometry in a two dimensional analysis. Note that in the context of linear elastic fracture mechanics the term stress intensity refers to the magnitude of the stress in the vicinity of a sharp crack tip in a linear, elastic, homogeneous and isotropic solid. Assuming far field tension and an edge crack geometry the stress intensity for the edge crack is given by

$$K = 1.12S_g\sqrt{\pi a}, \text{for } a/b \le 0.13 \qquad (2)$$

Which assumes that F=1.12. Equation (2) is accurate to within 10% of the actual value for small values of a/b [24]. For any value of a/b, the equation for the geometry factor F is

$$F = 0.265(1-\alpha)^4 + \frac{0.857 + 0.265\alpha}{(1-\alpha)^{3/2}}, \text{for } h/b \ge 1 \qquad (3)$$

Which is valid for specimens with an aspect ratio (*h/b*) greater than 1 (i.e. long and thin). As the crack depth increases ($a/b > 0.13$) the remaining specimen ligament begins to act as a hinge and the far field tension generates a local bending moment about the centerline of the specimen. Equation 4 is the calculation for *F* assuming a large aspect ratio and a far field tension which applies a local moment to the specimen in the vicinity of the crack.

$$F = \sqrt{\frac{2}{\pi\alpha}\tan\frac{\pi\alpha}{2}}\left[\frac{0.923 + 0.199\left(1 - \sin\frac{\pi\alpha}{2}\right)^4}{\cos\frac{\pi\alpha}{2}}\right], \text{for } h/b >> 1 \tag{4}$$

The displacements of the divider plate and tubesheet change as a function of location in the three dimensional finite element models. In three dimensions the two dimensional equations can be applied but they will only be valid at a single point. As an example, the gross section stress at a tubesheet radius of 34 inches can be used to calculate the stress intensity but that value will only be valid at a radius of 34 inches. There is also a difference between the displacement and stress results on the hot leg side of the divider plate and the cold leg side of the divider plate. Specifically, the surface of the cold leg side of the divider plate will have less stress placed on it compared to the hot leg surface of the divider plate. In the analysis of the three dimensional finite element results from Reference 24 the average axial section stress at the elevation of the stub runner weld was used to calculate the stress intensity. The average axial section stress is defined as

$$\sigma_{AVG} = \frac{\sigma_{HL} + \sigma_{CL}}{2} \tag{5}$$

Where σ_{HL} is the nodal stress on the hot leg surface of the divider plate at the elevation of the stub runner parallel to the global y-axis and σ_{CL} is the nodal stress on the cold leg surface of the divider plate at the elevation of the stub runner parallel to the global y-axis. See Figure 3-27 for a sketch of the coordinate system. The stress and stress intensity in the stub runner weld also changes as a function of the tubesheet radius. The average axial stress over the entire tubesheet radius is defined as

$$\sigma_{R,AVG} = \sum_{i=1}^{n}\frac{\sigma_{AVG}}{n} \tag{6}$$

Where *n* is the number of nodes along the hot leg surface of the divider plate at the elevation of the stub runner weld.

The mechanism of failure in the stub runner weld will most likely be fatigue failure and not brittle fracture of the cross-section. This is because the temperature of the reactor coolant stream as it enters the channel head is typically 600ºF or greater. The estimated depth of the crack for a brittle failure is given by the equation

$$a_c = \frac{1}{\pi}\left(\frac{K_C}{FS_{MAX}}\right)^2 \tag{7}$$

Where K_C is the fracture toughness of the specimen, S_{MAX} is gross section stress at the point in the loading with the maximum stress intensity and F is the geometry factor. The specimen may fail before the specimen reaches the maximum possible fracture toughness, even under ideal conditions. Therefore, K_C is not necessarily equal to K_{IC}, but it can be assumed to be equal to K_{IC} for the purposes of assessing the potential for brittle fracture.

It is more difficult to estimate the failure crack depth required for a material to fail plastically. An initial estimate, on a per unit length basis, can be calculated using:

$$l = \frac{P'}{S_m} \tag{8}$$

Where l is the length of the remaining ligament, P' is the estimated gross section load at failure and S_m is the average flow stress of the material. A better estimate of the crack depth at plastic failure can be obtained by iteratively comparing the gross section load and remaining ligament to the crack depth at failure using the equations

$$a_o = b\left(1 - \frac{P_{MAX}}{2b\sigma_o}\right) \tag{9}$$

$$S_{MAX} = \frac{P_{MAX}}{2b} \tag{10}$$

Where P_{MAX} is the maximum applied section load per unit length, b is the thickness of the uncracked and un-deformed specimen, and S_{MAX} is the maximum applied gross section stress. Replacing b in Equation 10 with the crack depth, a, and calculating the applied section stresses using Equations 9 and 10 makes it possible to iteratively compare the crack depths at the calculated failure loads. When the difference between the two results is acceptably low, the solution is assumed to be converged.

There are two methods for calculating fatigue life for a weld in this situation. The first is to estimate the number of cycles of a given type of loading that will exceed the fatigue resistance of the weld. The second is to estimate the fatigue resistance of the weld from various test results. The answer to the first approach is the estimated fatigue life of the divider plate cross section as given by a closed form solution of the Walker equation [24] given in Equation 11.

$$N_{if} = \frac{a_f^{1-m/2} - a_i^{1-m/2}}{C\left(F\Delta S\sqrt{\pi}\right)^m \left(1 - m/2\right)}, m \neq 2 \tag{11}$$

The $F\Delta S\sqrt{\pi}$ term in the denominator of Equation 11 is equal to the change in the stress intensity divided by the square root of the crack depth, *a*. The variables *m* and *C* are tabulated parameters that are dependent on load configuration and material [24]. The terms a_f and a_i refer to the crack depths at failure and at initiation, respectively.

The result of Equation 11 is the estimated number of cycles that are required to fail a specimen assuming that the initial crack size is much smaller than the crack size at failure and that the crack growth is due only to mechanical cycling on the specimen. The number of cycles to failure for a specimen that is exposed to both mechanical cycling and corrosive effects (e.g. PWSCC) is

$$N = N_{if} - N_{CHEM} \tag{12}$$

Where N_{CHEM} is the number of cycles to failure for a specimen exposed to corrosive effects and an initial crack size equal to the one assumed in Equation 11. The value of N_{CHEM} is taken from calculations based on the available literature or direct experimental results.

In the second method for estimating the fatigue life of the weld, the crack results from PWSCC sensitized specimens are analyzed to obtain a predicted rate of crack growth in terms of change in crack length per unit time. These results are combined with the results for purely mechanical fatigue crack growth in terms of change in crack length per cycle of applied loading as determined by a Paris law. The Paris law model for change in crack length is typically given as:

$$\frac{da}{dN} = C(\Delta K)^m \tag{13}$$

Where *C* and *m* are material specific parameters and ΔK can be determined by experiment or finite element results.

The combination of the change in crack length per unit time and per cycle is represented by Equation 14:

$$da = \frac{da}{dt}t + \frac{da}{dN}N \tag{14}$$

Where *t* is the period of time under evaluation (i.e. 1 year, 10 years, etc.) and *N* is the number of mechanical loading cycles expected in the given time period. Note that each of the two fatigue life methods described above focus on different behavior. The estimated number of cycles based on the finite element results and input to the Walker equation will tend to under estimate the effect of PWSCC on the weld. Conversely, the time based component of the PWSCC estimate will over estimate the crack growth because the test conditions which lead to the crack growth rate are not likely to be consistently duplicated for a consistent length of time in the steam generator. However, the results from Equations 12 and 14 are useful and can form the basis for a bounding analysis on the fatigue life of the stub runner to divider plate weld.

The Model 51 steam generator divider plate is analyzed under three different operating conditions: normal operating (NOP), loss of load (LOL) and main feedline break (FLB). The three conditions are applied to the finite element models as steady state boundary and loading conditions. The loss of load and feedline break cases were chosen because they are the limiting upset (LOL) and faulted (FLB) conditions for the Model 51 steam generator with respect to the pressure differential across the tubesheet. The pressure differential across the tubesheet is the primary source for the tension on the divider plate to stub runner weld and therefore it is the primary concern for crack growth in the weld.

The safety margin for the weld can be determined two different ways. First, the number of cycles required to grow a crack through the thickness of the weld can be compared to the average number of cycles in a year, using the results of Equation 11. This safety margin will give a good estimate of the importance of mechanical stresses on the crack growth in the weld and is defined by the ratio:

$$n = \frac{\text{Number of Cycles to Fail the Weld}}{\text{Number of Cycles per Year}}$$

The second method is to determine the potential crack growth over a year using the results of Equation 14. This safety margin will provide an estimate of how sensitive the weld is to PWSCC. The crack growth safety margin is defined by the ratio:

$$n = \frac{\text{Divider Plate Thickness}}{\text{Crack Growth per Year}}$$

Both safety margins should be considered estimates that will require field experience and data to verify.

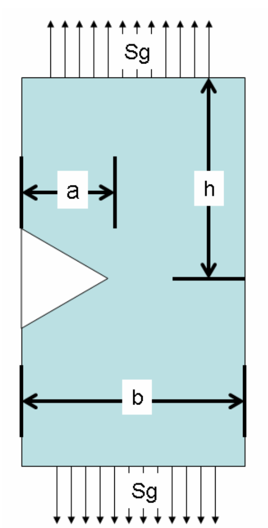

Figure 4-1
Assumed 2D Specimen Geometry with a Thickness, t, and Edge Crack with Far Field Tension

4.2 Summary of Divider Plate Crack Indications

There have been cracking indications in the divider plates of several French steam generators. These indications have occurred in units at the Chinon, Saint-Laurent, Dampierre, Gravelines and other nuclear power plants [1, 2, 3, 4, 5]. The cracks were observed on the hot leg side of the divider plate. There has been one documented case of cracking in heat affected zone on the cold leg side of the divider plate [4]. The cracks were observed in the stub runner divider plate weld, in the stub base metal and in the divider plate. The cracks occur more commonly in steam generators with 34 mm (1.34 inch) thick divider plates. The cracks tend to coalesce into long branched chains (up to nearly 6 feet in length) but remain shallow (typically less than 2 mm or 78.7 mils deep). In one case to date, a crack has been noted to progress to a depth deeper than 2 mm, to a maximum depth of 7 mm (~0.28 in).[5] The cracks tend to be horizontal and, when they have been noted to grow, they grow longer but not deeper. As the cracks near the triple point of the TS-CH complex, the cracks tend to turn and curve up. Several different phenomena appear to be causing the cracking, such as:

- Heat Treatment
- Weld Defects
- Material Defects
- Damage due to loose parts in the channel head
- PWSCC

A list of steam generators in the foreign nuclear fleet reported to have divider plate cracking is given in the table below.

Plant	Year Reported -	Length in	Max. Depth in
Blayais	2006	Varies	0.276
Chinon	2002	70.44	0.016
Dampierre	1993	Varies	0.008
Gravelines	1994	Varies	0.011
Ringhals	2004	Varies	Surface Only
St. Laurent-B	1996	Varies	0.0748

The shallow nature of the cracks suggests that only the heat affected zone and surface layer of the weld is cracking. This is reasonable because the layers underneath the last weld bead are effectively annealed, or heat relieved, by the application of the last weld layer. The surface weld layer in contact with the primary water is not annealed and therefore may be susceptible to residual stress induced cracking and more sensitive to PWSCC.

[5]: This indication was reported during Fall 2006 outage inspections at Blayais. This information was related to WEC Engineers as a personal communication and no formal documentation that details the entire geometry of the crack is yet available. It is a significant finding because it represents a change in crack depth due to SG operation/PWSCC and not loose parts.

In some cases, loose parts that were present during early testing and commissioning of the SG led to impacts and damage in the divider plate and channel head. These impacts resulted in a "cold working" effect which made cracking easier in the affected metal. It is thought that the weld, material and loose part damage in the SG occurred before the units were operational.

The PWSCC occurred after the SG units became operational. The deepest crack that was verified as PWSCC in the reports was 75 mils deep, but most cracks were on the order of 15 mils or less. The combined effect of the material and weld defects most likely contributed to the PWSCC in some of the plants. A significant finding from the EPRI MRP reports is that the cold working caused by the impingement of the loose parts on the divider plate material made it easier to initiate PWSCC. It is thought the cold working created regions of dense dendrite-like structures that made it easier to wedge the surrounding softer metal apart during the crack propagation process. The deepest PWSCC observed was on the divider plates that had sustained the most damage from loose parts.

There have been no reported instances of divider plate cracking in domestic steam generators to date. A summary of the reported crack indications discussed in the EPRI EDF MRP reports is provided below.

4.2.1 Indications at Dampierre Unit 1

Dampierre Unit 1 SG 3 was replaced in 1990. One triple point specimen, which included the stub runner partition plate and channel head, was removed from the SG for destructive examinations [4]. The destructive examinations revealed shallow PWSCC, <200 μm (8 mils), in the stub, in the weld and in the partition plate. The Alloy 600 partition plate and stub runner material was sensitized to PWSCC. The Alloy 600 surface exhibited some very coarse grains, dimensions of approximately 1 mm or 40 mils. The results of the indications led to the French inspecting a sample of the steam generators in their fleet from 1993 up to the present day (2007).

4.2.2 Indications at Chinon

The 2002 PT of the stub/partition plate weld of the Chinon B4 SG 2, evidenced a series of linear indications, reaching a total length of 1790 mm (5.87 feet) [5]. The 2004 metallographic replica taken from the middle of this series of indications, which has been judged as representative of the entire series of indications, showed PWSCC just underneath the surface (-0.3 to -0.4 mm; -12 to -16 mils after grinding for the surface preparation). Most of the PWSCC cracks were located in the stub base metal. Very short PWSCC cracks have been observed in the weld too. In 2004, the cracks network morphology looks similar to the corresponding 2002 RFO13 PT network of indications.

4.2.3 Indications at Saint-Laurent B

The examinations at Saint-Laurent B Unit 1 revealed [1] multiple impacts of loose parts all over the channel head, the tubesheet and in the radius in between. The examinations also revealed:

- PT indications at the hammered areas

- PWSCC corresponding to PT indications in both A82 and A182 alloys
- The deepest crack, from the above indications, was 1.9 mm (75 mils) deep.
- Crack faces exhibiting columnar grains with branched cracking and embedded precipitates.

A cold worked zone in the region of the stub runner weld was also identified, 2.34 mm (92 mils) deep, stemming from a 310 μm (12 mils) deep impact. The cracks that generated PT indications were found in this zone. The PWSCC is limited to the cold work material. These features are PWSCC typical and point out the deleterious role of cold work generated by loose parts. Embedded hot cracking was found in the A82 tubesheet cladding which highlighted the differences in morphology between PWSCC and hot cracking.

The hot leg side channel head of SG #52 at Saint-Laurent B NPP Unit 1 [2], had been hammered by loose parts during its commissioning tests. This SG had been replaced after 10 EFPYs of operation. The PT of the hot channel head revealed numerous indications. Two specimens were removed from the partition plate so that the PT indications could be characterized. The destructive examinations showed that these indications were PWSCC. A series of hardness measurements also showed that the PWSCC was limited to the cold worked regions of the specimens.

4.2.4 Indications at Gravelines Unit 1

Two PT indications have been observed on the left triple point (the connection of the tubesheet, divider plate and channel head) of Gravelines Unit 1 SG #2 [3]. The micrography shows these two indications are located in the weld. The first one is linear and corresponds to a flaw at the interface between 2 weld passes. The second is round and stems from interdendritic defects extending on 1.9 mm and 255 μm (10 mils) deep. The SEM examination confirms the interdendritic nature of the round defect and evidences a surface corrosion of all the dendrites. The 5.5 mm (0.22 inch) long indication is a lack of fusion. The 7 mm (0.28 inch) round indication is an interdendritic corrosion that most probably occurred prior to SG commissioning. Several PWSCC cracks, 280 μm (11 mils) have been observed at the outer rim of the partition plate specimen.

4.2.5 Conclusions Relative to Crack Geometry in Finite Element and Fracture Analysis

The indications from Chinon [5] and Gravelines [3] support the assumed crack geometry. It is conservative, but appropriate, to consider a crack that has already propagated the full length of the divider plate to stub runner weld and then proceeds to increase in depth. However, the thresholds for concern when using the worst field indications should also be questioned. For example, is it possible to propagate a crack through the divider plate given the shallow crack geometries observed from the field indications? Therefore, two specific structural and material thresholds must be checked. First, will the tubesheet displacements, which are closely related to the crack opening displacement available to a crack in the stub runner to divider plate, increase by a measurable amount due to cracking in the divider plate weld connections? Secondly, is it possible for the cracks in the divider plate to stub runner connection to propagate further into the weld material?

In the context of this analysis the limit of a measurable increase in vertical tubesheet displacement due to the crack is an increase of 2% or greater compared to the limiting vertical tubesheet displacement on the TS-CH complex with no cracks in the divider plate. The limit for Mode I crack propagation in Alloy 600 material is given in Reference 30 as 4.5 $ksi\sqrt{in}$. If the stress intensity caused by a given crack geometry exceeds that value then it is possible for the crack to grow into the divider plate.

4.3 Limiting Mechanical and Material Properties

The values for the fracture analysis of the Alloy 600 weld were taken from the ASME Code [16]. The values for *m* and *C* in the Walker equation were taken from Reference 24 using comparable materials as a reference. All of the properties used for the fracture analysis assume that the weld and surrounding metal are at 600ºF. If sequential effects (e.g. specifying an order of events and transients instead of assuming a steady state analysis) were also to be considered then it is expected these values would change. The material properties used in this analysis are listed in Table 4-1.

The residual effects of welding the stub runner to the divider plate will affect the material properties and behavior of the weld. This includes the residual stress distribution in the weld material and the surrounding heat affected zone. The distribution of residual stresses and material affects, such as phase transitions, due to a multi-pass welding process is complex. There are several simplifying assumptions that can be made in modeling the heat affected zone. Research by Hall [25] and Dong et al. [26] show that the residual stress distribution in the weld material peaks at the outer surfaces and reaches a minimum near the center of the welded section. This means that the assumed crack geometry will essentially negate the effect of the residual stresses because the region that would be in tension due to the residual stress effects is already cracked through. The residual stress effects are not a concern in the channelhead to tubesheet weld because that weld is heat treated (PWHT) after it is made. Secondly, the layers of the weld build-up below the outer surface are exposed to a high temperature during the application of the weld beads. The Alloy 182/Alloy 600 weld material has been shown to exhibit some stress relief at temperatures as low as 900 ºF [27, 28]. The applied weld temperatures during a multi-pass weld build-up can easily approach that temperature [29]. Therefore, the combination of the lower residual stress field in the interior of the weld section and the potential heat relief effects mean that the majority of the weld material in the stub runner to divider plate connection can be assumed to be heat treated as well. Applying the combination of these results means that the mechanical properties of the Alloy 182/Alloy 600 material in the heat affected zone do not need to be modified to account for residual affects.

The threshold crack propagation value for the stress intensity of Alloy 600 under mechanical loading is assumed to be 4.5 $ksi\sqrt{in}$ [30]. This value is based on assumptions and tests previously performed at Westinghouse for a load ratio, $R = 0$ ($R = S_{MIN}/S_{MAX}$) in air at room temperature. The threshold stress intensity value will change based on the environment and the loading ratio. The data indicate that the threshold value for crack propagation will increase slightly as R increases and that there is no significant change in the threshold value of Alloy 600 from R = 0 to R = 0.05. However, the change in the material properties of Alloy 600, in a primary water environment, at a temperature of 600ºF would likely increase the threshold for crack propagation [30]. Therefore, the use of 4.5 $ksi\sqrt{in}$ in this analysis is conservative.

Recent research [31, 32] indicates that the most conservative assumption with respect to PWSCC in Alloy 600 is to assume that there is no threshold value. This means that the only barrier to crack propagation in the Alloy 600 weld is the mechanical resistance of the metal to crack growth. Therefore, if the estimated crack tip stress intensity exceeds a value of 4.5 $ksi\sqrt{in}$ the crack is conservatively assumed to grow into the depth of the divider plate. The K_{IC} value was estimated based on the best available data. Comparing the data available in Reference 24 and Reference 31 one can infer that a reasonable value for the critical fracture toughness of the material is 7.5 times the stress intensity value of a specimen at the arrest of the final crack growth in a test specimen. The estimated K_{IC} value for the divider plate Alloy 600 weld material therefore is 215 $ksi\sqrt{in}$.

The crack growth data and the crack propagation information for the Alloy 600 material were taken from several references in the literature [22, 23, 32, 33]. The crack length at failure and the value of N_{CHEM} were taken from data used to analyze nozzle weld cracking at Ringhals [31, 32]. The best estimate data were used to reflect realistic crack growth in Alloy 600. Table 4-5 lists the best estimate data from Reference 31.

The unmodified geometric factor, see Equation 2, was used to calculate the average stress intensity in the stub runner weld. No geometric factor is necessary to calculate the stress intensity in the vicinity of the crack tip as a function of tubesheet radius. This is because actual stresses in the vicinity of the crack are used instead of gross section stresses so that there is no need for an additional modification to the section stress. The crack growth rate for PWSCC and mechanically induced cracking in the Alloy 600 weld were from the preliminary law developed by Electricité du France (EdF) and published in Reference 33 as:

$$\frac{da}{dt} = 0.51 \cdot 10^{-10} K^{0.4}, (\mathrm{m/s}) \qquad (15)$$

Where K is the stress intensity (in units of $MPa\sqrt{m}$) and *da/dt* is the crack growth rate in meters per second. Multiplying *K* by 0.910047 and *da/dt* by 39.37 converts the stress intensity and crack growth rate into the English Units terms of $ksi\sqrt{in}$ and inches per second. The crack growth rate curve is shown in Figure 4-2.

4.4 Design Basis Information and Estimated Fatigue Life Analysis

The information in Table 4-6 is a summary of the transient and design basis events from the Sequoyah Unit 2 steam generator stress report [34]. The design basis information for Sequoyah is typical of a Model 51 SG operating under the as-designed specifications and conditions. The number of events and the operating conditions (pressure, temperature, etc.) during the event listed are for the originally specified lifetime of the steam generator in the as-built condition. The data in Table 4-6 do not include the effects of power uprating or modifications to the original steam generator design. The values for temperature and pressure are the maximum values listed in the steam generator stress report. In the fatigue analysis these values are considered the maximum values for determining stress amplitude ranges and calculating the R ratio (S_{MIN}/S_{MAX}).

The estimated fatigue life of the stub runner to divider plate weld is determined using Equation 12. Typical fatigue life estimates assume that the loading on the cracked material is cyclical and applied at a defined rate for a defined period of time in a known environment. This is not necessarily the case for the divider plate to stub runner weld. The possible exception to that statement is if a plant plans to load follow during operation. The steam generators in the United States are not typically used in a load follow situation. The term “load follow” implies that the power output from the nuclear power plant varies significantly during any given day in response to demand for output (e.g. full power generation in the morning and evening and low power generation at night). Domestic nuclear power plants are used for baseload power generation to maintain grid demand and therefore do not significantly increase or decrease the amount of electricity produced in a given day under optimal conditions. One difference between the steam generators with divider plate cracking cited in Reference 1 through Reference 5 and the domestic steam generators is that the French nuclear power plants typically do load follow.

There are several assumptions that were made in the fatigue life estimate analysis:

1. Normal operation, upset and faulted conditions are assumed to occur in a single calendar year.
2. The conditions for each event are applied in a cyclic fashion to the divider plate weld.
3. The divider plate weld, and the hot leg face of the divider plate, will always be in tension.
4. No sequential effects will effect crack growth.
5. The crack growth rate is constant.
6. The steam generator begins the year in normal operation.

The assumptions listed above are conservative, but reasonable, from a perspective of bounding the scope of the problem. The collected list means that a crack in the divider plate is always able to grow once it initiates. The first assumption is particularly conservative because a steam generator would likely be inspected prior to further operation after a severe upset or faulted condition and not continue to operate in an unacceptable condition during the remaining portion of the year. The fourth assumption is potentially an issue because it is likely that the order of the events is capable of affecting crack growth (either retarding or accelerating). Including these effects in an analysis can be done by means on a Monte Carlo simulation to randomly sample the set of available events based on the frequency of occurrence of each event. However, the current method is sufficient to obtain information on the nature of the problem and would be required for comparison against different methods. There are other methods for calculating fatigue resistance during service life, such as Miner’s Rule [16], but they typically do not include the initial and final crack lengths for a material as variables in the problem.

4.5 Results from Finite Element Analysis

The fracture analyses described in this report use the results of a limiting finite element analysis described in the Appendices. The two dimensional finite element studies provided the local divider plate stiffness values for various crack depths and the gross section stress data for comparison against the classical two dimensional edge crack models described in Reference 24. The three dimensional finite element analyses provided the stress and displacement information used in the three dimensional fracture analysis.

The gross section stress in the two dimensional fracture analysis was taken from the finite element model using the elements ahead of the crack tip and outside of the theoretical process zone [24]. The finite element results were compared to the results using the gross section stress as calculated using traditional mechanics of materials solutions (e.g. $\sigma = P/A$). The gross section stress values used to calculate the stress intensity for the two dimensional comparison are listed in Table 4-2.

The average section stress values used to calculate the stress intensity for the three dimensional comparison are listed in Table 4-3. The average gross section stress at the elevation of the stub runner weld was used to calculate the stress intensity in the three dimensional fracture analysis. The reason for using the average value is that the stress on the hot leg surface of the weld is much greater than the stress on the cold leg surface of the weld. It would be overly conservative to use the hot leg surface axial stress value as a representative of the stress state in the stub runner weld. See Figure 4-3 for a plot of the hot leg and cold leg axial surface stresses during normal operating conditions. See Figure 4-4 for a plot of the average axial stress at the stub runner weld during normal operating, loss of load and feedline break conditions. Table 4-4 lists the maximum tubesheet displacements for the cracked and uncracked conditions as calculated by the three dimension finite element model. The maximum tubesheet displacements are important for future crack analysis because they are representative of the maximum crack opening displacement at the stub runner elevation.

Table 4-1
Summary of Alloy 600 Material Properties

Temp (ºF)	Y_s (ksi)	Y_{ut} (ksi)	S_m (ksi)
100	30.00	80.00	55.00
200	27.50	80.00	53.75
300	25.60	80.00	52.80
400	23.90	80.00	51.95
500	22.50	80.00	51.25
600	21.40	80.00	50.70
650	21.00	80.00	50.50

Table 4-2
Gross Section Stresses from 2D Finite Element Analysis

a (%)	S_g (psi)
8	2329.63
32	2586.80
64	2691.88
96	10758.64

Table 4-3
Average Section Stresses from 3D Finite Element Analysis

Condition	S (ksi)
NOP	19.8
LOL	23.5
FLB	32.0

Table 4-4
Summary of Maximum Vertical Tubesheet Displacements

	NOP (in)	LOL (in)	FLB (in)
Uncracked	0.05152	0.6127	0.08225
Cracked	0.12022	0.14364	0.19624

Table 4-5
Best Estimate Data from Ringhals Unit 3 Hot Leg Safe End Nozzle Weld Crack Specimens

	Crack Depth		Extension	Avg. CGR		Stress Intensity Factor		
Specimen #	Initial, a_1 (in)	Final, a_2 (in)	Δa (in)	606 ºF (in/s)	617 ºF (in/s)	Initial, K_1 (Ksi $in^{0.5}$)	Final, K_2 (Ksi $in^{0.5}$)	Mean, K_{avg} (Ksi $in^{0.5}$)
1	0.35	0.51	0.16	5.51E-09	7.09E-09	26.8	30.5	28.7
2	0.35	0.63	0.28	9.45E-09	1.26E-08	26.8	33.2	30.0

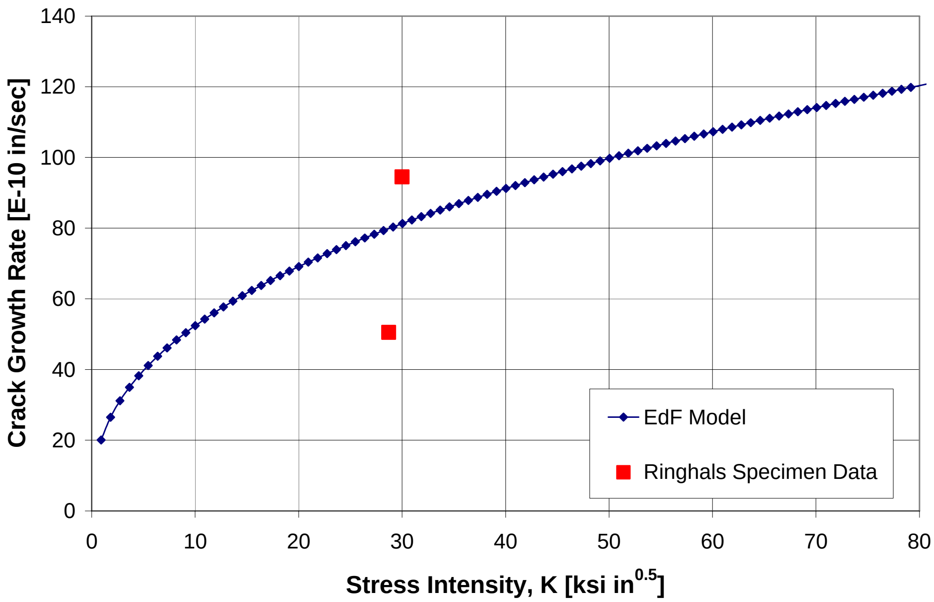

Figure 4-2
Crack Growth Rate Estimates using Model Fit from EdF Data [33]

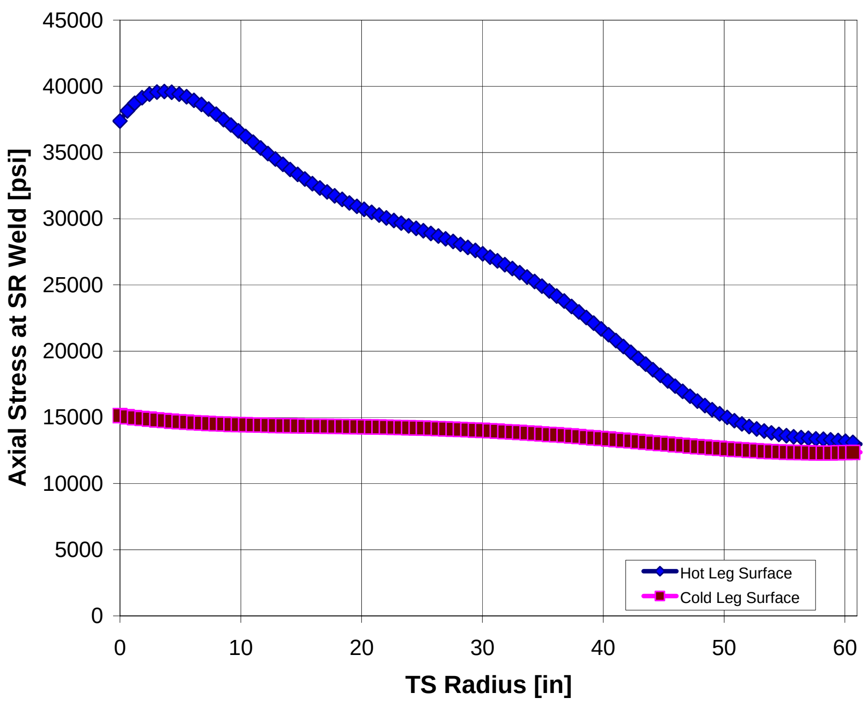

Figure 4-3
Comparison of Hot Leg and Cold Leg Surface Stresses from 3D Finite Element Model at the Elevation of the Stub Runner Weld at NOP Conditions

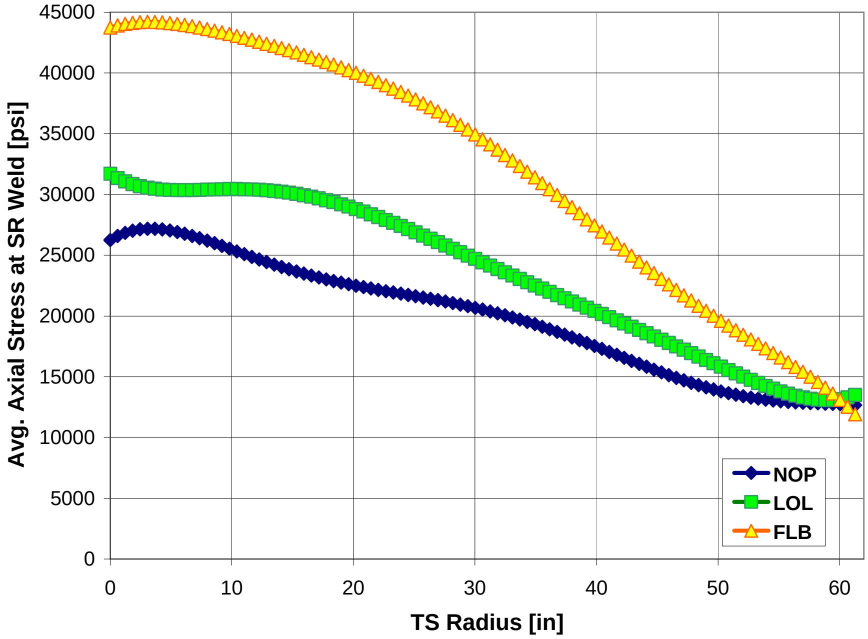

Figure 4-4
Plot of the Average Axial Stress at the Elevation of the Stub Runner Weld for the NOP, LOL and FLB Conditions

Table 4-6
Summary of Transient and Design Basis Events for Sequoyah Model 51 Steam Generator [34]

Category	Event	Total Years = 40				Temp. (ºF)	Primary (psi)	Sec (psi)	DP across TS (psi)
		Lifetime	Frequency	Prob	% Prob.				
Normal	Heat-Up	200	5	0.00	0.33	547.00	2250.00	735.00	1515
Normal	Cool Down	200	5	0.00	0.33	70.00	480.00	0.40	479.6
Normal	Plant Loading (5%/Min)	18300	457.5	0.30	30.44	605.00	2250.00	784.80	1465.2
Normal	Plant Unloading (5%/Min)	18300	457.5	0.30	30.44	547.00	2250.00	1020.00	1230
Normal	Small Step Increase	2000	50	0.03	3.33	560.00	2325.00	1151.60	1173.4
Normal	Small Step Decrease	2000	50	0.03	3.33	542.00	2228.00	900.30	1327.7
Normal	Large Step Decrease	200	5	0.00	0.33	562.00	2335.00	1399.30	935.7
Normal	Hot Standby	18300	457.5	0.30	30.44	547.00	2235.00	1020.00	1215
Normal	Turbine Roll Test	10	0.25	0.00	0.02	490.00	2000.00	550.00	1450
Upset	Loss of Load	80	2	0.00	0.13	577.00	2550.00	1413.00	1137
Upset	Loss of Power	40	1	0.00	0.07	567.00	2500.00	1413.00	1087
Upset	Loss of Flow	80	2	0.00	0.13	512.00	2200.00	1198.20	1001.8
Upset	Reactor Trip	400	10	0.01	0.67	537.00	1900.00	1346.70	553.3
Faulted	Feedline Break, SLB	1	0.025	0.00	0.0017	560.00	2650.00	0.00	2650
		Total Events	**1503**						

4.6 Fracture Evaluations and Results

4.6.1 Crack Initiation, Brittle and Plastic Failure of the Divider Plate Cross Section

The detection threshold for cracks in the divider plate is taken as the crack initiation depth in the fatigue life estimates using the stress intensity values calculated from the 3D finite element data. The crack initiation data from Table 4-5 was used to calculate the estimated fatigue life of the divider plate section due to combined mechanical and PWSCC effects.

The results of using Equations (7) and (8) and the iteration scheme with Equations (9) and (10) are shown in Table 4-3. It is unlikely that the divider plate will fail as a brittle material because the temperature of the metal in the TS-CH complex during NOP exceeds 600 ºF. It is much more likely that the divider plate section, with the assumed crack geometry, will fail plastically as the remaining ligament yields in tension.

4.6.2 Two Dimensional Crack Model Results

The stress intensities for a two dimensional, plane strain, edge crack calculated using an unmodified, modified and moment adjusted shape factor are shown in Figure 4-5. The modified and moment adjusted calculation results over estimate the stress intensity in the section compared to the finite element results. The unmodified stress intensity results are the most similar to the finite element results.

4.6.3 Three Dimensional Crack Model Results

Figure 4-6 shows the stress intensity calculated using the unadjusted average section stresses at the elevation of the stub runner weld during NOP as a function of tubesheet radius for four different crack depths. The stress intensities for a three dimensional edge crack calculated using the average section stresses is shown in Figure 4-7. The stress intensity exceeds the threshold for propagation at each point along the tubesheet for all of the crack depths shown. The stress intensity for each crack depth reaches a maximum value along the tubesheet at a radius of roughly 3 inches and a minimum value along the periphery of the tubesheet. This result is reasonable because the observed PT indications at St. Laurent [2] were concentrated towards the center of the tubesheet. The fact that the stress intensity exceeds the threshold value along the entire length of the divider plate is also reasonable because of the cracking observed in the triple point specimens taken from Gravelines [3] and Dampierre [4].

Figure 4-7 shows the adjusted average stress intensity as a function of crack depth for NOP, LOL and FLB conditions. The adjusted average stress intensity curves predict that a crack will exceed the threshold at a depth of 0.05 inch or less (i.e. less than a 3% crack depth). This result indicates that it is much easier to propagate a crack with the assumed geometry than it is to propagate a smaller crack. A conservative interpretation of the three dimensional stress intensity results is that if a crack has propagated along the entire length of the divider plate then it will exceed the threshold for crack propagation and can grow into the depth of the divider plate.

4.6.4 Life Estimates from Mechanical Cycling and Combined Effects on the Weld

The state of stress during NOP must be defined in order to calculate the load ratio, R (S_{MIN}/S_{MAX}). The average section stress, taken from the 3D finite element analysis results, for an uncracked divider plate at the elevation is roughly 26 ksi during the as-specified NOP condition. The smallest pressure differential across the tubesheet in a Model 51 steam generator occurs during Cool Down and is 0.48 ksi (See Table 4-6). The average uncracked section stress during Cool Down at the elevation of the stub runner is obtained by comparing the average section stress in the two dimensional FE model for a 1000 psi pressure differential to the 480 psi pressure differential. This yields an average section stress of roughly 1.2 ksi for the Cool Down condition with an uncracked divider plate. The ratio of the Cool Down section stress to the NOP section stress is equal to 1.2 divided by 26, or 0.046. Rounding this value up to the nearest decimal place gives an estimated load ratio of R = 0.05 for NOP conditions in an uncracked divider plate. The minimum and maximum stresses in the divider plate will change as the crack depth increases which will change the R ratio. But the initial uncracked condition is a useful piece of data to gauge how the fatigue resistance of the divider plate will change as the crack length increases.

Figure 4-8 shows the estimated fatigue life for the divider plate stub runner weld as a function of crack depth for several different values of R. Note the vertical axis of the plot is taken as logarithmic scale. The results show that a stub runner weld with a crack that extends the length of the divider plate and is 0.25 inch or less in depth requires more than 1 million cycles to failure at an R value of 0.05. Assuming that the crack growth increases the R ratio in the divider plate by a factor of 10 (R = 0.5), there is still ample margin to accommodate the estimated 1503 cycles in an average year from cracks less than 1.10 inches deep. The crack in the weld would need to be more than 1.20 inches deep and the R ratio more than 0.68 in order to potentially fail the divider plate weld within one calendar year. This is a highly unlikely possibility given the deepest weld crack indications currently observed are 0.28 inch deep or less and the estimated R ratio for NOP is 0.05.

4.6.5 Fatigue Life Estimate from Combined Corrosive and Mechanical Effects

Table 4-9 summarizes the results of calculating the change in crack length using Equation 14 and Equation 15 for a period of 1, 2, 5 and 6 calendar years of service at NOP conditions. The results in Table 4-9 assume that all of the weld material is sensitized to PWSCC and that the driving mechanism of the crack growth will be PWSCC combined with mechanical fatigue. The K data in the table are read from a polynomial fit of the average stress intensity NOP curve in Figure 4-7 at each given crack length. The ΔK is taken as the difference in the final stress intensity value under NOP conditions at the final crack length for that period of time and the stress intensity value at the unloaded state at the beginning of the cycle.

Table 4-10 summarizes the estimated time to failure (in calendar years) for a cracked divider plate under NOP conditions and an initial crack depth with the assumed conservative crack geometry of 0.16 inch. Figure 4-9 and Figure 4-10 show the estimated number of cycles to failure as a function of R ratio for various conditions. Note the vertical axes of the plots are taken as logarithmic scales. Figure 4-9 compares the results of Equation 11 using the stress intensity data from the Ringhals specimens and the average stress intensity data from the three dimensional finite element analysis. The results for the two different analysis inputs were compared assuming NOP conditions and an initial 0.16 inch crack with the assumed crack geometry. Figure 4-9 shows that the finite element results are approximately 7% lower than the Ringhals results. Taking the absolute value of the difference between the two curves gives an estimate for the value of N_{CHEM}. The results of the three dimensional finite element study give the values for N_f as a function of R ratio. Subtracting N_{CHEM} from N_f gives an estimate for the fatigue life of a divider plate exposed to PWSCC, under NOP, with an initial crack depth of two times the detection threshold. The estimated fatigue life of 1.05 million cycles is roughly 700 times the average number of cycles expected during a calendar year. Figure 4-11 is a plot of the safety margin of the weld, with respect to the estimated number of cycles to fail weld. Figure 4-12 is a plot of the safety margin of the weld with respect to crack growth. Note that at the currently observed crack depths Figure 4-12 shows a safety margin of more than 12.

Figure 4-10 shows the estimated number of cycles to failure for an initial 0.16 inch deep crack under NOP, LOL and FLB conditions. Recall that the assumptions in the analysis assume that the pressure differentials during each condition are assumed to be applied cyclically. Also, the minimum stress applied to the stub runner weld section will increase as the crack depth increases, thereby increasing the R ratio value. The results of the fatigue analysis indicate that failure of the divider plate to stub runner weld would require more than 5500 cycles of the pressure differential from the limiting accident condition (FLB), which is more than 3.5 times the average number of events in a calendar year. The design specification for the Model 51 assumes that only one steam line break (SLB) or FLB occurs during the lifetime of the SG.

The results of the above crack growth analyses are summarized in Table 4-10. The four entries in Table 4-10 represent different assumptions about the failure mode of the divider plate. All of the results in Table 4-10 assume that the divider plate has an edge crack with an initial depth of 0.16 inch that runs the length of the divider plate and that the divider plate experiences 1503 loading cycles equivalent to NOP conditions each calendar year. All of the results in Table 4-10 use the average stress intensity results calculated using the average stresses from the 3D finite element model. The entry for “FEA w/Ringhals Data” assumes that the crack growth is driven by mechanical fatigue and is based on the Ringhals nozzle specimen crack growth data in Reference 31 assuming that the crack will propagate through the weld. The entry for “FEA w/Plastic Failure” assumes that the crack growth is also driven by mechanical fatigue but that the weld will fail when the remaining ligament reaches the plastic limit. The entry for “$N_f - N_{chem}$” assumes that the crack growth is driven by mechanical fatigue but the weld material is sensitized to PWSCC. These results indicate that mechanical fatigue of the weld is not a concern under NOP conditions. The final entry in Table 4-10, “Finite Element CGR Estimate”, assumes that a combination of PWSCC and mechanical fatigue will act to grow the crack, but the dominate mechanism in the crack growth is PWSCC. The “Finite Element CGR Estimate” is taken from Table 4-9 and it is the most limiting case for the cracked divider plate.

The conclusion for the fatigue life estimate curves shown in Figure 4-10 is that it is highly unlikely that a cracked divider plate to stub runner weld will fail during normal operation, upset or accident conditions in a given calendar year. However, the results that are summarized in Table 4-10 suggest that it is possible for a crack to propagate through the weld in a relatively short period of time, 5.11 years. More data and field experience are necessary to validate these analysis results or provide guidance on potential inspection requirements.

Table 4-7
Comparison of Estimated Crack Lengths at Failure during NOP

Method	Crack Length (Inch)
Estimated Brittle Failure	1.800
Estimated Plastic Failure	1.915
Iterative Solution	1.945

Table 4-8
Percent Crack Depth that Exceeds Crack Propagation Threshold Calculated using 2D Methods for a 1000 psi Pressure Differential Across the TS

Model	Percent Cracked
Unmodified	58.0
Modified	25.5
Moment Adjusted	26.0
Finite Element	38.0

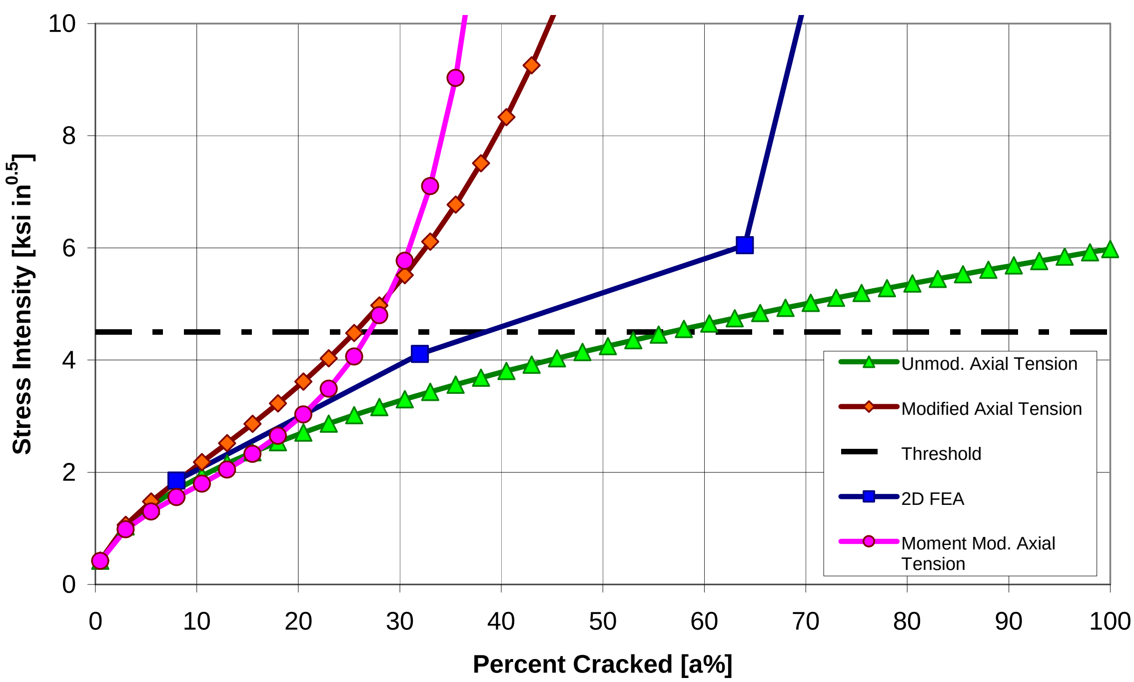

Figure 4-5
Plot of 2D Stress Intensity as a Function of Crack Length for a 1000 psi Pressure Differential Across the TS

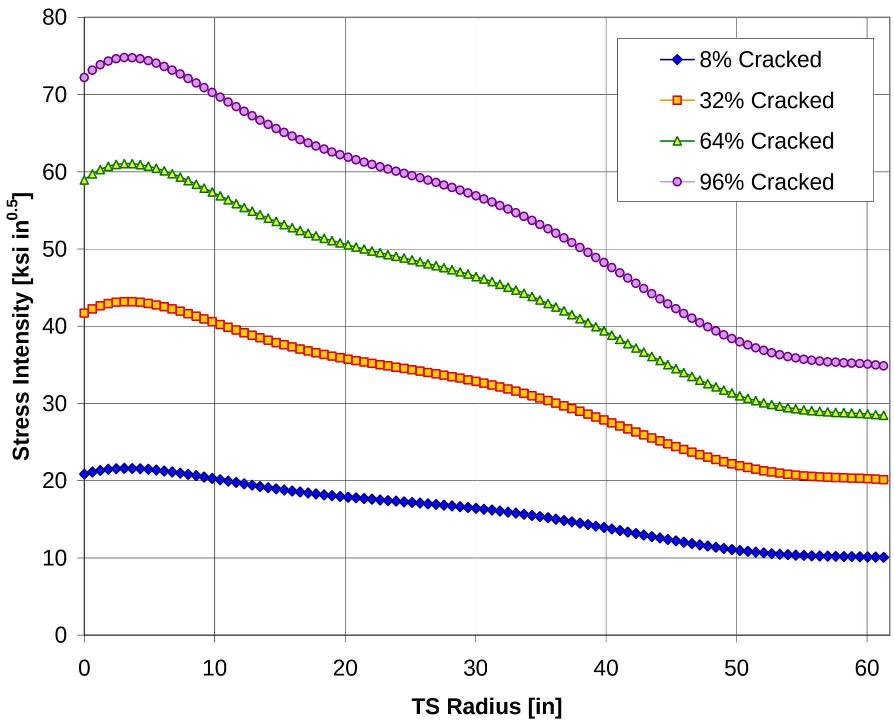

Figure 4-6
Plot of Stress Intensity in the Vicinity of the Crack Tip During NOP as a Function of Tubesheet Radius

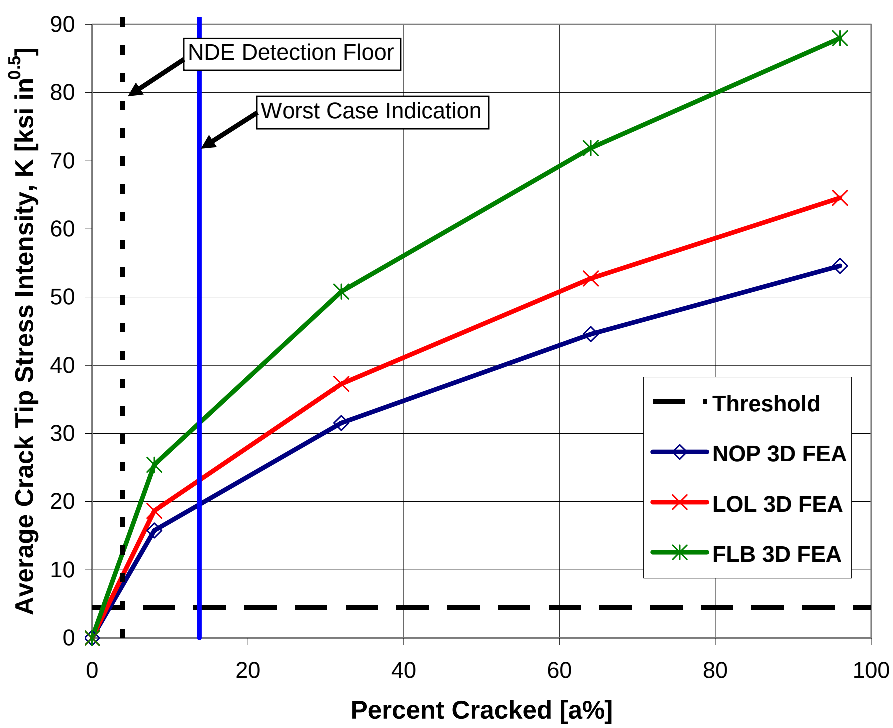

Figure 4-7
Plot of Average Stress Intensity as a Function of Percent Crack Depth

Table 4-9
Estimated Fatigue Crack Growth using Finite Element, and EdF CGR Data

Time Years	Estimated n #	Initial Crack Length in	Avg. Final K ksi $in^{0.5}$	ΔK ksi $in^{0.5}$	PWSCC CGR E-10 in/sec	Fatigue CGR in/cycle	Change in Crack Length in	Final Crack Length In
1	1503	0.16	15.76	15.76	62.82	1.378E-05	0.22	0.38
2	3006	0.16	23.83	23.83	74.12	4.763E-05	0.54	0.70
5	7515	0.16	30.72	30.72	82.61	1.020E-04	1.76	1.92
6	9018	0.16	48.79	48.79	98.72	4.087E-04	2.48	2.64

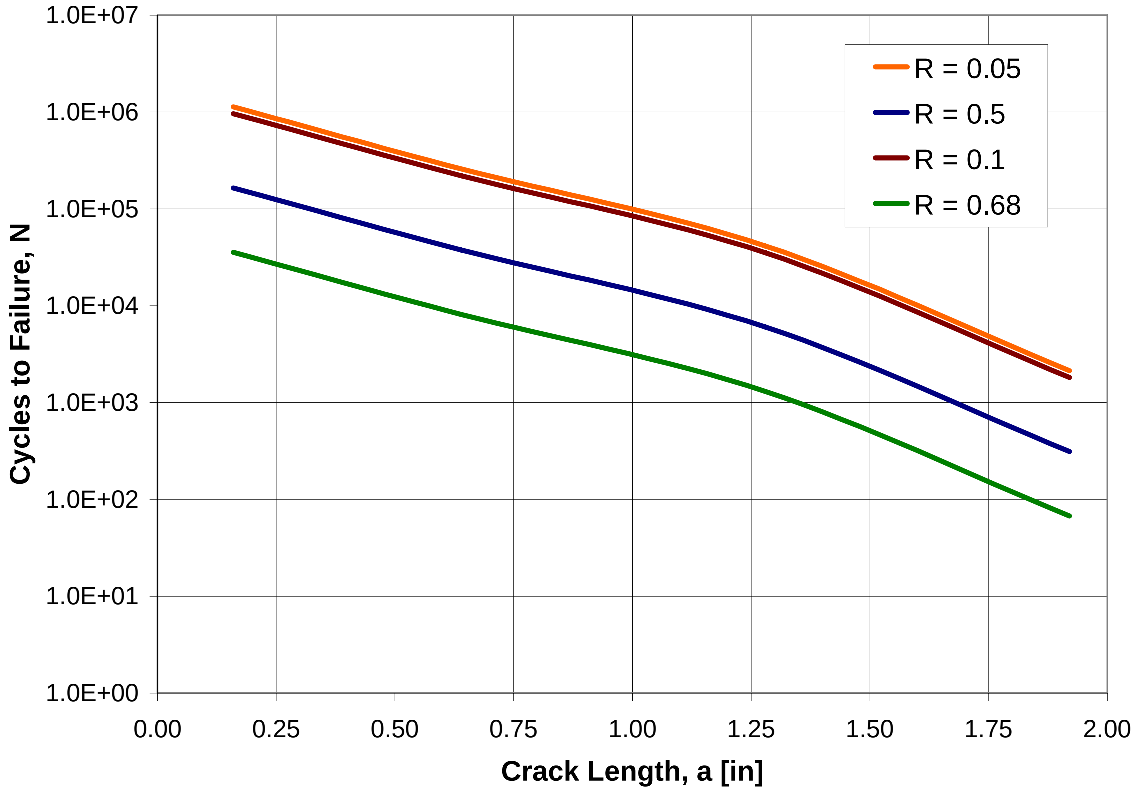

Figure 4-8
Plot of Cycles to Failure as a Function of Crack Length for Different R Ratio

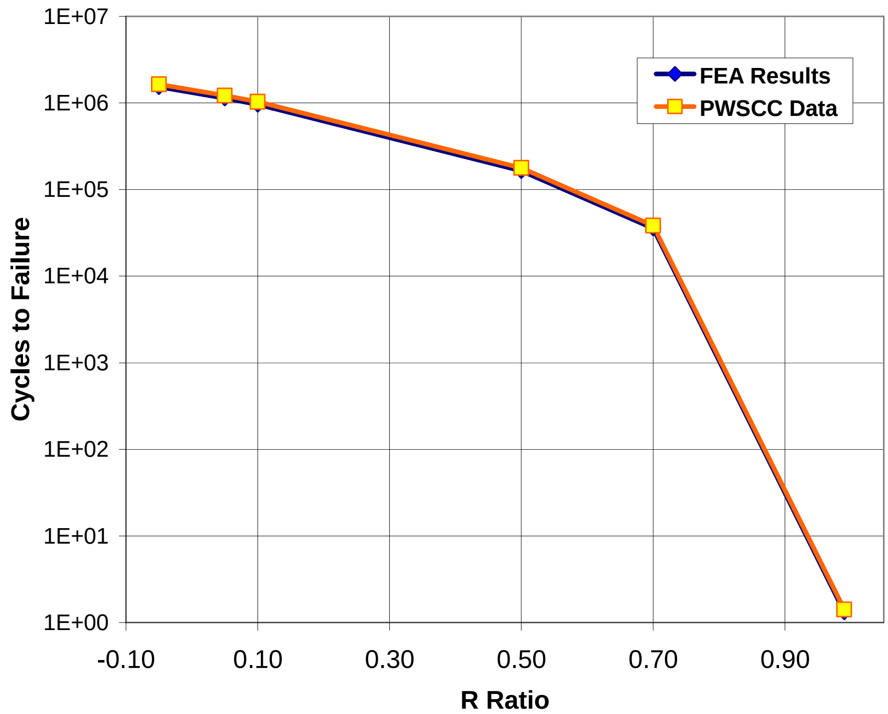

Figure 4-9
Comparison of Estimated Fatigue Life during Normal Operation for a Divider Plate with an Initial 0.16 inch Deep Crack Using Data from 3D FEA Studies and PWSCC Data from [31]

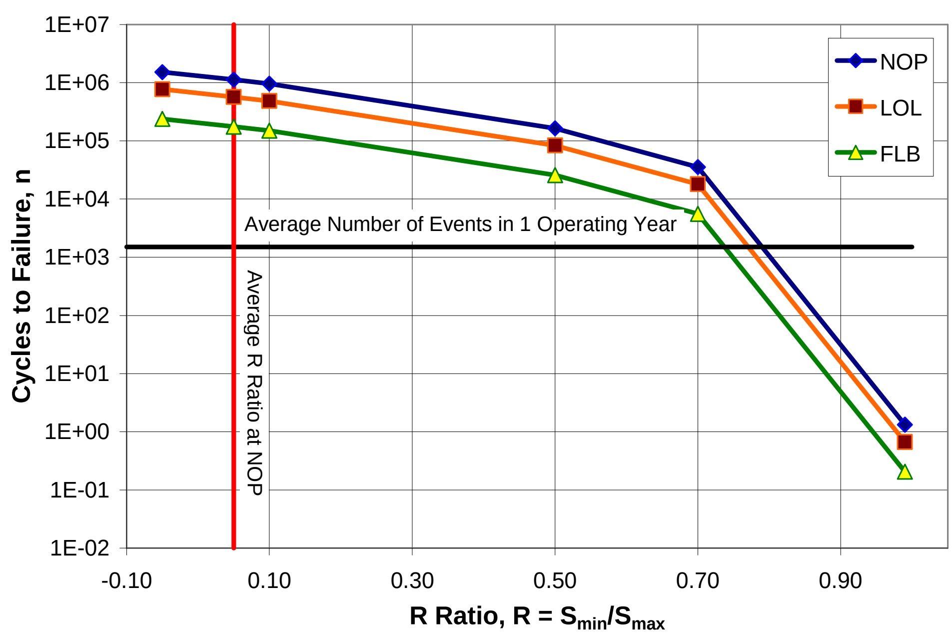

Figure 4-10
Plot of Cycles to Failure as a Function of R Ratio for Different Operating Conditions Assuming an Initial 0.16 inch Deep Crack in the Divider Plate

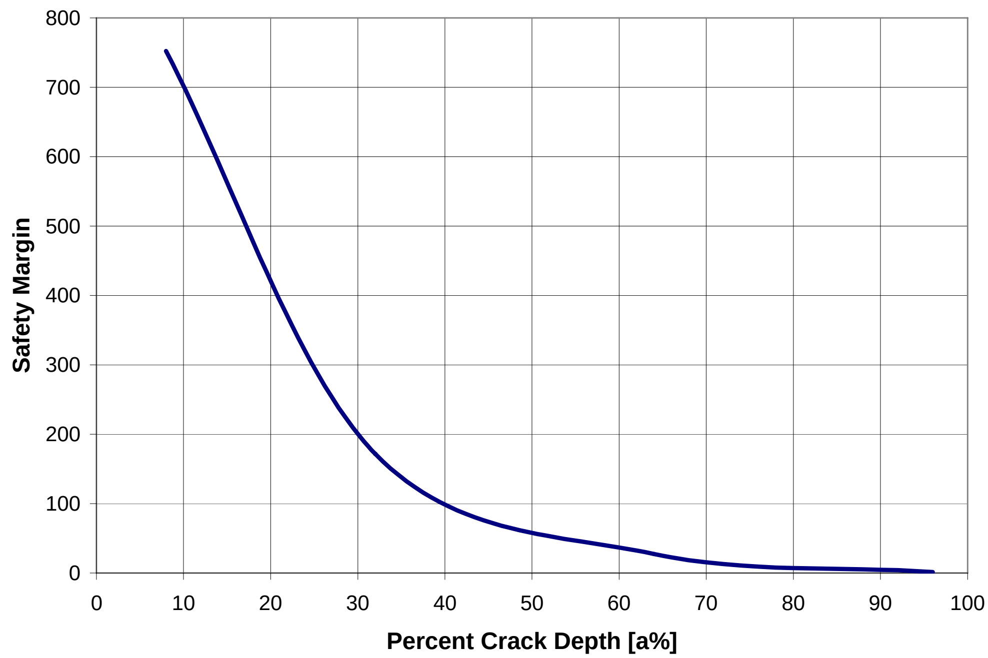

Figure 4-11
Plot of Cycle Safety Margin as a Function of Percent Crack Depth in the Divider Plate during Normal Operation for an Average Number of Events during a Calendar Year

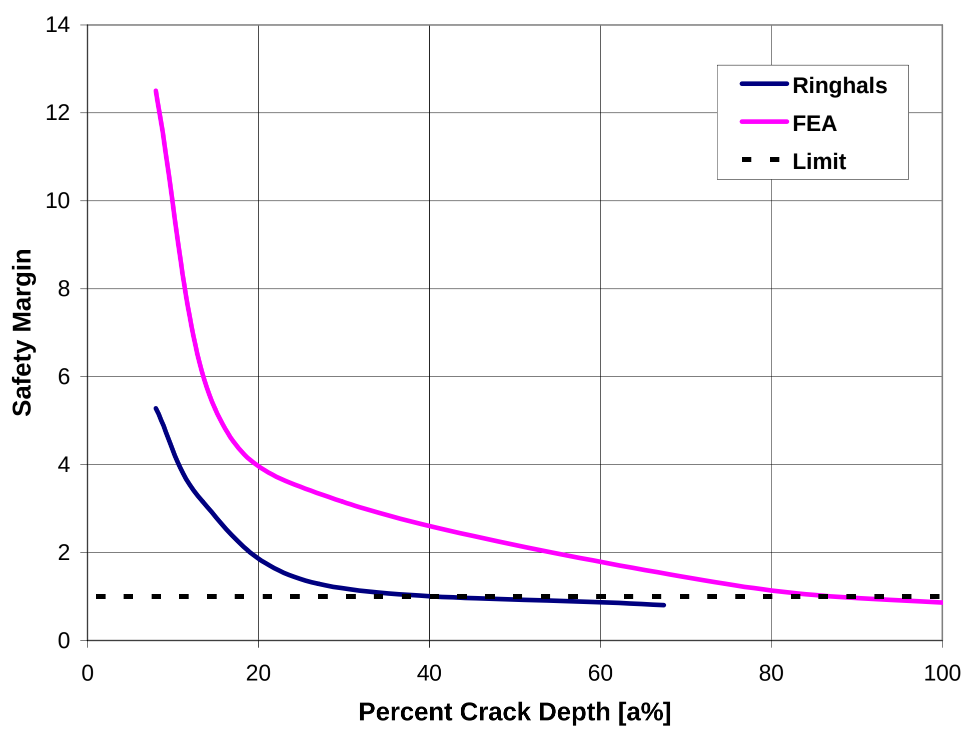

Figure 4-12
Plot of Cycles to Failure as a Function of R Ratio for Different Operating Conditions Assuming an Initial 0.16 inch Deep Crack in the Divider Plate

Table 4-10
Summary of Estimated Fatigue Life of a Cracked Divider Plate during NOP Assuming an Initial 0.16 inch Crack Depth and 1503 Cycles per Calendar Year

Source	Years
FEA w/Ringhals Data	805.1
FEA w/Plastic Failure Limit	751.8
N_f- N_{CHEM}	698.6
Finite Element CGR Estimate	5.1

5
REFERENCES

1. MRP-EDF-SGPP05, SAINT-LAURENT B NPP - Unit 1 – SG #52 – Loop #2 - Examination of specimen harvested from a hammered partition plate.
2. MRP-EDF-SGPP01, SAINT-LAURENT B NPP - Unit 1 - Steam generator #52 - Loop #2 - Examination of two specimens taken out from the SG channel head divider plate.
3. MRP-EDF-SGPP03, GRAVELINES NPP - Unit 1 - Destructive examination of the triple point of the SG2 channel head.
4. MRP-EDF-SGPP02, DAMPIERRE 1/2 NPP - Unit 1 - Steam generator #27 retired from loop 3 when the SGs were replaced in 1990 - Chemical, metallurgical and mechanical characterizations of the weld joining the partition stub, the divider plate and the channel head bowl.
5. MRP-EDF-SGPP04, CHINON B NPP - Unit 4 - Characterization of indications discovered on the SG #2 stud / partition plate weld surface.
6. "51 Series Steam Generator Calculated and Measured Strains and Deflections for Steam Generator Tubesheet Channel Head Model Under Limit Conditions", MPR 201, Volume 1 of Two Volumes, November, 1969.
7. "51 Series Steam Generator Divider Plate Analysis", E.W. Pianka, April 1972.
8. "51 Series Steam Generator Channel Head-Tubesheet-Stub Barrel Steady State Analysis", P. DeRosa, 1970.
9. "51 Series Steam Generator Channel Head-Tubesheet- Stub Barrel Transient Analysis", P. DeRosa, Dr. L. Conway, August, 1970.
10. CN-NCE-CP1RSG-17, "Delta 76 Replacement Steam Generator Divider Plate Analysis Comanche Peak Unit 1," C.A. Weindorf, July, 2006.
11. SG-90-02-026, "Steam Generator Information Report," Rev. 6, February 1990.
12. Thomas Slot, "Stress Analysis of Thick Perforated Plates," Technomic Publishing Co., Inc., Westport, Connecticut, 1972.
13. Terakawa, T., Imai, A., Yagi, Kazushige, Fukada, Y., Okada, K., "Stiffening Effects of Tubes in Heat Exchanger Tube Sheet", Journal of Pressure Vessel Technology Transactions, ASME Vol. 106, No.3, August 1984.
14. WCAP-16640-P, "Steam Generator Alternate Repair Criteria for Tube Portion Within the Tubesheet at Salem Unit 1," G.W. Whiteman, 09/06/2006.
15. Roark's Formulas for Stress and Strain, 7th Ed., Ed: W.C. Young, R.G. Budynas, McGraw-Hill, New York, New York, 2002.

16. ASME Boiler and Pressure Vessel Code, Section II Part D, “Materials,” 1998 Edition, 1999 Addenda, The American Society of Mechanical Engineers, New York, New York.

17. CN-SGDA-03-99, “Evaluation of the Tubesheet Contact Pressures for Wolf Creek, Seabrook, and Vogtle 1 & 2 Model F Steam Generator,” Thurman, A.L., 09/30/2003.

18. LTR-CDME-05-32-P, “Limited Inspection of the Steam Generator Tube Portion within the Tubesheet at Byron 2 & Braidwood 2,” Keating, R.F., 05/10/2005.

19. LTR-SGDA-06-136, “Letter of Transmittal for H.B. Robinson Unit 2 True B* Spreadsheets for WCAP-16627,” Cassino, C.D., 08/03/2006.

20. Flurry, R., “51 Series Steam Generator Tube-To-Tubesheet Junction Analysis”, 1971.

21. Fisher, M. J., “Release of ANSYS 8.1 for XP, Solaris 8, HPUX 11.0, and HPUX 11.23,” LTR-SST-04-44, October 29, 2004.

22. Bibollet, C., Beroni, C., Raimbault, S., Stindel, M., Verdiere, N., Gauchet, J., “EDF Field Experience on Steam Generator Divider Plate Examinations,” 6th International Symposium of the Contribution of Material Investigations to Improve the Safety and Performance of LWRs, September 2006.

23. Verdiere, N., Pons, S., Amzallag, C., Bibollet, C., Rayel, P., “Maintenance Strategy of Inconel Components in French PWRs,” 6th International Symposium of the Contribution of Material Investigations to Improve the Safety and Performance of LWRs, September 2006.

24. N.E. Dowling, <u>Mechanical Behavior of Materials</u>, 2nd Ed., Prentice Hall, New Jersey, © 1999.

25. Hall, J.F., Molkenthine, J.P., Prevéy, P.S., “XRD Residual Stress Measurements on Alloy 600 Pressurizer Heater Sleeve Mockups,” Proceedings of the Sixth International Symposium of Materials in Nuclear Power Systems-Water Reactors, 1993, TMS, ANS, NACE, San Diego, CA, pp. 855-861.

26. Dong, P., Hong, J.K., Bouchard, P.J., “Analysis of Residual Stresses at Weld Repairs,” Int. Journal of Pressure Vessels and Piping, Vol. 82 (2005), pp. 258-269.

27. WNEP-9725, “The Westinghouse Tube-to-Tubesheet Joint Hydraulic Expansion Process – Design, Qualification, Manufacturing, and Performance,” July 1997.

28. STD-DP-1997-8015, Rev. 0, “Data Package for Leak Testing of Vogtle Unit 1 Steam Generator Tube to Tubesheet Joint per STD-TP-1997-7951 Rev. 1,” 6/3/97.

29. LTR-SGDA-03-191, Rev. 0, “H* Testing of Model D5 and F Tube-to-Tubesheet Joint Specimens,” August 3, 2003.

30. Internal Westinghouse Electric Company Communication, “Threshold stress intensity for Inconel 600,” 03/10/1998. (This document is attached to CN-SGDA-07-10 in EDMS).

31. White, G.A., Nordmann, N.S., Hickling, J., Harrington, C.D., “Development of Crack Growth Rate Disposition Curves for Primary Water Stress Corrosion Cracking (PWSCC) of Alloy 82, 182, and 132 Weldaments,” Proceedings from the 12th International Symposium on Environmental Degradation of Materials in Nuclear Systems - Water Reactors, 2005.

32. Materials Reliability Program (MRP) Crack Growth Rates for Evaluating Primary Water Stress Corrosion Cracking (PWSCC) of Alloy 82, 182, and 132 Welds (MRP-115), EPRI, Palo Alto, CA: 2004. 1006696.

33. Valliant, F., Boursier, J., Amzallag, C., Bibollet, C., Pons, S., “Environmental Behavior and Weldability of NI-Base Weld Metals in PWRs,” 6th International Symposium of the Contribution of Material Investigations to Improve the Safety and Performance of LWRs, September 2006.

34. General Order #CO-60001-AR6-AR5, P. DeRosa, “TVA/TEN Sequoyah Units 1 & 2 51 Steam Generator Stress Report – Sections 1 & 2,” March 1974.

35. ANSYS Inc. “Theory Reference – Structural Fundamentals”, Version 8.1, 2004.

A

APPENDIX A: APPROXIMATE MATERIAL MODELING

Analysis of Thick Perforated Plates using Anisotropic Material Models

The equivalent solid plate procedure greatly simplifies the structural analysis of a perforated plate, for the explicit modeling of each penetration is not necessary [10]. The perforated plate is treated as an orthotropic homogeneous material with in-plane effective elastic constants, $\overline{E}^*, \overline{\nu}^*$, and $\overline{G}^*$, and out-of-plane effective elastic constants E_z^*, ν, and G_z^*, which are used to account for the effect of the holes on the stiffness of the plate. For square penetration patterns, the in-plane behavior of the plate is isotropic and the anisotropy of the equivalent material must only be considered for stresses in the thickness direction. The ANSYS finite element analysis code uses the orthotropic material properties for most element types when the element material is defined with the appropriate elasticity matrix constants.

The equivalent elastic constants are obtained from Equation 2.2 of Reference 12, and are shown below in matrix form for a Cartesian and Cylindrical coordinate system. In these equations, the Z coordinate is in the direction of the thickness of the plate. These constants are for a square hole penetration pattern and are derived based on generalized plane strain assumptions. The generalized plane strain assumption is appropriate because the tube plate is relatively thick compared to the radius of the plate.

Cartesian Coordinate System

$$\begin{Bmatrix} \varepsilon_x^* \\ \varepsilon_y^* \\ \varepsilon_z^* \\ \gamma_{yz}^* \\ \gamma_{zx}^* \\ \gamma_{xy}^* \end{Bmatrix} = \begin{bmatrix} 1/\overline{E}^* & -\overline{\nu}^*/\overline{E}^* & -\nu/E_z^* & 0 & 0 & 0 \\ -\overline{\nu}^*/\overline{E}^* & 1/\overline{E}^* & -\nu/E_z^* & 0 & 0 & 0 \\ -\nu/E_z^* & -\nu/E_z^* & 1/E_z^* & 0 & 0 & 0 \\ 0 & 0 & 0 & 1/G_z^* & 0 & 0 \\ 0 & 0 & 0 & 0 & 1/G_z^* & 0 \\ 0 & 0 & 0 & 0 & 0 & 1/\overline{G}^* \end{bmatrix} \begin{Bmatrix} \sigma_x^* \\ \sigma_y^* \\ \sigma_z^* \\ \tau_{yz}^* \\ \tau_{zx}^* \\ \tau_{xy}^* \end{Bmatrix}$$

Cylindrical Coordinate System

$$\begin{Bmatrix} \varepsilon_R{}^* \\ \varepsilon_\theta{}^* \\ \varepsilon_Z{}^* \\ \gamma_{\theta Z}{}^* \\ \gamma_{ZR}{}^* \\ \gamma_{R\theta}{}^* \end{Bmatrix} = \begin{bmatrix} 1/\overline{E}^* & -\overline{\nu}^*/\overline{E}^* & -\nu/E_z{}^* & 0 & 0 & 0 \\ -\overline{\nu}^*/\overline{E}^* & 1/\overline{E}^* & -\nu/E_z{}^* & 0 & 0 & 0 \\ -\nu/E_z{}^* & -\nu/E_z{}^* & 1/E_z{}^* & 0 & 0 & 0 \\ 0 & 0 & 0 & 1/G_z{}^* & 0 & 0 \\ 0 & 0 & 0 & 0 & 1/G_z{}^* & 0 \\ 0 & 0 & 0 & 0 & 0 & 1/\overline{G}^* \end{bmatrix} \begin{Bmatrix} \sigma_R{}^* \\ \sigma_\theta{}^* \\ \sigma_Z{}^* \\ \tau_{\theta Z}{}^* \\ \tau_{ZR}{}^* \\ \tau_{R\theta}{}^* \end{Bmatrix}$$

The equivalent matrix that is used by ANSYS in determining the orthotropic constants is given in Equation 2-4 of the ANSYS Theory Manual (Reference 35) and is shown below.

ANSYS Orthotropic Material Matrix

$$\begin{Bmatrix} \varepsilon_x{}^* \\ \varepsilon_y{}^* \\ \varepsilon_z{}^* \\ \gamma_{yz}{}^* \\ \gamma_{zx}{}^* \\ \gamma_{xy}{}^* \end{Bmatrix} = \begin{bmatrix} 1/EX & -NUXY/EY & -NUXZ/EZ & 0 & 0 & 0 \\ & 1/EY & -NUYZ/EZ & 0 & 0 & 0 \\ & & 1/EZ & 0 & 0 & 0 \\ & & & 1/GYZ & 0 & 0 \\ & \begin{pmatrix} symmetric \\ ratios \end{pmatrix} & & & 1/GXZ & 0 \\ & & & & & 1/GXY \end{bmatrix} \begin{Bmatrix} \sigma_x{}^* \\ \sigma_y{}^* \\ \sigma_z{}^* \\ \tau_{yz}{}^* \\ \tau_{zx}{}^* \\ \tau_{xy}{}^* \end{Bmatrix}$$

The ν/E ratios for the off diagonal terms in the lower portion of the matrix are automatically calculated by ANSYS such that the matrix is symmetrical. The terms EX, EY, EZ, NUXY, NUYZ, NUXZ, GXY, GYZ, and GXZ in the matrix are supplied as user input. The appropriate equivalent material constants to be entered for each of these terms are determined by comparison of the terms in the ANSYS matrix to the terms in the equivalent plate matrix.

The required inputs are different for a general three-dimensional analysis and for an axisymmetric analysis as shown below.

ANSYS Inputs for a General 3-Dimensional Analysis

$$EX = \overline{E}^* \qquad GXY = \overline{G}^* \qquad NUXY = \overline{\nu}^*$$
$$EY = \overline{E}^* \qquad GYZ = G_z^* \qquad NUYZ = \nu$$
$$EZ = E_z^* \qquad GXZ = G_z^* \qquad NUXZ = \nu$$

X and Y are in the in-plane direction of the plate
Z is in the direction of plate thickness

ANSYS Inputs for an Axisymmetric Analysis

$$EX = \overline{E}^* \qquad GXY = G_z^* \qquad NUXY = \nu$$
$$EY = E_Z^* \qquad GYZ = G_z^* \qquad NUYZ = \frac{\overline{E}^*}{E_z^*}\nu$$
$$EZ = \overline{E}^* \qquad GXZ = \overline{G}^* \qquad NUXZ = \overline{\nu}^*$$

X is in the radial direction of the plate
Y is in the direction of plate thickness
Z is in the theta direction of the plate

The equivalent material constants are a function of the perforated hole pattern, the ligament efficiency, and the thickness of the perforated plate. The hole penetration pattern for the Model 51 Steam Generator tube plate is shown in Figure A-1. It can be seen from the figure that the perforated hole pattern is triangular, and the plate is relatively thick, indicating that the generalized plane strain assumption is appropriate. The ligament efficiency is calculated below.

Tube Hole Diameter: d = 0.875” (nominal)

Tube Hole Pitch: P = 1.281”

Tube Hole Ligament: h = P - d = 1.281 – 0.875 = 0.406

The resulting ligament efficiency is: $\eta = \frac{h}{P} = \frac{0.406}{1.281} = 0.3169$

From Table B.2 of Reference 12, the following equivalent elastic constants are obtained by linear interpolation using a ligament efficiency of $\eta = 0.3169$ and a Poisson’s Ratio of $\nu = 0.3$.

$$\frac{\overline{E}^*}{E} = 0.4375 \qquad \frac{\overline{G}^*}{G} = 0.2112 \qquad \overline{\nu}^* = 0.1803$$

From Table 4.2 of Reference 12, the following equivalent elastic constants are obtained by linear interpolation using a ligament efficiency of η = 0.3169.

$$\frac{E_z^*}{E} = 0.6345 \qquad \frac{G_z^*}{G} = 0.4615$$

The temperature dependent equivalent material constants are obtained by substituting the values of E and G at different temperatures into the above equations. The results are shown in Table A-1. The additional stiffness from the portion of the steam generator tubes within the tubesheet acts to increase the value for E_z in the ANSYS model. The stiffness modified tubesheet properties are shown in Table A-2. The unmodified isotropic tubesheet properties are shown in Table A-1 to A-3 for comparison.

Table A-1
Orthotropic Material Properties

Temperature (°F)	$\overline{E}^*$ (x 10^6 psi)	$\overline{G}^*$ (x 10^6 psi)	$\overline{\nu}^*$	E_z^* (x 10^6 psi)	G_z^* (x 10^6 psi)
600	1.16E+1	2.35	0.0541	1.67E+1	4.68

Table A-2
Modified Orthotropic Material Properties

Temperature (°F)	$\overline{E}^*$ (x 10^6 psi)	$\overline{G}^*$ (x 10^6 psi)	$\overline{\nu}^*$	E_z^* (x 10^6 psi)	G_z^* (x 10^6 psi)
600	1.26E+1	2.35	0.0374	1.83E+1	4.68

Table A-3
Unmodified Isotropic Material Properties

Temperature (°F)	E (x 10^6 psi)	G (x 10^6 psi)	ν	E_z (x 10^6 psi)	G_z (x 10^6 psi)
600	26.4	10.15	0.3	26.4	10.15

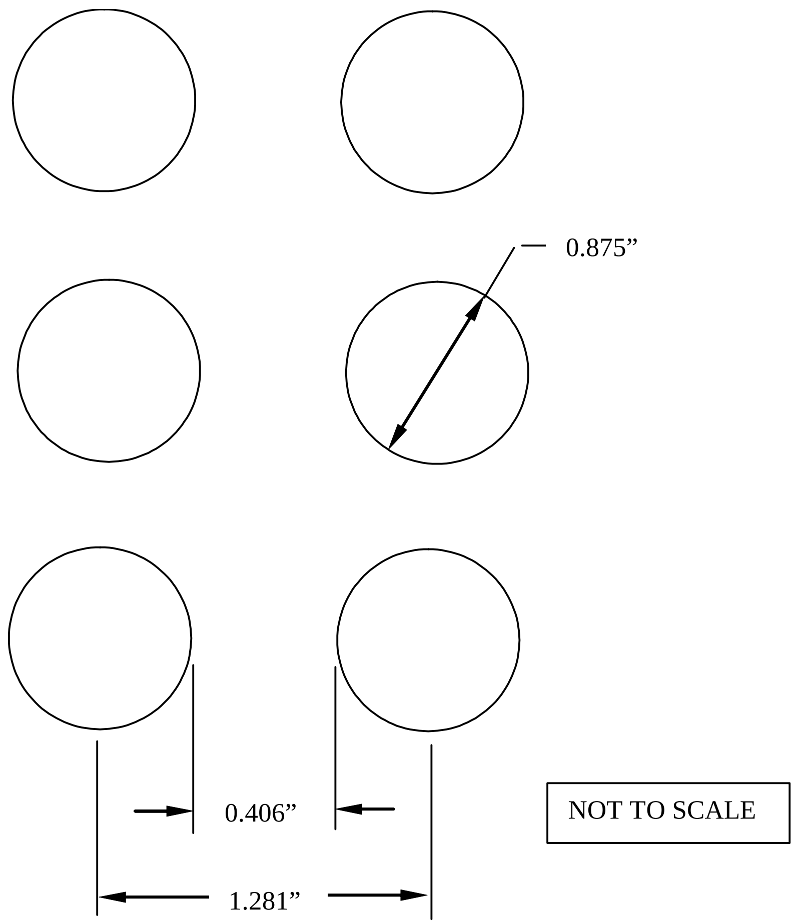

Figure A-1
Tube Plate Hole Penetration Pattern

Export Control Restrictions

Access to and use of EPRI Intellectual Property is granted with the specific understanding and requirement that responsibility for ensuring full compliance with all applicable U.S. and foreign export laws and regulations is being undertaken by you and your company. This includes an obligation to ensure that any individual receiving access hereunder who is not a U.S. citizen or permanent U.S. resident is permitted access under applicable U.S. and foreign export laws and regulations. In the event you are uncertain whether you or your company may lawfully obtain access to this EPRI Intellectual Property, you acknowledge that it is your obligation to consult with your company's legal counsel to determine whether this access is lawful. Although EPRI may make available on a case-by-case basis an informal assessment of the applicable U.S. export classification for specific EPRI Intellectual Property, you and your company acknowledge that this assessment is solely for informational purposes and not for reliance purposes. You and your company acknowledge that it is still the obligation of you and your company to make your own assessment of the applicable U.S. export classification and ensure compliance accordingly. You and your company understand and acknowledge your obligations to make a prompt report to EPRI and the appropriate authorities regarding any access to or use of EPRI Intellectual Property hereunder that may be in violation of applicable U.S. or foreign export laws or regulations.

The Electric Power Research Institute (EPRI), with major locations in Palo Alto, California; Charlotte, North Carolina; and Knoxville, Tennessee, was established in 1973 as an independent, nonprofit center for public interest energy and environmental research. EPRI brings together members, participants, the Institute's scientists and engineers, and other leading experts to work collaboratively on solutions to the challenges of electric power. These solutions span nearly every area of electricity generation, delivery, and use, including health, safety, and environment. EPRI's members represent over 90% of the electricity generated in the United States. International participation represents nearly 15% of EPRI's total research, development, and demonstration program.

Together...Shaping the Future of Electricity

Program:

Nuclear Power

Printed on recycled paper in the United States of America

1014982

Electric Power Research Institute
3420 Hillview Avenue, Palo Alto, California 94304-1338 • PO Box 10412, Palo Alto, California 94303-0813 USA
800.313.3774 • 650.855.2121 • askepri@epri.com • www.epri.com